Porous Complexes for the Unambiguous Structural Determination of Non-Crystalline Compounds

Lilian M. Hayes

Supervised by Prof. Claire Carmalt

and Prof. Derek Tocher

Thesis submitted for the degree of Doctor of Philosophy (Chemistry)

University College London

2017

DECLARATION

I, Lilian M. Hayes confirm that the work presented in this thesis is my own. Where information has been derived from other sources, I confirm that this has been indicated in the thesis.

Lilian Hayes

ABSTRACT

The ability of the metal-organic framework (MOF) [{$(ZnI_2)_3$(tris (4-pyridyl)-1,3,5-triazine)$_2.x$(solvent)}$_n$] (**1**) to act as a 'crystalline sponge' for the analysis of non-crystalline compounds *via* single-crystal X-ray diffraction (SCXRD) has been assessed and a host of new encapsulation complexes presented. Firstly, studies have been performed to investigate the most reliable protocol for its synthesis, which resulted in the discovery of three novel, non-porous Zn-TPT forms along side **1**. Repeat encapsulation experiments with simple, aromatic guest molecules demonstrated the reproducibility of the technique and the specificity of site uptake by guest molecules within the pore space of **1**. Systematic studies of guest-host interactions determine how **1** displays such unique abilities of guest ordering. Analysis of encapsulation compounds with chemically related guests of systematically varying size and functionality showed guest ordering is governed predominately by $\pi\cdots\pi$ and CH$\cdots\pi$ interactions, bolstered by multiple guest-host and guest-guest van der Waals interactions and hydrogen bonds.

Parallel work has sought to develop alternative crystalline sponges through reticular synthesis for the encapsulation of large guest molecules. Three organic compounds have been synthesised using Stille and Suzuki coupling reactions including the previously unreported 2,4,6-tri(4'-(pyridin-4-yl)-[1,1'-biphenyl]-4-yl)-1,3,5-triazine (**TPPPT**) Together they form a series of potential linkers with similar functionality and chemical properties to tris(4-pyridyl)-1,3,5-triazine (used in **1**) whilst displaying systematic variation in size. Work focused on developing interfacial syntheses to produce novel porous MOFs in single-crystalline form. This yielded four novel MOFs: [{$(Zn_4(OAc)_6)$(TPT)•2(H_2O)}$_n$] (**2**); [{$(ZnI_2)_2$(TMDP)•$C_6H_5NO_2$}$_n$] (**3**); [{Co(TMDP)(mand)$_2$}$_n$] (**4**); and [{$Zn(C_9H_6N_7O)_2$•0.56(DMF)}$_n$] (**5**). The latter of which was shown to display crystalline sponge properties, with proof provided by the successful encapsulation and SCXRD analysis of *trans*-cinnamaldehyde and 2,4,6-trimethylaniline.

ACKNOWLEDGMENTS

First and foremost I would like to thank my supervisors at UCL, Professor Claire Carmalt and Professor Derek Tocher. That I have enjoyed studying for my PhD so much is predominantly down them. Their high standards and willingness to guide me through challenging areas afforded me independence in my research whilst always being supported and encouraged. This support and encouragement also emanated from those of the extended Carmalt/Parkin conglomerate I had the pleasure of sharing an office and lab with. Special thanks go to Rachel Wilson, Dom Potter, Dr Nicholas Chadwick, Merina Corpinot, Dr Francesco Di Maggio, Monika Jurkic, Dr Caroline Knapp, Dr Michael Powell, Dr Will Peveler and Dr Joe Bear.

I would like to thank my industrial supervisor Dr Neil Press at Novartis for the opportunities I had to visit Switzerland and for welcoming me into his group to undertake some of my research there. Also, my literature section owes a lot to his committed forwarding of new publications! I would also like to thank Dr Christel Guibourdenche for her kindness and guidance during my placement at Novartis, it was invaluable.

I would like to give honourable mention to Professor Paul Wright who first introduced me to the fascinating field of MOFs at the University of St. Andrews, and my 6^{th} form chemistry teacher Dr Paul Maddren, the original inspiration.

Of course, the past three years have been all work, but occasionally there was time for fun. For its provision I would like to thank Becky Bottle and Hannah, my climbing pals Nick, Rob, Anna and Finn, and many of the Carmalt/Parkin conglomerate.

To my family who I love very much, Miranda, Simon, Magda, Toby, Oliver and Maciej, thank you so much. I can't wait to hear your verdicts on the crystalline sponge!

I come to the end of this PhD with so much more than a thesis and a couple of publications. I have learnt so much, grown to have great confidence in my own abilities, and an even greater appreciation for the knowledge of others!

Thank you all very much.

PUBLICATIONS

Lilian M. Hayes, Caroline E. Knapp, Karina Y. Nathoo, Neil J. Press, Derek A. Tocher and Claire J. Carmalt. **The crystalline sponge method: a systematic study of the reproducibility of simple aromatic molecule encapsulation and guest-host interactions**. *Cryst. Growth Des.*, 2016, **16**, 3465 - 3472

Lilian M. Hayes, Neil J. Press, Derek A. Tocher and Claire J. Carmalt. **Intermolecular interactions between encapsulated aromatic compounds and the host framework of a crystalline sponge**. *Cryst. Growth Des.*, 2017, **17**, 858 - 863

CONTENTS

LIST OF TABLES

ABBREVIATIONS

a, *b*, *c*	Unit cell axis
α, β, γ	Unit cell angles
ADP	Atomic displacement parameter
BAPE-PP	4-(4-pyridyl)phenylboronic acid pinacol ester
cm	Centimeter
DCM	Dichloromethane
DMF	Dimethylformamide
DMA	Dimethylacetaminde
EI	Electron impact
ESI	Eectrospray ionisation
eq	Equivalent molar quantity
hrs	Hour(s)
IR	Infrared spectroscopy
J	spin-orbit coupling
K	Kelvin
LCMS	Liquid chromatography-mass spectrometry
M	Metal
mand	D-mandelic acid
mg	Milligram(s)
min	Minute(s)
MOF	Metal organic framework
mp	Melting point
MS	Mass spectrometry
nm	Nanometer(s)
NMR	Nuclear magnetic resonance
Ph	Phenyl
ppm	Parts per million
R_1	R-factor
SCXRD	Single-crystal X-ray diffraction
SMR	Suzuki-Miyaura reaction
T	Temperature
TBPT	2,4,6-tris(4-bromophenyl)-1,3,5-triazine
TIMTZ	4,6-tri(imidazol-1-yl)-1,3,5-triazine
TMDP	4,4'-trimethylenedipyridine
TPPPT	2,4,6-tri(4'-(pyridin-4-yl)-[1,1'-biphenyl]-4-yl)-1,3,5-triazine
TPPT	2,4,6-tris(4-(pyridin-4-yl)phenyl)-1,3,5-triazine
TPT	tris(4-pyridyl)-1,3,5-triazine
wR_2	Weighted R-factor

Part I

INTRODUCTORY CHAPTERS

1

INTRODUCTION

The premier analytical technique available for unambiguous structural determination is single-crystal X-ray diffraction (SCXRD). Aside from instrumental availability and training the only requirement is the possession of a suitable crystal. Although other valuable analytical techniques are available only SCXRD can provide bond lengths and angles, atom positions, elemental composition, site ordering information, and stereochemistry (see Table 1.1). By definition SCXRD is limited to single crystals and so comes its greatest limitation. Many samples demand an unreasonable time outlay to be obtained as single crystals of sufficient quality to produce usable diffraction patterns. Indeed some are never obtained in crystalline form. A technology allowing precise molecular structure determination of any compound (whether it be liquid, amorphous or crystalline) in low quantities would be one of the holy grails of chemistry.

1.1 CRYSTAL-FREE CRYSTALLOGRAPHY

In 2013 Fujita and co-workers at the University of Tokyo published a ground-breaking paper introducing a technique that claimed to overcome these inherent limitations of SCXRD.[1] Fujita's solution, nicknamed 'crystal-free crystallography',[2] was a simple one; encapsulate your non-crystalline compound within a crystalline framework. Through the formation of strong guest-host interactions, it may be rendered regularly ordered and thus capable of creating Bragg peaks and a diffraction pattern. It is not the idea of studying a

	IR	NMR	MS	SCXRD
Sample	Solid Liquid Gas	Solid Liquid	Solid Liquid Gas	Crystal
Suitable atoms	All	Limited	All	All but H
Absolute structure determination	x	Indirect	x	Directly
Conformational determination	x	Indirect	x	Directly
Data interpretation	Indirect	Indirect	Indirect	Direct

Table 1.1: Comparison of structural determination methods.

guest enclatherated in a host framework that was novel (small guest molecules have been studied in clathrates)[3] but the use of a specific metal-organic framework (MOF) displaying extraordinary properties.

1.1.1 *Application to Biomedical Research*

Developing and applying this technique beyond Fujita's proof-of-principle study to protein function determination could have a huge impact on biomedical research. The most significant potential applications are:

1. Enabling the unambiguous structural determination of compounds not amenable to conventional study. Research times could be cut by providing identification of unknown compounds quickly and with absolute accuracy. Examples of such areas of application are:
    - Novel active compounds enabling medicinal chemistry optimisation and probing of protein function with new molecular tools.
    - Metabolite structures, accelerating the evaluation process.
    - Reaction side product structures enabling reaction optimisation.
2. The technique could be used to investigate the adopted conformation of molecules. This is vital to biomedical research as knowledge of the conformation of molecules with an affinity to proteins allows accurate computer assisted docking into crystallographic structures or homology models of the protein and its binding site(s).

1.2 METAL-ORGANIC FRAMEWORKS

MOFs are a type of coordination network made up of multifunctional organic linkers coordinated to metal ions or clusters through moieties such as carboxylates, pyridines and phosphates. A MOF network may extend infinitely in one-, two-, or three-dimensions of repeating units often producing a network of uniform permanent voids (seen in Figure 1.1) on the microporous ($<$2 nm) or mesoporous (2 - 50 nm) scale.[4,5] MOFs may also be referred to as hybrid framework compounds to reflect their incorporation of both organic and inorganic building blocks.

By judicious selection of inorganic and organic moieties a MOF's hybrid architecture may be tailored to fulfil the demands of a specific application. This huge chemical versatility has lead to ultra high porosity and high thermal and chemical stability .[6] The extraordinary synthetic flexibility of the combination of metal-containing units

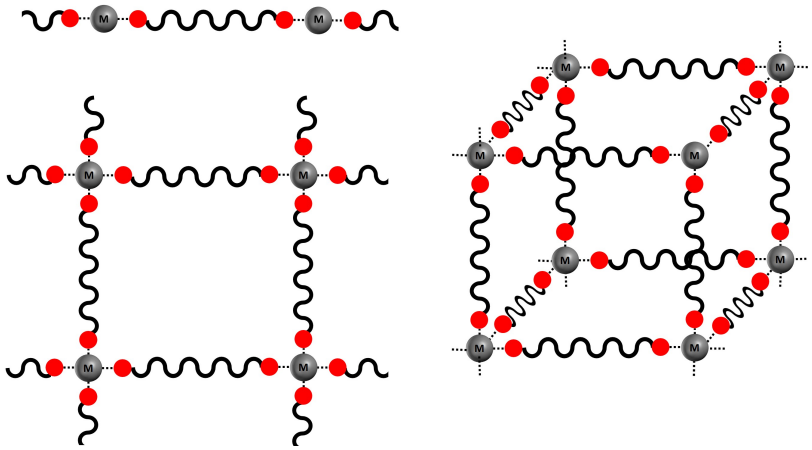

Figure 1.1: Schematic represenatations of one-, two-, and three-dimentional metal-organic structures. Metal centres represented by grey spheres and organic linkers as black lines terminated by red donor atoms.

and organic linkers is a great advantage over other classes of porous materials, such as purely inorganic zeolites, and has enabled researchers to push the boundaries of solid-state science. Indeed, they trump all competition in terms of surface area. The structure $[Zn_4O(BTE)_{4/3}(BPDC)]$ (MOF-210) displays ultra high porosity with a Langmuir surface area of 10400 $m^2\,g^{-1}$. MOF-210 is formed from $Zn_4O(CO_2)_6$ units and two linkers, which are shown in Figure 1.2 along with the extended structure. As a result of its porosity it shows exceptional gas (hydrogen, methane, and carbon dioxide) uptake capacities.[7] MOFs also exhibit positively outrageous pore volumes. Bio-MOF-100, based on the same biphenyldicarboxylate (BPDC) linkers as MOF-210 and zinc-adeninate (Figure 1.3), has a BET surface area of >4000 $m^2\,g^{-1}$ and a pore volume of 4.3 $cm^3\,g^{-1}$.

1.2.1 *History of MOFs*

As a result of these astonishing properties, since first appearing in the literature some 20 years ago,[6] MOFs have become a workhorse serving fields as varied as gas storage and sequestration, chemical sensing, biomedical applications and catalysis.[7,10–13] Initial excitement surrounded their high surface areas and potential for the storage of gases such as methane or hydrogen, and later carbon dioxide sequestration. However, their potential extends more broadly with MOFs capable of luminosity (conjugated linkers),[11] charge transfer,[14] electrical properties,[15] catalysis,[16] and drug delivery.[17]

Over 20,000 types of MOFs have been created since the term was first coined in 1995 by Yaghi *et al* with the hydrothermal synthesis of $[Cu(4,4'\text{-bpy})_{1.5}{\bullet}NO_3(H_2O)_{1.25}]$ framework.[6] They became

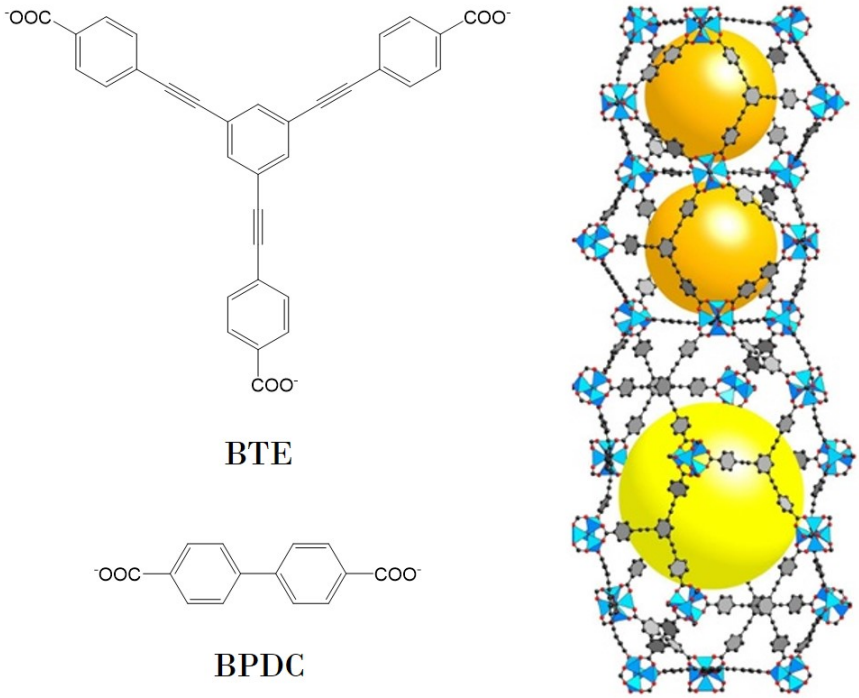

Figure 1.2: The organic linkers BTE and BPDC which make up the extended structure of $[Zn_4O(BTE)_{4/3}(BPDC)]$ (MOF-210) with yellow and orange spheres to indicate pore space.[7]

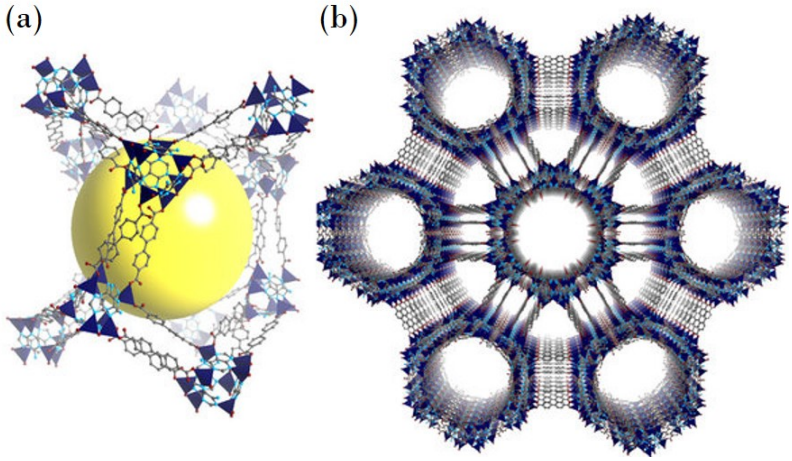

Figure 1.3: Crystal structure images of BIO-MOF-100; (a) yellow sphere indicating pore space within channels of (b) the extended structure.[8]

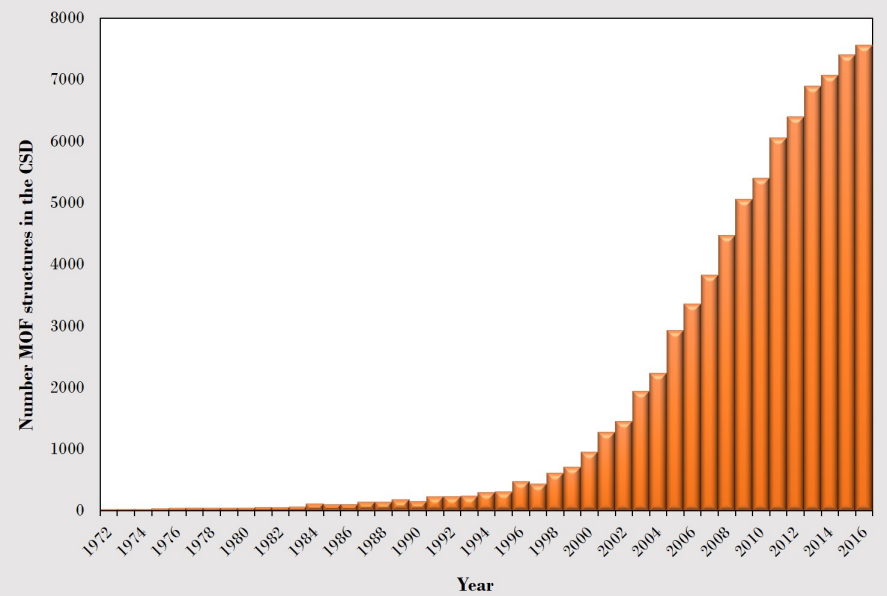

Figure 1.4: Growth of MOF entries in the CSD from 1972 to 2016, defined according to the CSD MOF subset.[9]

one of the fastest growing classes of material in the discipline of chemistry as demonstrated by the sheer number of MOF structures submitted to the CCDC, increasing every year (Figure 1.4). Initially, the fragile structures produced compared unfavourably to well established, rugged zeolites and some scientists remained sceptical of their use. However, by 1999 the robust and highly porous framework [{Zn_4O(benzene-1,4-dicarboxylate)•x(solvent)}$_n$] (MOF-5) had been characterised by Yaghi *et al* as having 61% porosity (by gas-sorption) and an incredibly high surface area of 3000 m^2g^{-1}, beginning to challenge the likes of zeolites and activated carbon.[18] In the same year the robust and now highly studied MOF [{Cu_3(benzene-1,3,5-tricarboxylate)$_2$(H_2O)$_3$}$_n$] (HKUST-1) was published. It is stable up to 240 °C with a pore size of 1 nanometer and solvent accessible voids of about 40% unit cell volume in the solid.[19] The publication of these structures lit the fire under global research interest in this new field of supramolecular chemistry.

1.2.2 *Applications*

Certainly their chemistry provokes fascination but after two decades the lack of promising industrial application provokes some scepticism as to their value. Whilst the interest in their application remains high, some researchers are disappointed, with questions surrounding their thermal, chemical and mechanical stability. The rush to report new crystalline structures is no longer a priority, although it remains an interest, compared to the delivery of valuable

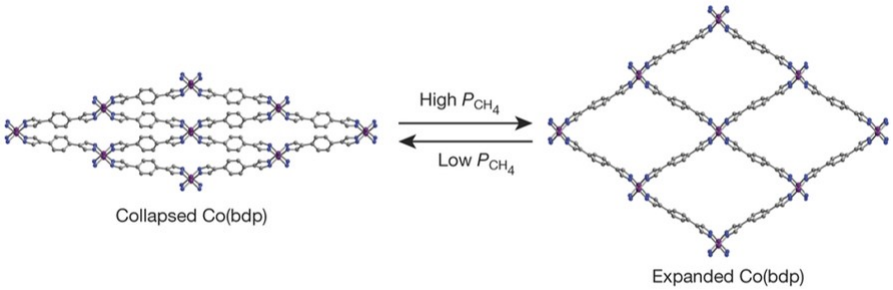

Figure 1.5: The crystal structures of the MOF Co(bdp) in its collapsed form (at 0 bar partial pressure of methane) and expanded form (at 30 bar).[22]

industrial applications. However, in the last couple of years a handful of structures have begun to live up to expectation and make their way to market, transcending the realm of purely synthetic interest.[20] A few of the most interesting and promising products are discussed below.

Energy storage

Natural gas is cleaner-burning than petrol and although there are nearly 150,000 vehicles running on compressed natural gas in the US, to compete with traditional cars on driving range and convenience lower pressure methane tanks are required. The low volumetric energy density of natural gas at ambient temperature and pressure present a substantial challenge, especially for lighter private vehicles. Therefore, BASF worked with pioneering MOF chemist Omar Yaghi using MOFs to store methane at upto triple the volume possible in a conventional fuel tank.[21] Whilst the identity of the structures investigated by BASF are secret, in order to cope with cycles of discharge and refuelling one might speculate on the candidates being MOFs with flexible or 'breathing' frameworks. For example, a flexible MOF developed by Long *et al* at Berkeley can store methane at 35 - 65 ATM, compared to a tank at 250 ATMs.[22] The mechanism of this breathing behaviour is shown in Figure 1.5. However, the progress of this project has largely stalled, with its success largely dependant upon global oil prices remaining high to provide a financial incentive for alternative fuels.

Antimicrobial coatings

Biologically active compounds such as nitric oxde (NO), active in host defence by preventing the proliferation of bacteria and hydrogen sulfide, a vasodilator, have been stored in MOFs and targeted delivery was shown to be possible.[23,24] This process has been exploited by MOFGen, a spin out company from the Russell Morris

group at the University of St Andrews. The company is developing antimicrobial coatings for medical devices such as catheters with the aim of reducing infection rates, with some products already supplied commercially. As well as the storage of biological agents in the pores, the MOF structure itself can be design to include active elements such as copper or silver ions, and potentially be applied to wound healing applications.

Food packaging

The spoiling of food and its subsequent wastage is a increasing problem along all points of the supply chain, from the farm to the consumer's fridge. A portion of this problem is the over-ripening of fruits and vegetables stimulated by the release of the plant hormone ethylene. This mechanism was the target of world's first commercial MOF produced by the companies MOF Technologies and Ducco. Called TruPick^{TM} for 'post-harvest freshness management', the MOF stores and releases the gas 1-methylcyclopropene which preferentially binds to plant enzymes inhibiting the action of ethylene. It is currently sold in US and Turkey, and is seeking approval for use in the EU.[25] BASF also has a interest in this area having registered a patent for a bioldegradable polymer embedded MOF for the adsorption of ethylene.[26]

Crystalline sponge

In 2014 the Japan Science and Technology Agency awarded Makoto Fujita at the University of Tokyo US$15 million over 5 years to commercialise the crystalline sponge method for the structural detrmination of non-crystalline compounds by SCXRD. The product is expected on the shelves in the next few years. Although Fujita has been reported informally as saying '*You know the Apple iPhone? They first released the iPhone 3. Our crystal is the iPhone zero.*'[27]

1.3 SYNTHESIS OF CRYSTALLINE MOFS

MOF structures are generally crystalline and in the context of this project focus is placed on the growth of single-crystalline MOFs. However, it is interesting to note that amorphous MOFs do exist. ZIF-4, a MOF with zeolitic structure, has been shown to undergo a crystal-amorphous transition at elevated temperature.[28]

Exploratory synthesis for the production of novel crystalline MOFs is not simple, remains highly empirical and to some extent requires a 'give-it-a-go' attitude. A consolation however can be sought in the fact that once a successful set of experimental conditions are identified as viable for the chosen components modification for optimisation is more straightforward. Indeed the crystal engineering

goal to synthesise crystals with predictable structures based on desired properties has proven a challenge when it comes to MOFs. Many synthetic factors play a role in whether a MOF will crystallise and the form the structure will take. These factors can be separated into compositional parameters and process parameters and include temperature, pressure, solvent properties, molar ratios of reactants and often the pH of the reaction mixture.[29] If available, high-throughput methods are a powerful tool to aid the discovery of novel compounds, using small scale parallel reactors to rapidly screen reagent combinations or assess the effect of small changes in experimental conditions.[30,31]

1.3.1 *Rational Design*

The range of established and undiscovered MOF structures is vast and judicious selection of ones study subject is tantamount to efficient research. Whilst the potentials of many known MOFs have yet to be reached, targeted synthesis of novel MOFs is highly desirable as it would allow structures with specific topologies and physical properties to be designed.[32] However, the relationship between the structure of organic linkers and the properties of the corresponding polymeric structures are not always clear. This challenging problem has been skillfully tackled by editing MOFs with an already understood structure-property relationship with particular advances made by Yaghi and O'Keefe.[18,33–37]

The term recticular synthesis is used to define this process of assembling specifc molecular building blocks into orders of systematic network structures.[37] An excellent example of this synthetic possibility is the study by Yaghi *et al.* describing the systematic design of MOF pore size and functionality for application to methane storage.[38] Pore functionality and size were varied across a series of frameworks based on the skeleton of MOF-5, creating an isoreticular series (one having the same framework topology but varied pore size). Figure 1.6 shows part of the series of ditopic carboxylate linkers employed in this study and the corresponding crystal structures. In creating structures with a precision akin to organic chemistry, the authors demonstrated synthetic control can be taken by combining extended linkers with the same metal-containing units. Such control is extremely desirable in the development of crystalline sponges capable of encapsulating specific classes of molecules and overcoming limitations.

1.3.2 *Design of Linkers*

In order to undertake such systematic MOF design one must be able to design and synthesise linkers relevant to the specific application.

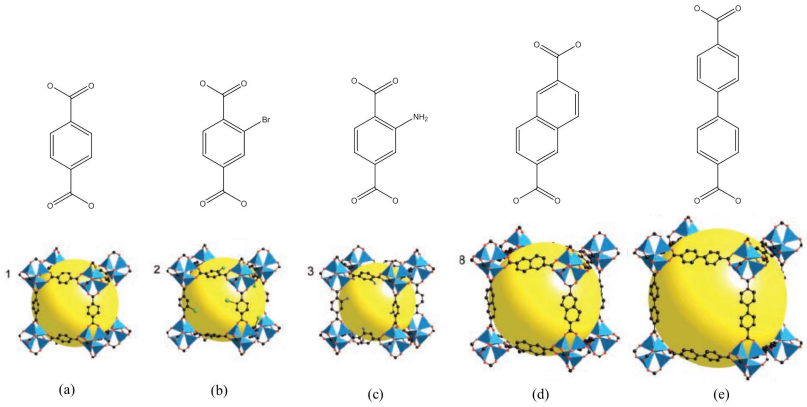

Figure 1.6: Dipotic carboxylate linkers and their corresponding isoreticular crystal structures. The yellow spheres represent the lagest van der Waals sphere that would fit in the cavities.[38]

Whether this be the incorporation of polarizable N=N bond for hydrogen anchoring, deprotonation sites for heterogeneous catalysis or highly conjugated linkers for fluorescence. For example, in the design of MOFs for hydrogen and methane storage Zhao *et al* focused on 'the gas affinity of frameworks by using ligands with different geometries to control the pore size and effectively introduce unsaturated metal centers (UMCs) into the framework'.[39] In order to improve a MOF's performance by judicious ligand design it is vital to understand the mechanism of the specific process.[40]

An interesting study performed by Yaghi *et al* showed that a large number of differently functionalised organic linkers can be incorporate in the same MOF structure, creating a multivariant series.[41] Starting with the well studied MOF-5, the authors edited its linker benzene-1,4-dicarboxylate (BDC) to produces a series of nine functionalised BDC compounds, including NH_2-BDC, Br-BDC, $(CH_3)_2$-BDC and $(OC_7H_7)_2$-BDC. By virtue of the unchanged length and connectively of the linkers, the authors aimed to assemble multiple structures and assess their properties. In total 18 multivariate MTV-MOF-5 type structures containing up to eight distinct functionalities in one phase were synthesised. Due to the different combinations of functionalities the pores were endowed with multiple levels of complexity that may allow their properties to be fine tuned (see Figure 1.7). It was noted that the properties of the MTV-MOFs were not simply a linear combination of each additional functional group. One of the structures containing 3 of the variants exhibited 400% better selectivity for CO_2 over CO compared with the original non-functionalised MOF-5.[41] The concept of multivariant MOFs has since been applied to a number of other studies.[42,43]

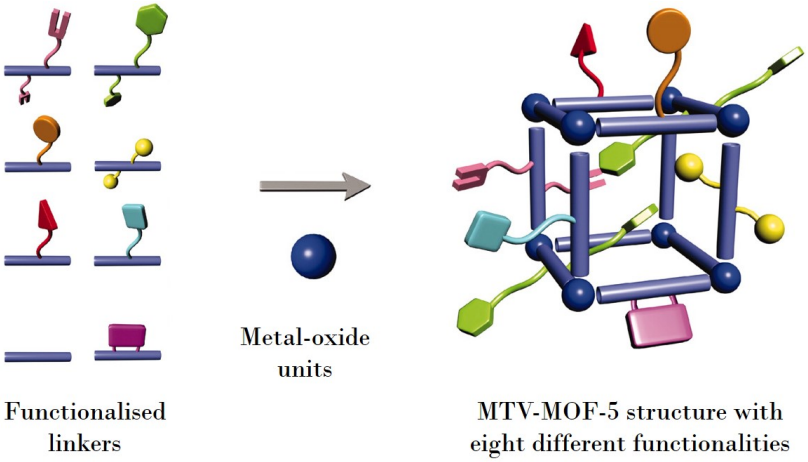

Figure 1.7: A structure from the MTV-MOF-5 series.[41]

1.4 THE MOF OF CRYSTAL-FREE CRYSTALLOGRAPHY

1.4.1 *General Properties and Requirements*

For application as a crystalline sponge, the MOF must contain pores of volume and aperture size appropriate to the intended guest molecules, and be capable of strong interaction with an absorbed guest. Of equal importance is that the MOF structure itself is crystalline and can present its captured guests for SCXRD analysis in an inclusion complex. Therefore, optimisation of the synthetic conditions is crucial, to ensure crystals are not only of sufficient quality for SCXRD but that they remain so once guest encapsulation has been completed. A final and related requirement is that the solvent used in synthesis, and thus present in the pores, is sufficiently labile that upon immersion of the crystalline sponge in the guest liquid or solution it will readily be exchanged. Non-aromatic solvents such as cyclohexane or chloroform have proved optimal.

1.4.1.1 *Embodiment of Required Properties*

The linker used in Fujita's MOF is the large panel like tris(4-pyridyl)-1,3,5-triazine (TPT) (Figure 1.8), a well-established component used in container-compounds[44,45] and 3D networks.[46] TPT's high aromaticity and electron deficiency imparts an ability to form $\pi \cdots \pi$, CH$\cdots\pi$ and charge-transfer interactions with electron rich molecules. By incorporation into a MOF structure, these properties can be exploited and enhanced through the creation of 'sticky' hydrophobic pores. This property was reported in two MOFs specifically – $[\{(Co(NCS)_2)_3(TPT)_4 \cdot x(solvent)\}_n]$ and $[\{(ZnI_2)_3(TPT)_2 \cdot x(solvent)\}_n]$ (**1**).[1] As the Zn analogue has proven the

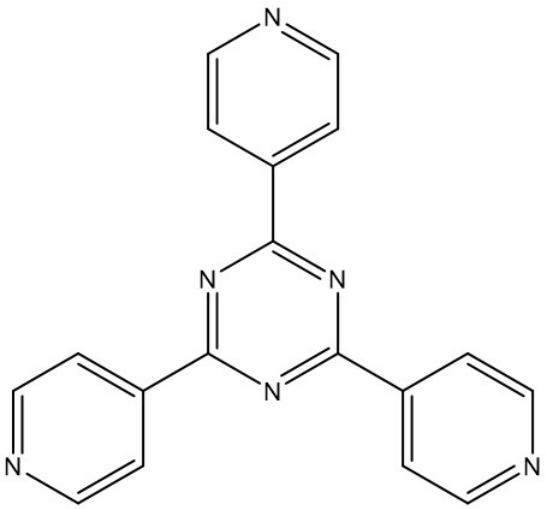

Figure 1.8: Tris(4-pyridyl)-1,3,5-triazine (TPT).

most successful in this application it alone will be considered from here onwards.

1.4.2 *Development of the Crystalline Sponge*

Large solvent molecules were first observed in the pores of a Zn-TPT based MOF in 2002[47] where benzene was ordered sufficiently to be refined isotropically once exchanged into the pores of the crystalline interpenetrating MOF with structure $[\{(ZnI_2)_3(TPT)_2 \cdot 6(C_6H_5NO_2)\}_n]$ (one of many known interpenetrated TPT networks).[46] In the same paper, the synthesis of the first non-interpenetrated TPT MOF was reported, obtained by the use of bromoform/methanol in place of nitrobenzene. Crystals of the complex $[\{(ZnI_2)_2(TPT)_2 \cdot 2(CHBr_3)\}_n]$ were obtained with disordered bromoform molecules occupying the channels (Figure 1.9). This non-interpenetrating structure is currently the most frequently and successfully used crystalline sponge, albeit with different solvent molecules occupying the pores. Subsequently in 2004, the inclusion of large guest molecules (triphenylene, anthracene and perylene) was reported, confirming that donor-acceptor interaction strongly control guest geometry.[48]

A similar biporous structure was published in 2005 by Fujita *et al.* The interpenetrating coordination network $[\{(ZnI_2)_3(TPT)_2(\text{triphenylene})].x(\text{nitrobenzene}).y(\text{methanol})\}_n]$ was shown to be capable of selectively taking up a series of guests from a mixture.[49] Its biporous nature arose from two distinct channels formed in the structure, shown in Figure 1.10. Molecules of triphenylene were encapsulated through co-crystallisation (see Figure 1.12b) by strong π-stacking with TPT molecules. As a result, they were trapped in the framework and could not undergo guest

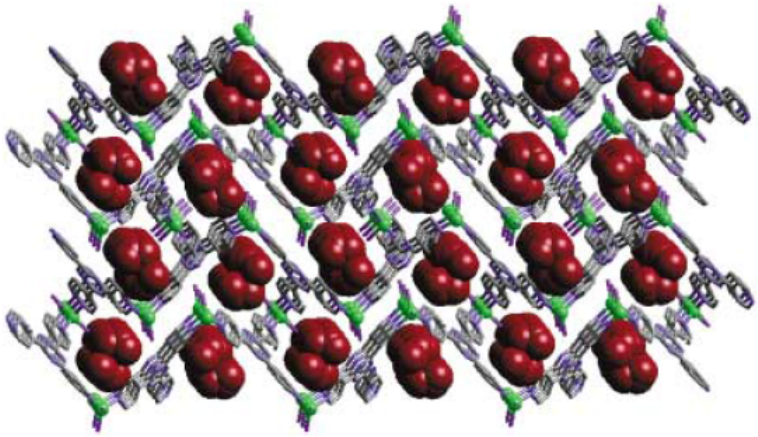

Figure 1.9: Illustration of the extended 3D network of $[\{(ZnI_2)_2(TPT)_2.2(CHBr_3)\}_n]$.[47]

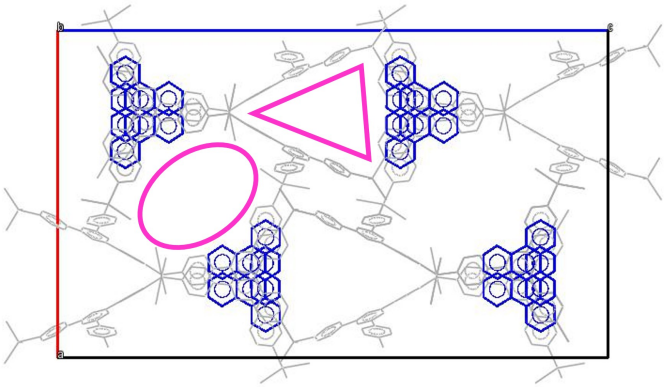

Figure 1.10: The biporous nature of the TPT based coordination network $\{[(ZnI_2)_3(TPT)_2(guest)]\cdot x(nitrobenzene).y(methanol)\}_z$ highlighted in pink. Structure generated from CCDC refcode XAPCOH.[49]

exchange. The π-stacking interactions were evidenced by UV/Vis spectroscopy as a broad charge-transfer absorption band in the 400–600 nm range. Guests such as naphthalene, nitrobenzene and cyclohexane where then shown to be separately included into the two channels. The main application reported was to enable the storage of otherwise incompatible compounds, for example, an acid/base pair.

The Zn-TPT MOF next reappeared in the literature in 2009, being used to observe a transient hemiaminal (see Section 1.6.2).[50] Latterly in 2010, the synthesis of the MOF was optimised, using a 4:1 nitrobenzene/methanol solvent mixture and subsequent solvent exchange to obtain $[\{(ZnI_2)_3(TPT)_2.x(cyclohexane)\}_n]$, the form used in Fujita's 2013 Nature paper. Here it was used to catalyse the *cis-trans* isomerization of the olefin retinal.[51] Again, the guest was visualised by SCXRD in the pores to a sufficient degree to confirm the presence of the *trans* isomer but not its *cis* partner.

1.4.3 *Mechanism of Guest Encapsulation*

With common MOFs and other porous networks, absorbed guests are rarely observed by SCXRD and in the few cases they are observed severe disorder abounds.[14,52,53] The adsorption of small molecules into MOFs is generally a kinetic process characterised by the rapid movement of guests (usually gases) into permanent vacuum pores. For example, [{$Mg_2(H_2O)_2$(2,5-dihydroxyterephthalic acid)•$x(H_2O)$}$_n$] (Mg-CPO-27) must be thermally dehydrated and kept under vacuum before it can be used as a methane storage material (Figure 1.11). By application of sufficient thermal energy chemisorbed water molecules octahedrally-coordinated to metal cations (yellow octahedra) are removed. The cation takes up a coordinatively unsaturated square pyramidal geometry resulting in the strong binding of absorbates such as CO_2. Conversely, the encapsulation of guests into the pores of the crystalline sponge **1** is a thermodynamic process where molecules are absorbed slowly by exchange with the solvent (similar to host-guest complexation in solution). This results in guests of equilibrated geometry and regular ordering. This is key. Guest molecules are then capable of creating Bragg peaks and contributing to a diffraction pattern amenable to crystallographic analysis.

There are three mechanisms by which guest molecules can obtain such order within a framework structure.[12] Detailed in Figure 1.12, these are (a) through guest exhange within the pre-assembled porous framework, (b) encapsulation at the point of framework assembly through co-crystallisation and (c) pre- or post-synthetic anchoring of the guest. The mechanism of guest encapsualtion by **1** is predominatly (a), making use of rapidly exchangeable inert solvents such as $CHCl_3$ or cyclohexane.

Encapsulation into **1** has also been achieved through mechanism (b) co-crystallisation. This was reported for a mechanistic study of Palladium-mediated aromatic bromination, through preparation of an organopalladium-embedded porous network,[55] and the observation of transient hemiaminal species (see Section 1.6.2).[50] However, this undermines the idea of a universally applicable technique as crystallisation conditions could vary for every new guest.

1.4.4 *Absolute Structural Determination*

Such is the ordering of molecules in **1** that absolute structural determination may be performed on chiral compounds. As a diffraction object enantiomeric pairs are indistinguishable. At any given direction of diffraction the phase difference of diffracted X-rays

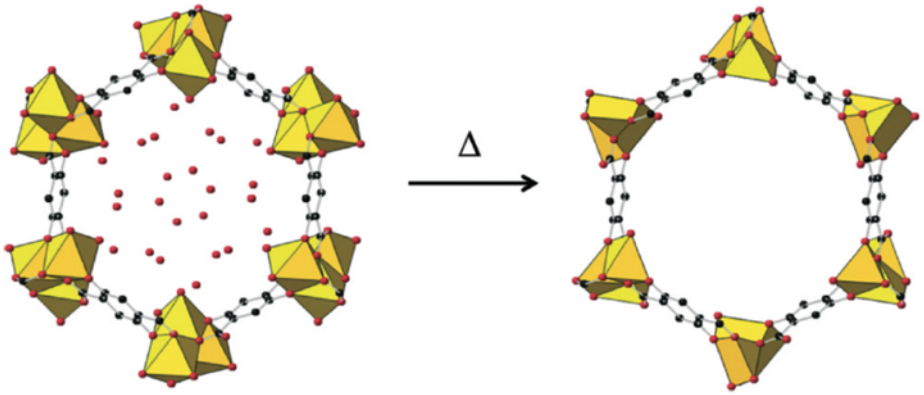

Figure 1.11: The dehydration of metal organic framework Mg-CPO-27 viewed down the *c* axis. Water molecules are chemisorbed to octahedrally coordinated metal ions in the hydrated form (left). Removal of water on the application of sufficient heat energy leaves the cation in coordinatively unsaturated square pyramidal geometry (right).[54]

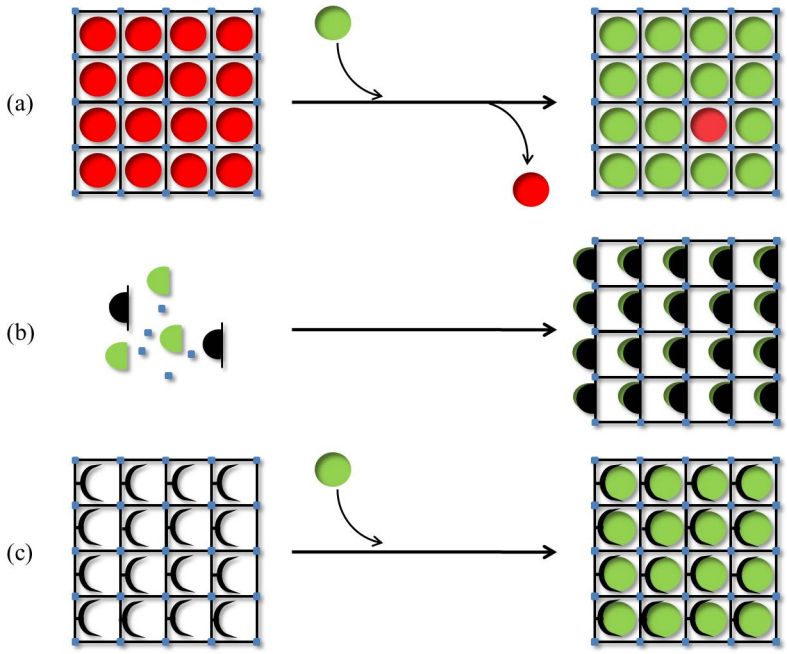

Figure 1.12: A schematic representation of the mechanism for guest encapsulation; (a) guest exchange (b) guest encapsulation by co-crystallization (c) pre- or post-synthetic anchoring of the guest at a non-structural position of the framework.

will be of equivalent magnitude (but opposite phase) whether taken from the front or back of a crystal plane, as stated by Friedel's law:[56]

$$|F_{hkl}| = |F_{\bar{h}\bar{k}\bar{l}}| \tag{1.1}$$

Where F is the amplitude of the reflections h, k, l and $\bar{h}, \bar{k}, \bar{l}$, which are Friedel pairs. Based on this it should be impossible to determine absolute structure by SCXRD. However, if the energy of the incident X-ray is close to the resonance frequency of an electron it will be scattered out of phase, affecting a small shift in amplitude and violating Friedel's law. In such cases, a noncentrosymmetric crystal may be distinguished from its inverted pair. This second-order effect is known as anomalous scattering and is observed for inner shell electrons of heavy atoms. After a series of studies, the technique was first applied to an organic molecule by J. M. Bijvoet in 1951 who assigned the absolute configuration of (+)-tartrate using its sodium rubidium salt.[57–59] The Flack parameter, is an alternative method also making use of resonance scattering and is measured directly from intensity data.[60,61] x is the molar fraction, defined as:

$$C = (1 - x)X + x\bar{X} \tag{1.2}$$

Where C is the crystal structure made up of two inversely orientated domains X and $\bar{X}$. A value of $x = 0$ implies the crystal contains none of its inverted form, compared to $x = 1$ where it is fully inverted, with fractions in between representing a range of inversion twining. Due to the presence of heavy elements (Zn and Iodine) in the crystalline sponge, the Bijvoet method can be used directly on inclusion complexes of **1**.

1.5 NOVELTY OF THE CRYSTALLINE SPONGE TECHNIQUE

The concept of guest encapsulation for crystallographic analysis is not wholly novel. Clathrates and container molecules are well-known crystalline materials containing void space into which guest molecules may be trapped and host-guest structures visualised by SCXRD. Whilst clathrates are extended structures with channels and pores, container compounds are macrocyclic units containing isolated cavities. In contrast to the crystalline sponge method, both are formed by the *in situ* crystallisation of host components and guest molecules together (by a similar mechanism to co-crystallisation in Figure 1.12). The following paragraphs detail some examples of their use to highlight the innovation of the crystalline sponge method and where its novelty lies.

1.5.1 *Clathrates and Container Molecules*

Clathrates are defined by the IUPAC as 'inclusion compounds in which the guest molecule is in a cage formed by the host molecule or by a lattice of host molecules'.[62] Their name comes from the Latin *clathratus* meaning 'to be enclosed by the cross bars of a grating'. Clathrates are guest-host complexes in which one component (the host) has an open structure containing cavities and channels which encapsulate compounds of comparable size (the guest) and allowing it to be structurally refined. Although MOF encapsulation compounds are a class of clathrates, here we make the distinction with clathrates formed through a complexation process of two (or more) components making use of multiple weak dispersive interactions to organise and maintain a stable porous molecular material. In this case, host components are large, rigid and highly symmetrical molecules that cannot pack efficiently in three dimensions. Therefore, they readily form inclusion compounds with smaller guest molecules to achieve efficient packing. Such structures can be analysed by SCXRD to reveal the structures of both components. A hugely versatile class of host material is porphyrins.[3,63–65] Examples of inclusion compounds with tetraarylporphyrin sponges are shown in Figure 1.13 providing a brief picture of the variety of guests that may be structurally assessed by this method.

Working on similar principles, container compounds have interior cavities suitable for hosting guest molecules. These may be close-surface voids where the guest is permanently incarcerated or contain molecular sized pore apertures such as in molecular flasks.[67] For example, hemicucurbiturils are macrocyclic host molecules that have electron-deficient cavities capable of encapsulating complementary sized anions. An example crystal structure is shown in Figure 1.14 with a (R)-cyclohexanohemicucurbit[8]uril unit encapsulating SbF_{6-}. The strength of complexation is governed by the size, shape and charge distribution of the anion.[66] Container molecules however accommodate only a limited range of guest molecules and, although container moelcules for organic non-charged guest are being developed,[68] guest ordering is not routinely sufficient for anisotropic guest refinement. Overall, due to the nature of the *in situ* crystallisation required, there can be no certainty or predictability of a host-guest system being formed. This points to the core driving force behind crystalline sponge development; enabling the routine analysis of non-crystalline materials by a reliable method.

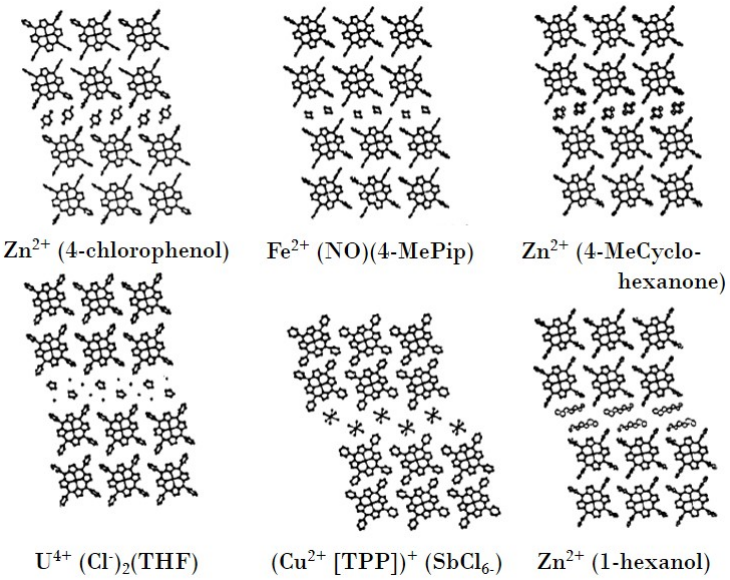

Figure 1.13: Crystal lattices of clathrates based on M-tetraarylporphyrins in which sheets of guests molecules are separated by double sheets of host molecules.[3]

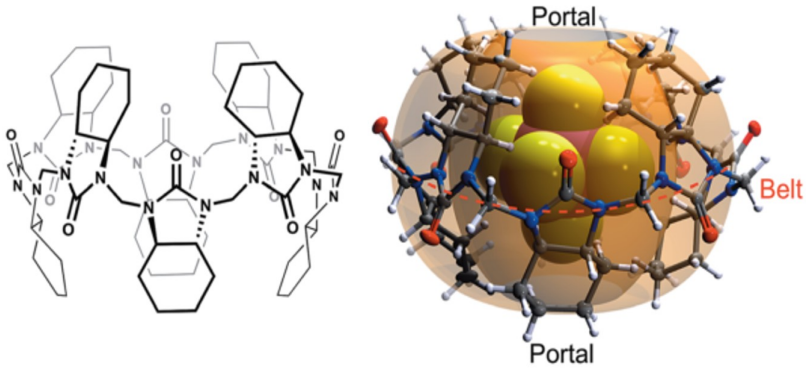

Figure 1.14: Moleculer and X-ray structures of a hemicucurbituril inclusion complex with SbF_6^-.[66]

1.6 APPLICATION OF THE TECHNIQUE

Since the initial publication of the crystalline sponge concept a steady stream of compounds have been observed in the pores of **1** and their structure determined. The attractions of the technique to researchers are manifold; predominately these are based on its ability to work with nano-gram quantities, provision of suitable reaction environment for mechanistic studies, and determination of absolute stereochemical information. These overlapping areas will be discussed in this section using extensive examples from the literature.

1.6.1 *Overview of Reported Inclusion Compounds*

The structures of a number of compounds exhibiting various types of chirality have been reported, increasing monthly. These include the (S) and (R) enantiomers of an axially chiral o-substituted biaryl and a macrocyclic bisbenzimidazole with planar chirality,[69] a tetrahydrobenzofuranone bearing a chiral tetrasubstituted stereogenic carbon center, along with simpler chiral molecules such as (1R)-(-)menthyl acetate.[70] The crystalline sponge method has also been exploited in mechanistic studies to probe reactive intermediates and to observed metal species.[71] With an overview of the structures so far analysed using this method (chiral and achiral) we can build an idea of the range of sizes and functional groups compatible with **1**. The functional group present on successfully encapsulated guests reported in the literature include: hydrocarbons (*e.g.* guaiazule); aldehydes and ketones (*e.g. trans*-anethole); shielded amines (*e.g.* 2,6-diisopropyl aniline); hydroxyl and ethers (*e.g.* 4-hydroxy-3-methoxy benzaldehyde); nitro groups (*e.g.* 1,4-nitrobenzaldehyde); and halides (*e.g.* 9-bromophenanthrene).

1.6.2 *Chemical Reactions and Mechanistic Studies*

Crystalline porous frameworks had been shown to provide an environment in which reactions may occur before development of the so-called crystalline sponge.[72,73] However, while time-resolved X-ray crystallographic studies had been performed to analyse reaction mechanisms and transformations, the analysis of unstable and non-isolable intermediates presented a particular challenge. The first example of work breaking this barrier dates to 2009 before the idea of the 'crystalline sponge method' had been presented and presents a transient hemiaminal species observed by SCXRD trapped in Zn-TPT MOF framework.[50] The mechanism of the reaction between an amine and an aldehyde forms the Schiff-base product *via* a rarely observed hemiaminal intermediate. The amine investigated

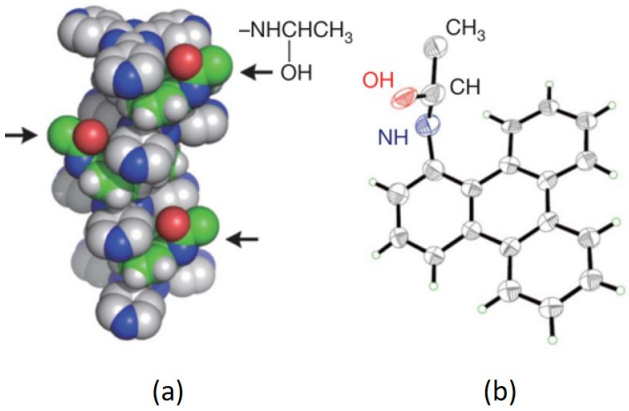

Figure 1.15: The direct observation of a hemiaminal intermediate in the crystalline sponge.[50]

was encapsulated into the porous framework by co-crystallisation and exposed to an aldehyde substrate by its diffusion into the pores. On reaction the trapped aromatic was converted to the hemiaminal which was kinetically trapped by a reaction temperature of 215K. Thus it was observable *in situ* by SCXRD, the structure of which is shown in Figure 1.15. This work illustrated the unobtrusive use of a porous framework to enable reaction monitoring, providing previously unknown mechanistic insight.

Subsequently, the reaction of Diels-alder substrates (a diene and dienophile) was performed in the pores of **1** with the aid of a radical initiator. Ikemoto *et al* reported enhanced selectivity to that observed in either solution phase or would be possible in diffusion driven guest encapsulation.[74] As in the hemiaminal study, the importance of strong guest-host $\pi \cdots \pi$ donor-acceptor interaction was highlighted. The flexible diene molecule was geometrically fixed within an alternating guest-linker column, exposing one double bond only for effective orbital overlap with incoming dienophiles. Thus a regio- and stereo-controlled transformation was promoted. A more recent example of an encapsulated chemical reaction used gas-phase reagents in solvent-free conditions. Knichal *et al* reported the iodine vapour-induced cyclisation of a diarenynyl and an oxidation reaction mediated by molecular oxygen.[75]

Latterly, time-dependent X-ray diffraction was used to visualise the palladium mediated bromination of an aromatic compound within the framework.[55] This impressive study resulted in the observation of a rare [Ar-Pd(Br)(CH_3CN)] species (of a type observed only once before by crystallisation) and its conversion to the final product (Figure 1.16). The crystallographic observation was confirmed by the appearance and/or disappearance of electron density associated with Pd-Br and C-Br bonds. The authors were careful to note that'

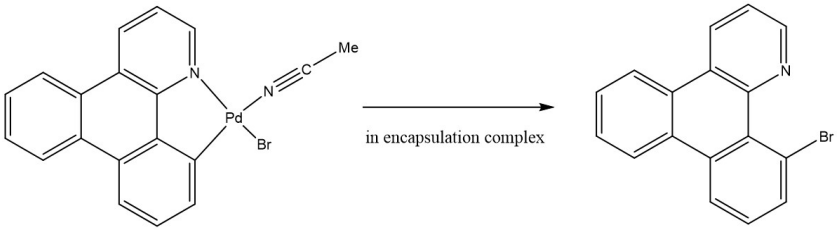

Figure 1.16: The palladium mediated bromination reaction performed in the crystalline sponge.[55]

these results are not necessarily conclusive...since the reaction pathway is more or less biased by a crystalline state' as 'the apical positions on the Pd atom in the crystal are blocked by the π-stacking ligand'. Nevertheless, it was a highly informative study and demonstrated the successful use of the crystalline sponge method for mechanistic studies.

The final and most recently reported study presented an *in situ* observation of a reversible Michael addition reaction between thiol nucleophiles and the drug cyanoenonesthiol.[76] The Michael adducts had only previously been observed spectroscopically in solution. Crystals of **1** where treated with the substrate in CH_2Cl_2, followed by mercaptoethanol. The authors describe the use of many different encapsulation conditions (reaction time, temperature, thiol reagent, and co-solvent) and the use of an X-ray scanner for high-throughput screening to select the highest quality crystals. The unstable thiol Michael adduct was successfully detected, giving strong support for the previously postulated mechanism.

1.6.3 *Nano-gram to Micro-gram Quantities*

In the original crystalline sponge paper, the ability of the technique to work with only very small, nano-gram to micro-gram quantities was stressed as a key advantage.[1] The authors theorised that to fully occupy the void space of one crystal ($\sim$ 0.1 mm^3, with $\sim$ 50% guest-accessible voids) required only 0.5 $\mu\mathrm{g}$ (at $1\,\mathrm{g\,cm}^{-1}$). This is likely to still be an over estimation as some solvent may remain in the void space after guest exchange, and the average occupancy of the guest molecules may be <100%. Indeed, a successful encapsulation experiment was performed using as little as 80 ng of guaiazulene for one single crystal of **1**. Working at such low guest concentration raises the possibility of very low site occupancy factors. It is therefore vital for the compound of interest to be high purity and, in order to avoid erroneous structure solutions by the encapsulation of impurities, the authors recommend the complimentary use of other methods such as NMR and mass spectrometry.

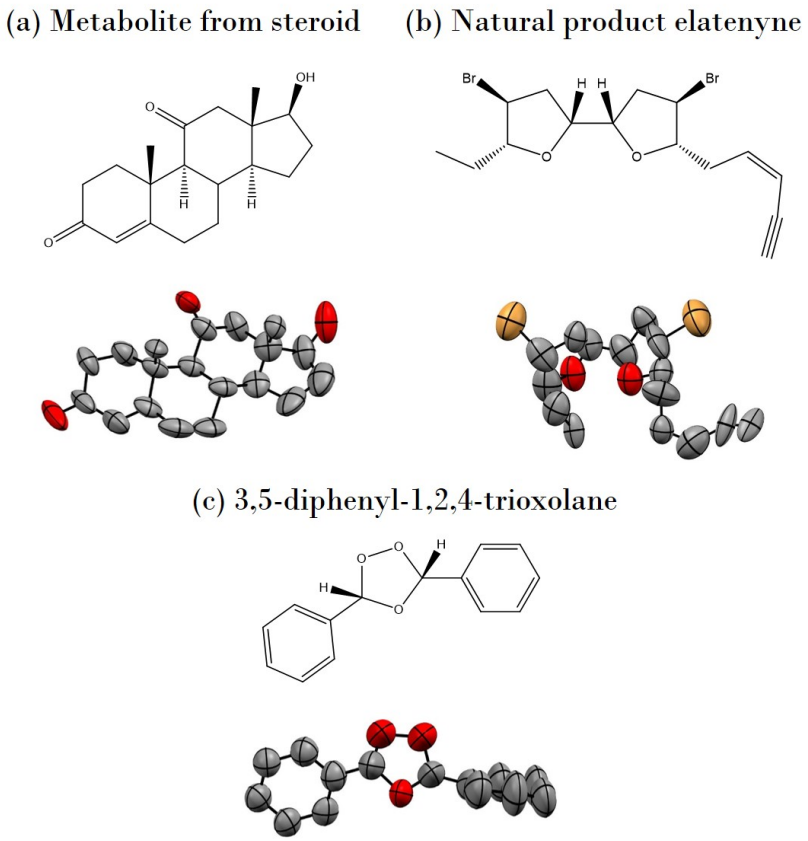

Figure 1.17: Examples of compounds encapsulated in **1** on the microgram scale: (a)metabolite from steroid[77] (b)marine natural product elatenyne[78] (c) 3,5-diphenyl-1,2,4-trioxolane.[79]

Since this publication, other systems have been analysed. For example, biosynthetically produced metabolites are obtained in low yield (on the microgram scale) with many unpredictable impurities making then difficult to fully characterise. A proof of applicability study for their analyis in the crystalline sponge was performed by Fujita *et al* on products of enzymatic reduction reaction by bakers yeast of 1,1-bis(4-chlorophenyl)-2,2,2-trichloroethane (DDT), tetralone and a metabolite from adrenosterone.[77] Extreme care was taken to remove all impurities and therefore the procedure was coupled with HPLC (and a strong recommendation of pre-purification by PTLC or LC-LC). This combination has proved useful in other studies.[1,69,80] This led to successful analysis of the metabolite at concentrations of $\sim 1\ \mu g \cdot \mu L^{-1}$, with excellent guest ordering as shown in Figure 1.17a. Similarly, Urban *et al* determined the absolute structure of the marine natural product elatenyne, an oily product (Figure 1.17b).[78] Experiments proceded with cyclohexane solution of elatenyne at a concentration of $1\ \mu g \cdot \mu L^{-1}$. Overall the experiments led to a successful structural characterisation, requiring approximately 100 μg of guest compound, of which 95 μg was recoverable.

In addition to being advantageous for scarce products, this technique can be used when it is simply not safe to handle higher quantities. Ozonides are a class of unstable, reactive compounds that are formed during ozonolysis - the conversion alkenes or alkynes into alcohols or aldehydes by ozone. They are highly explosive and their concentration must be carefully avoided. As a result routine crystallographic study of such compounds is restricted. However, with the requirement of only micrograms, Fujita *et al* were able to use ozonide solutions of <1 $\mu g \cdot \mu L^{-1}$ to determine the crystal structure (Figure 1.17c) whilst avoiding the risk of explosion.[79]

1.7 ASSOCIATED CHALLENGES AND SOME SOLUTIONS

Whilst the value of the crystalline sponge method has been clearly demonstrated, it cannot yet be seen as a universal solution to unambiguous structural determination of non-crystalline compounds. Currently, it is more a curious possibility. In order to develop the technique into something more universal its limitations must be identified and addressed. The challenges are primarily associated with (i) the structure of **1** and (ii) the procedure.

1.7.1 *Limitations of the Sponge*

The main limitation of the crystalline sponge method is the MOF – or, perhaps more accurately, our ability to synthesise MOF structures with properties suitable for the encapsulation of any intended guest molecule. The main limitations are:

(i) Pore size - the intrinsic requirement is that guest molecules are smaller than the pores. With the maximum cross-section of crystalline sponge 8 × 15 Å many potential guests are excluded.

(ii) Electronics - the pores are electron deficient and hydrophobic limiting the procedure to hydrophobic, electron rich guests. The quality of the diffraction data is highly dependent on the extent of guest ordering, relying on sufficient guest-host interactions (in quantity and/or strength) being formed.

1.7.2 *Process Limitations*

Other factors relating to the guest, such as purity and solubility, may also impede encapsulation. A significant aspect to the protocol for guest encapsulation is the lack of universal procedure. With each new compound of interest the researcher must optimise the experimental conditions such as the temperature and solvent. However, this is not uncommon, and is seen in other widely used techniques such as chromatography and can be over come with experience. Experience

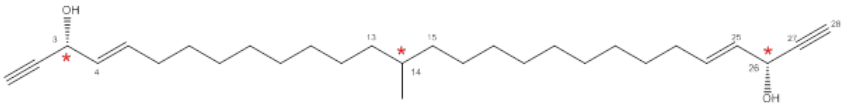

Figure 1.18: Miyakosyne A, the first molecule reported to have its stereochemistry unambiguously determined by the crystalline sponge method. Asymmetric carbons are labelled *.

is also vital for accurate crystallographic analysis, especially with the analysis of chiral compounds.

This warning was very clearly demonstrated with Fujita's original Nature paper. Perhaps its most intruiging claim made was that of absolute structural elucidation of the natural product miyakosyne A. This molecule contains three stereocentres shown in Figure 1.18. Two of which had known absolute configurations (C3 and C26 are 3R and 26R respectively) whilst the third, C14, was unknown. After a successful encapsulation experiment, analysis of the inclusion complex's crystal structure led Fujita *et al* to the report the stereochemistry as 14S. This conclusion was reached once it was found that the least-square refinement converged for this form alone. However, the authors were forced to rescind this assertion after 'previous unnoticed ambiguities in the crystallographic data' came to light, declaring ina corrigendum that the assignment was incorrect.[81] Although this does not affect the other conclusions of the paper, it is a pertinent reminder of the challenges associated with absolute structural determination.

Experience and time investment can overcome these associated challenges, but to produce an analytic technique as valuable and convenient as it is promising, alternative MOFs must be produced to overcome these limitations, with clear protocols to guide the non-specialist user.

1.7.3 *Development of the Technique*

> *'The growing interest in this strategy as a characterization tool coupled with the vast potential for designing new host frameworks of predetermined functionality and structure metrics means this area is poised for exciting new developments.' From 'X-ray Crystallography in Open-Framework Materials' by Doonan et al.*[12]

Although the original crystalline sponge **1** has proved exceedingly valuable there are limitations to its use. In order to expand the technique to allow the structural determination of potentially any compound their chemical diversity must be reflected by a range of alternative sponges. The following sections look at ways in which

$[\{(ZnI_2)_3(\text{tris(4-pyridyl)-1,3,5-triazine})_2].x(CHCl_3)\}_n]$ (**1**) may be edited to improve its performance.

1.7.3.1 *Varying the inorganic component*

Making just a subtle adjustment to the structure of **1**, Clardy *et al* synthesised bromide and chloride analogs of the zinc iodide crystalline sponge (Figure 1.19) to investigate the effect and possible benefits of lowering the electron count of the terminal ligand on the location and ordering of guest molecules.[82] The effects were assessed by analysis of the diffraction data from inclusion complexes with (1*R*)-(-)-menthyl acetate. All three as-prepared sponges exhibited a centrosymetric monoclinic *C*2/*c* spacegroup and refinement statistics of the three encapsulation compounds were broadly similar (see Table 1.2). However, the unit cell expansion of the iodide analog upon encapsulation yielded a challenging refinement scenario taking weeks to resolve to publication standard. Conversely, the Br and Cl analogues lacked major cell expansion and displayed a reduction in symmetry to $P2_1$. Structure solution in these cases took a matter of hours.

1.7.3.2 *Varying the Organic Component*

As of yet, alternative linkers to TPT have not be reported for using in reticular synthesis and thus presents a clear area for study.

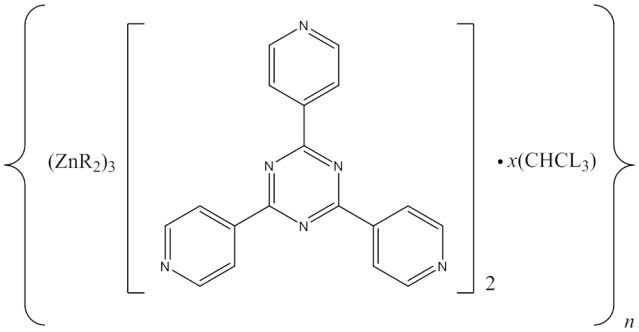

Figure 1.19: Zn-TPT based crystalline sponges synthesised from various zinc halides where R = Cl, Br, I.

Termainal ligand	R_1 / %	wR_2 / %
I	6.19	19.09
Br	7.10	22.98
Cl	8.47	27.30

Table 1.2: Refinement statistics by terminal ligand.[82]

1.8 ALTERNATIVE CRYSTALLINE SPONGES

In the years since Fujita *et al* first presented the idea of crystal-free crystallography, other groups have published alternative structures and reported encapsulations compounds of previously unobserved guest molecules. The main features of these structures, a comparison between them and the extent of their innovation is discussed in this section.

1.8.1 *Porous Organic Materials*

The use of a porous organic material (POM) assembled from a semiridgid macrocyclic tetraimine and EtOAc template was reported and offered as an alternative to **1**.[83] The crystalline sponge presented was the macrocyclic tetraimine shown in Figure 1.20. A range of guests were successfully encapsulated and characterised by SCXRD, including the determination of absolute configuration. They were *S*-(-)-nicotine, nitromethane, diethyl squarate, ethylene glycol, anisaldehyde, *cis*-stilbene, *p*-xylene and (*R*)-(+)-limonene. The strength of the cohesive interactions were evaluated using theoretical calculations showing the favourable energy change on guest encapsulation.

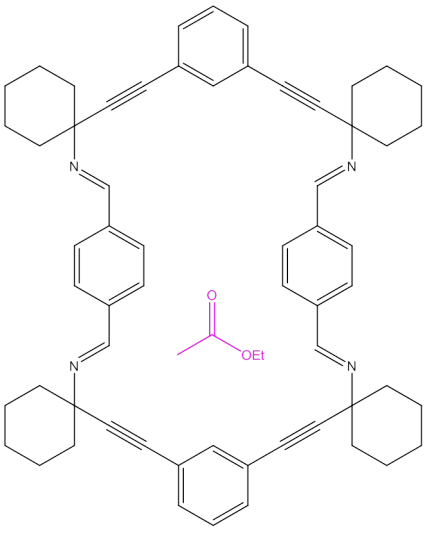

Figure 1.20: The macrocyclic tetraimine used as a crystalline molecular sponge for structural analysis of a variety of guests by SCXRD. Its one dimensional rectangular micropores (12 × 9 Å) allow for the encapsulation of a variety of small guest molecules.

1.8.2 *Chiral Metal-Organic Material*

A pair of entiomeric chiral metal-organic frameworks were synthesised by Zaworotko *et al* based upon [$Co(NO_3)_2.6H_2O$]z with mandelate (man) and 4,4'-pyridyl (bipy) linkers.[84] The enantiomeric 1-dimensional structures, [{Co_2(*S*-man)$_2$(bipy)$_3$}$(NO_3)_2$•guest] and [{Co_2(*R*-man)$_2$(bipy)$_3$}$(NO_3)_2$•guest], contain chiral channels of dimensions 8.0 Å x 8.0 Å lined by nitrate anions and phenyl groups. It was found that the nature of the guest solvent molecules (referred to as *cofactors* by the authors) affected the availability of chiral binding sites and thus selectivity. This suggests a potential application to chiral separation. The guests encapsulated were 1-phenyl-1-propanol, nitrobenzene, dichloromethane and cyclohexane. The authors investigated the interactions between guests and the host framework at specific binding sites. For example, guest molecules of (*S*)-1-phenyl-1-propanol were selectively taken up by the *S* form of the frameworks, taking up three crystallographically independent sites anchored by hydrogen bonds and aromatic interactions.

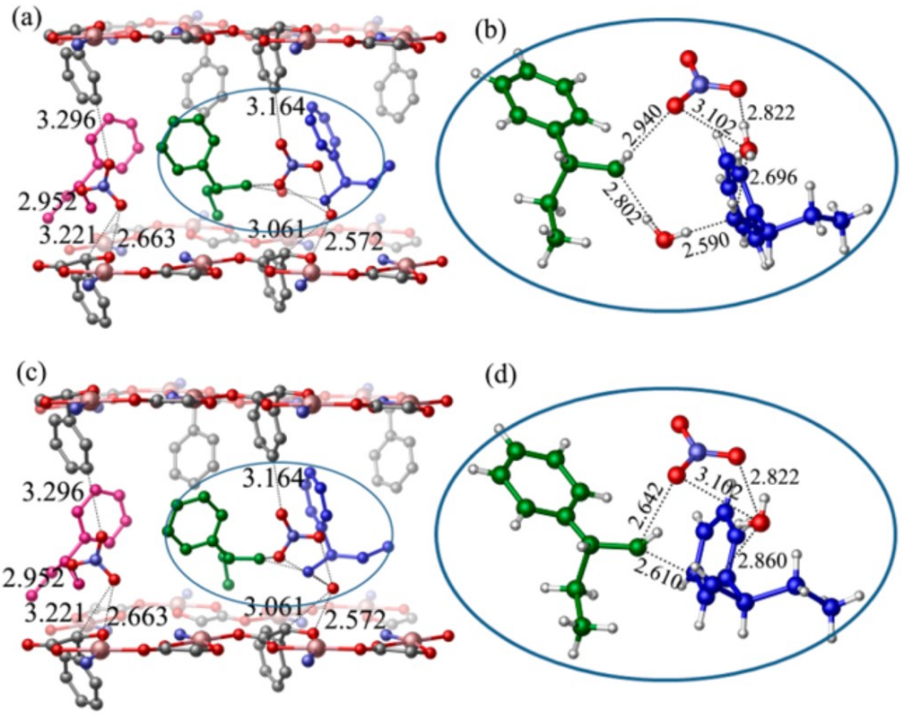

Figure 1.21: Views of the chiral [Co_2(*S*-man)$_2$(bpy)$_3$]$(NO_3)_2$•((*S*)-1 -phenyl-1-propanol), showing two positions of the guest.[84]

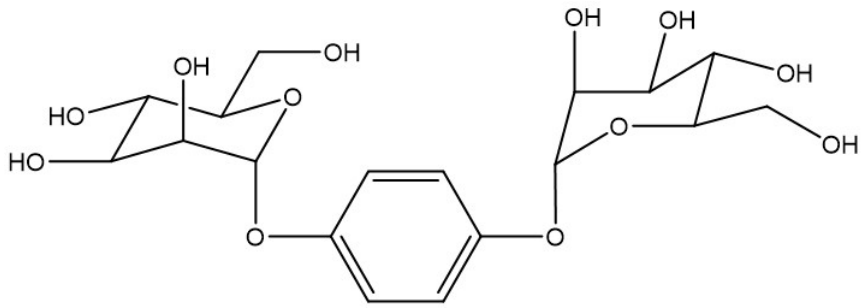

Figure 1.22: D-mannose-based sugar building block displaying both hydrophilic (D-mannose) and hydrophobic (phenylene) components.

1.8.3 *Saccharide-Based Crystalline Sponge*

Fujita *et al* reported a saccharide-based crystalline sponge (sugar sponge) constructed using a D-mannose-based ligand and sodium ions.[85] The saccharide building block shown in Figure 1.22 displays both hydrophilic and hydrophobic components, which it imparts on the chemical make up of the extended structure. In contrast to crystalline sponges with hydrophobic pores (e.g **1**) where weak intermolecular interactions and a low temperature of the diffraction experiment are responsible for the ordering of guest molecules in the host, the hydrophilic pores relied on rather stronger multiple hydrogen-bonding dipole-dipole interactions. It was utilised to analyse the structures of flexible alcohols and the absolute configurations of chiral epoxides.

1.8.4 *The Coordinative Alignment Method*

1.8.4.1 *MOF-520*

In 2016 Yaghi *et al* published work on a new strategy for the inclusion of guest molecules.[86] The well established MOF-520 ($[Al_8(OH)_8(BTB)_4(HCO_2)_4]$) was used to coordinatively bind guest molecules of varying size, complexity and functionality by the formation of covalent bonds to metal sites within its large octohedral pores. MOF-520 was chosen for its high crystallinity, robustness and chirality. The strucutre of the two MOF-520 enantiomporphs are shown in Figure 1.23, with chirality arising from the linker 1,3,5-tris(carboxylphenyl)benzene (BTB).[87] The chiral backbone of MOF-520 acted as a reference for the absolute structural determination of guest molecules, negating the need for heavy elements and avoids the pseudo-symmetry problems encountered in the use of some other crystalline sponges.[69,83] However, although each single crystal was enantiomorphically pure (Flack parameters

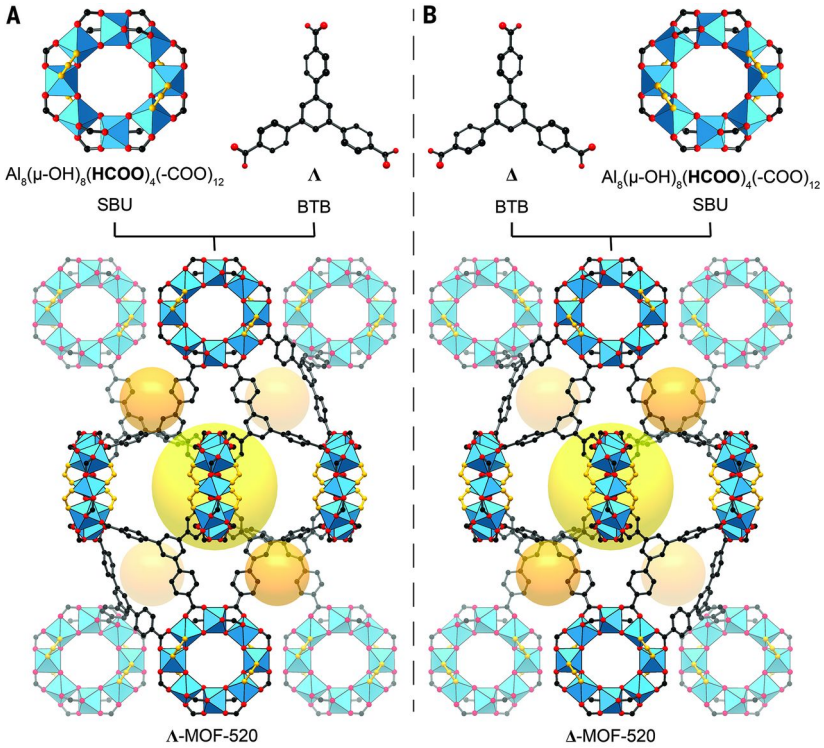

Figure 1.23: Structures of MOF-520 enantiomorphs ($\wedge$ and $\triangle$) and their building units comprising $Al_8(m\text{-}OH)_8(HCOO)_4(\text{-}COO)_{12}$, and 1,3,5-benzenetribenzoate linker. The yellow and orange spheres represent the two distinct pores. Colour code: black, C; red, O; blue polyhedra, Al.[86]

-0.049(17) for L and 0.031(11) for D) the overall bulk sample was a racemic mixture containing both enantiomorphs.

Referring to their procedure as the 'coordinative alignment (CAL) method', the authors successfully encapsulated 16 unique guests representing four common functional groups: primary alcohol, phenol, vicinal diol, and carboxylic acid. Guest molecules were covalently bonded to the MOF by immersing single crystals in a concentrated solution of the specific guest and heating (40 °C to 100 °C) for at least 12 hours. Guest structures determined included two forms of the plant hormone gibberellins and (±)-jasmonic acid (Figure 1.24), the enantiomers of which were separated by preferential binding to chiral sites of the MOF enantiomorphs.

1.8.4.2 *Flexible Zirconium MOF*

The coordinative alignment method has since been applied using a different species - the MOF PCN-700, formed by the coordination of $[Zr_6O_4(OH)_8(H_2O)_4]$ clusters with 2,2'-dimethylbiphenyl-4,4'-dicarboxylate linkers.[42] As a crystalline sponge PCN-700 is useful. It displays inherent flexibility thanks to

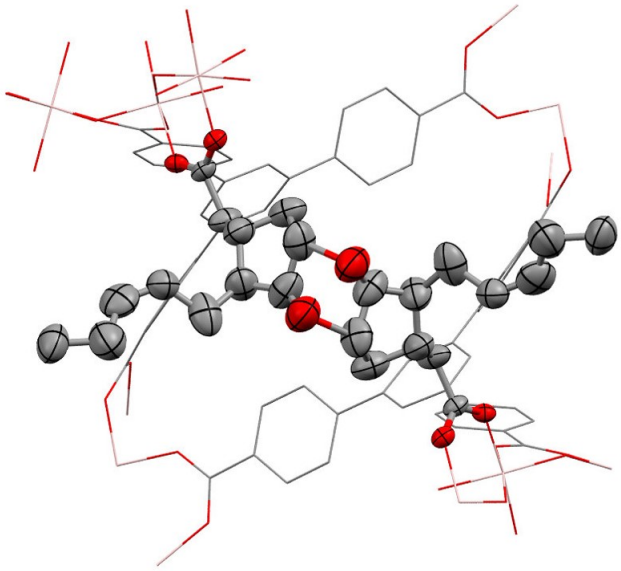

Figure 1.24: The structure of two jasmonic acid molecules (ellipsoids) coordinately alligned in the pore of MOF-520 (wireframe). Image produced using CCDC data.[86]

rotation of the biphenyl rings and -OH^-/H_2O ligands on Zr can be exchanged *via* acid-base reaction. These properties were identified and exploited by Zhou *et al* to encapsulate a family of organic dicarboxylate compounds, shown in Figure 1.25.[88] The dicarboxylate guests were identified crystallgraphically in the pores, bringing about a single-crystal to single-crystal transformation. The flexible PCN-700 framework was seen to 'breath' with the unit cell expanding roughly in line with the increasing length of the guest across the series. To demonstrate this the unit cell parameters of some of the encapsulation complexes are listed in Table 1.3.

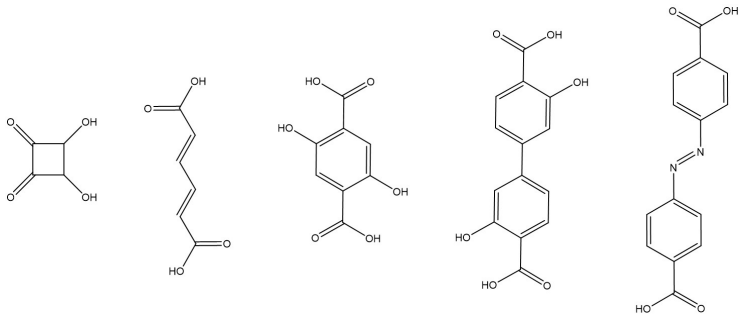

Figure 1.25: Some of the linear organic dicarboxylates encapsulated by PCN-700.

Guest	a/Å	c/Å	V/Å^3	Guest length/Å
None	24.35	14.92	8844	-
H2SA	23.87	15.89	9060	3.22
BDC	24.40	14.88	8861	7.00
MA	34.33	14.71	17327	7.44
DOBPDC	23.61	17.41	9549	11.35
AZDC	34.15	14.66	17096	13.25

Table 1.3: Breathing behaviour of PCN-700 upon encapsulation of some guest molecules, all of which crystallise in the tetragonal space group $P4_2/mmc$.[88]

1.8.5 *Comparison of crystalline sponges*

The publication of these alternative crystalline sponges has led to a broader opportunity to investigate non-crystalline compounds *via* the crystalline sponge method. Table 1.4 summarised the nature of the guest species successfully encapsulated by each of the sponges. The largest expansion in scope of the technique arises from the so-called sugar sponge allowing the investigation of hydrophilic guests, although no further studies have yet been published. Two major limitations that remain surround the encapsulation of amines and the encapsulation of larger guest molecules.

Structure	Guests
Zn-TPT MOF	hydrophobic guests, no amines
POM	aromatic and non-aromatic, nicotine
Chiral MOF	chiral aromatic and non-aromatic
Sugar sponge	hydrophillic
MOF-520 (CAL method)	alcohols, carboxylic acid
Zn-MOF (CAL)	dicarboxylates

Table 1.4: Comparison of known compatible guest species with each crystalline sponge.

1.9 NON-COVALENT INTERACTIONS

Weak non-covalent interactions formed between the host framework **1** and its guests are integral to the crystalline sponge technique as their formation render compatible guests regularly ordered. The most important of these will be discussed briefly here.

1.9.1 *van der Waals Interactions*

IUPAC definition: '*The attractive or repulsive forces between molecular entities (or between groups within the same molecular entity) other than those due to bond formation or to the electrostatic interaction of ions or of ionic groups with one another or with neutral molecules. The term includes: dipole–dipole, dipole-induced dipole and London (instantaneous induced dipole-induced dipole) forces. The term is sometimes used loosely for the totality of nonspecific attractive or repulsive intermolecular forces.*'[89]

Van der Waals interactions are the weakest of intermolecular forces (see Table 1.5) but when summed over many atom pairs at short distances ($\sim$3 - 6 Å) the effect can be substantial.[91,92] This can be easily comprehended by considering a gecko and his toes. Autumn *et al* investigated the mechanism of dry adhesion in the millions of setae in gecko toes, long since an area of scientific intrigue.[93] They tested the affinity of a gecko's toes for polar silicon dioxide and to apolar gallium arsenide (Figure 1.26). The lizard's hydrophobic toes were found to adhered to both surfaces, demonstrating the action of van der Waals forces - rather than mechanisms relying on high surface polarity such as capillary adhesion.

1.9.2 *Hydrogen Bonding*

IUPAC definition: '*An attractive interaction between a hydrogen atom from a molecule or a molecular fragment X–H in which X is more electronegative than H, and an atom or a group of atoms in the same or a different molecule, in which there is evidence of bond*

Force	Strength /kJ mol^{-1}	Distance /Å
van der Waals	0.4 - 4.0	3.0 - 6.0
Hydrogen Bonds	12 - 30	1.5 - 3.5
Hydrophobic interacions	$<$40	varies

Table 1.5: Strengths of weak intermolecular interactions.

	H						
H	2.40	C					
C	2.90	3.40	N				
N	2.75	3.25	3.10	O			
O	2.72	3.22	3.07	3.04	F		
F	2.67	3.17	3.02	2.99	2.94	Cl	
Cl	2.95	3.45	3.30	3.27	3.22	3.50	I
I	3.28	3.68	3.53	3.50	3.45	3.73	3.96

Table 1.6: van der Waals radii of common elements: $r(H)$, 1.20 Å; $r(C)$, 1.70 Å; $r(N)$, 1.55 Å; $r(O)$, 1.52 Å; $r(F)$, 1.47 Å; $r(Cl)$, 1.75 Å; $r(I)$, 1.98 Å.[90]

Figure 1.26: Tokay gecko (Gekko gecko) strongly adhering to the molecularly smooth hydrophobic surface of GaAs.[93]

formation.'[94]

In the literature, the presence of hydrogen bonds is generally noted as short contacts less than or equal to the sum of the van der Waals radii of the interacting atoms (see Table 1.6),[95] although this is debated.[96] Some will split the hydrogen bond into three classes; very strong (*e.g.* F-H-F), strong (O-H···O) or weak (C-H···O) according to the length of interaction (at 100%, ~100% and 30-80% the sum of van der Waals radii respectively). The latter especially has been the subject of intense scrutiny over recent years, although plenty of examples can be found in the literature.[97]

An example particularly relevant to this report is organic fluorine as its ability to form hydrogen bonds varies distinctly from what might be empirically expected. Linus Pauling wrote:

> *'It is interesting that in general fluorine atoms attached to carbon do not have significant power to act as proton acceptors in the formation of hydrogen bonds in the way*

> *that would be anticipated from the large difference in electronegativity of fluorine and carbon.'*[98]

This can be attributed to a combination of two factors (although these themselves are not fully understood):[99] (i) low proton affinity and (ii) an inabilty to overcome this by electron delocalization.[100] Still, however weak the interaction there is a great deal of evidence for the occurrence of F···H bonds.[101–104] However, due consideration must be given to the environment. For example, C-F is unable to compete with an O- or N- atom acceptor when the latter are present.[100]

1.9.3 *Aromatic Interactions*

Aromatic interactions play an important role in a broad range of intermolecular complexes and have been proposed to consist of van der Waals, hydrophobic and electrostatic forces.[105] TPT has a highly electron deficient and hydrophobic π-plane thought to be particularly important in the strong interaction with guest molecules (<40 kJ mol^{-1}, see Table 1.5). The required geometry of interacting rings is not clear and depends on the nature of those involved. However, they can be generally described as parallel face-centred, offset face-centred, perpendicular t-shaped and perpendicular y-shaped (Figure 1.27). The question of whether there is 'any unique attraction between aromatic pi systems that favours stacking and transends the suite of [interactions]...that influences the association of *all* molecules'[106] is much debated in the literature.[107–110] Unfortunately, this requires more discussion than is possible here. Therefore, it will simply be noted that the analysis of these types of interaction will be approached with caution.

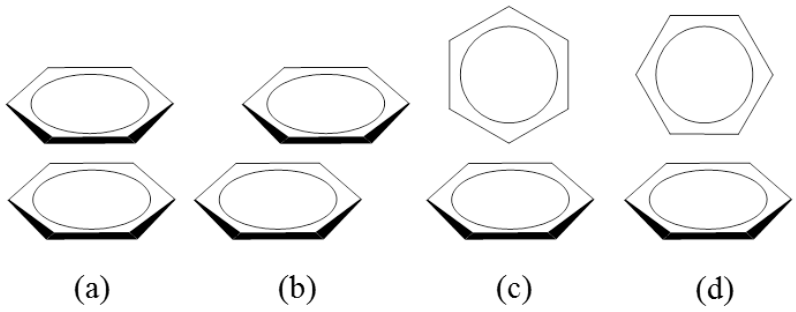

Figure 1.27: Aromatic stacking arrangements based on the electrostatic contribution to the interaction. Parallel (a) face-centred and (b) offset, perpendicular (c) t-shaped and (d) y-shaped.

2

RESEARCH QUESTION AND HYPOTHESIS

In order to expand the application of the crytalline sponge technique, a range of metal-organic frameworks (MOFs) are required to allow for the study of a diverse range of natural products and biologically active molecules, of varying size and functionality. Achieving a greater understanding of guest-host interactions will aid in the judicious selection of inorganic and organic moieties potentially allowing MOF hybrid architecture to be tailored to fulfil the demands of specific guest encapsulation. This has the potential to expand the technique to allow encapsulation of hydrophilic guests of varying steric requirements.

The first aim of this project is to optimise the crystalline sponge method to allow for the structural assignment of a range of non-crystalline compounds, to potentially allow for conformational analysis of protein structures in the future. In the shorter term the investigation will focus on the use of crystalline MOF $[\{(ZnI_2)_3(TPT)_2.x(solvent)\}_n]$ (**1**) as the crystalline sponge by replication of protocol reported in the literature. The aim is to incorporate a range of guest compounds (e.g. of varying chirality, functionality and molecular weight and shape) to obtain novel inclusion complexes and determine the method's robustness and versatility. On the way to achieving this aim, crystallographic studies detailing the uptake and specific locations of systematic series of chemically related simple functionalised aromatic guest molecules within the crystalline sponge, together with analysis of possible guest-host interactions will also be attempted. As no systematic study has been reported in the literature the aim is to develop the understanding of the currently used crystalline sponge and why it displays such unique properties.

A second aim is to synthesise alternative MOF structures with variable pore sizes and chemical properties suitable for use as crystalline sponges to extend the technique beyond aromatic, hydrophobic guests. Alternative linkers are needed to allow this, and those with similar functionality to TPT will be investigated primarily, focusing on varying pore size to develop a reticular series of crystalline sponges.

Part II

EXPERIMENTAL CHAPTERS

3

SYNTHESIS OF THE CRYSTALLINE SPONGE

3.1 AIMS

Experiments in this chapter have two main aims. Firstly, they seek to assess the reproducibility of the two literature synthetic protocols for the production of $[\{(ZnI_2)_3(TPT)_2.x(solvent)\}_n]$ (**1**) as high quality single crystals in a form that would be ready for guest encapsulation and amenable to single-crystal X-ray diffraction (SCXRD) studies. Experiments seek to determine and overcome any potential problems with implementation. A second aim is the comparison of the two methods' respective advantages and disadvantages, focusing on practicability, reliability, crystal quality and yield.

3.2 INTRODUCTION

The highly porous MOF $[\{(ZnI_2)_3(TPT)_2.x(solvent)\}_n]$ (**1**) has been developed as a so called 'crystalline sponge' for the encapsulation of guest molecules (Section 1.4.2). Through the formation of strong guest-host interactions, guest molecules may be rendered regularly ordered and thus amenable to SCXRD. This may overcome the inherent limitation of SCXRD - the requirement that the compound of interest be obtained in single-crystalline form. Still though to be of use the crystalline sponge **1** must itself be obtained reproducibly as a high quality single crystals, from the point of synthesis, surviving its encapsulation experiments, through to mounting on the diffractometer, and full data collection. The quality of a crystal is determined by three key factors; its diffraction power (it must be well-diffracting), minimal thermal movement and full occupancy of all the atoms with no disorder (of the host and any residual solvent molecules).

3.2.1 *Interfacial Synthesis*

MOF formation is a self-assembly process involving the reaction of a metal salt (commonly acetates, nitrates or sulphates) with the chosen organic linker. Solvothermal synthesis is most common, often making use of autoclaves to create a high pressure closed system using temperatures above the solvent boiling point. Such procedures have the attraction of favouring the condensation of M-OH bonds to M-O-M bonds.[111] Increasingly, room temperature

synthesises are being developed as lower energy alternative for scale up.[112] A lesser used laboratory method, but of particular relevance here, is interfacial synthesis where partially miscible reagent solutions are layered and react at the interface (Figure 3.1). By varying the solvent systems and reagent concentrations the rate of diffusion between layers can be controlled allowing for the growth of high quality single crystals.

Interfacial synthesis makes use of the slow diffusion of reagents across the interface between two miscible or immiscible solvents. The reaction of two or more reagents at the liquid-liquid interface may result in the nucleation and growth of a crystal lattice, commonly on the surface of the reaction vessel, as shown in Figure 3.1. The nucleation sites may be scratches or defects in the glass, or dust particles acting as seeds. An important growth condition for the formation of high quality single crystals is extended growth time at the liquid-liquid interface. To allow molecule by molecule addition to the crystal surface the continued precipitation of a solid phase must occur at conditions close to thermodynamic equilibrium *i.e.* the slower the introduction of building blocks the slower the rate of crystallisation. Therefore, the reaction of reagents from low concentration solutions by diffusion across a concentration gradient is a prime method for the production of high quality single-crystals for structural characterisation. This is especially useful for the synthesis of MOFs, which, by the insolubility of their infinitely extending structures assembly must be performed in a single step as recrystallisation is not possible. Many crystalline MOFs have been synthesised this way.[19,113–115] This technique has been used to obtain single crystals for structural characterisation and is thus hugely applicable to crystalline sponge synthesis.[116,117] The advantages of the interfacial method include being able to use metals with low reduction potentials (e.g. Cu^{2+}), and solvents unstable under commonly use solvothermal conditions. Furthermore, inorganic and organic precursors often have markedly different solubility leading to the widespread use of non-aqueous solvents and solvent mixtures to produce single phase MOF crystals.

3.2.2 *Published synthetic procedures*

In the original Naure paper presenting the crystalline sponge technqie Fujita *et al* used an interfacial synthesis based on nitrobenzene/methanol solvent combination for the dissolution of TPT, from here refered to as 'method **A**'.[1] (Although this paper did not report fully the synthetic procedure and it has since been updated twice).[80,118] This solvent combination was reported to reliably produce suitable single crystals of **1** with nitrobenzene in

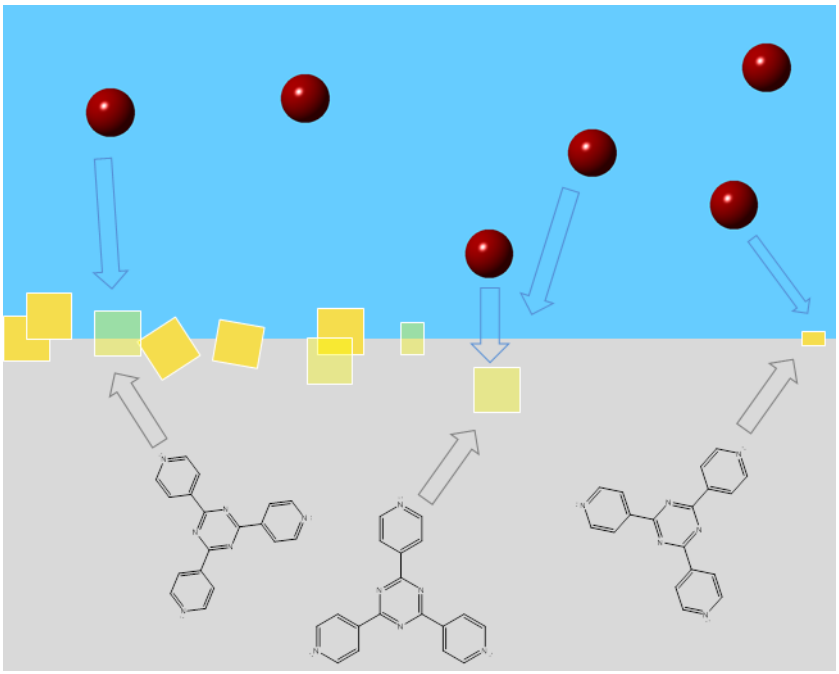

Figure 3.1: Interfacial synthesis of **1** crystals (yellow) from a methanol solution of ZnI_2 (blue) and a solution of the linker (grey). Adapted from literature.[113]

the pores (referred to as **1(**$C_6H_5NO_2$**)**). These electron rich molecules interact strongly with the electron poor TPT linkers making up the framework and would inhibit guest exchange. Therefore prior to guest encapsulation experiments the crystalline sponge was washed thoroughly with cyclohexane, an inert solvent, to obtain a structure referred to as **1(**C_6H_{12}**)**. Latterly an alternative practical guideline was published by Clardy *et al*, making use of the solubilty of TPT in chloroform to negate the need for nitrobenzene and thus eliminate the solvent exchange step, refered to here as 'method **B**'.[119] Both procedures are still in use, although the majority of papers published in the area follow Fujita's method.

More recently a procedure based not on interfacial synthesis but slow evaporation was published. The authors used microwell droplets to produce $\geqslant$90% yield of suitable crystalline sponge crystals. As it was published after the completion of this study it was not investigated here.[120]

3.2.3 *Crystalline phases*

Crystal formation is a far from simple process and great effort has been expended in attempts to understand it from practical and computational perspectives. Crystal nucleation and growth are distinct processes and a variety of factors can influence each.

In the last two decades interest in crystallisation technique that can be tailored to produce desired crystalline structures has surged.[121,122] This had led to a large increase in understanding as to appropriate design, preparation and characterisation of the material of interest and its specific crystal growth requirements. Whilst a great deal of time and effort is invested in determining the most reliable experimental procedure for the production of a particular compounds as high quality single-crystals (hence the work in the majority of this chapter), new crystal forms can emerge unexpectedly. These may be in the form of solvates, polymorphs and hydrates, as well as amorphous materials. This is not always a negative occurance, indeed fortuitous discovery of new and useful crystal structures have occured this way.[123] However, the unexpected production of crystalline forms of undesirable properties can be an inconvenience and, in extreme cases, result in the serious distruption of product development.[124,125] Current understanding of the process of crystallisation is limited meaning the cause of such phenomena is little known. Furthermore, methods to manipulate the mechanism of nucleation and crystal growth are often insufficient and too poorly understood to prevent such problems from arising, or dealing with them once they do.

3.3 RESULTS

3.3.1 *Synthesis of the Crystalline Sponge*

3.3.1.1 *Implementation of the technique*

Initial experiments focused on the original nitrobenzene based synthetic protocol, method **A**. Poor results demonstrated the importance of carefully layering the two reactant solution to ensure the formation of a clean interface. Insufficient care or an unsteady hand was seen to resulted in the formation of fluffy, unusable solid (Figure 3.2). This indicated that although the synthetic procedure is in principle quite simple it is a delicate process, both in initial synthesis and in the subsequent careful handling required to maintain the integrity of the obtained single crystals.

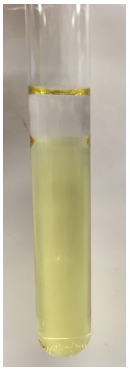

Figure 3.2: The formation of clean interface between solvent layers gives rise to quality crystals of **1($C_6H_5NO_2$)**.

After some practice and by the use of an Eppendorf pipette for solvent layering, suitable single crystals of **1($C_6H_5NO_2$)** were obtained from method **A** and soon after **1($CHCl_3$)** from method **B**. The identity of the crystals were confirmed by the determination of the unit cell parameters on the single-crystal diffractometer. All cell parameters matched those reported in the literature confirming structures of $[\{(ZnI_2)_3(TPT)_2.x(solvent)\}_n]$ had been successfully formed. The unit cell parameters are reported in Table 3.2 showing only small differences as a results of varying solvent in the pores.

3.3.1.2 *Single-crystals of* ***1***

Crystals of **1** can be roughly classified according to morphology. The first are rod shaped and around 50 - 250 μm in length, indicated by the green arrow in Figure 3.3. These are most desirable being the most resilient to harvesting, having the highest integrity and lowest incidence of cracking or intergrowth. The second morphology, indicated by the orange arrow, are plates frequently cracked and

	1($C_6H_5NO_2$)	1($CHCl_3$)
Crystal system	Monoclinic	Monoclinic
Space group	C2/c	C2/c
a/Å	35.860(14)	35.2913(7)
b/Å	14.866(5)	14.7032(2)
c/Å	31.241(3)	31.2290(6)
α/°	90	90
β/°	102.85(5)	101.5328(18)
γ/°	90	90
volume	16239(18)	15877.4(5)

Table 3.1: Experimental unit cell parameters.

often twinned. Like the rod shaped crystals these present the expected unit cell parameters for **1** but are poorly diffracting and unusable for full data collection. The third morphology identified are clusters of microcrystals, which are too small for SCXRD analysis (red arrow).

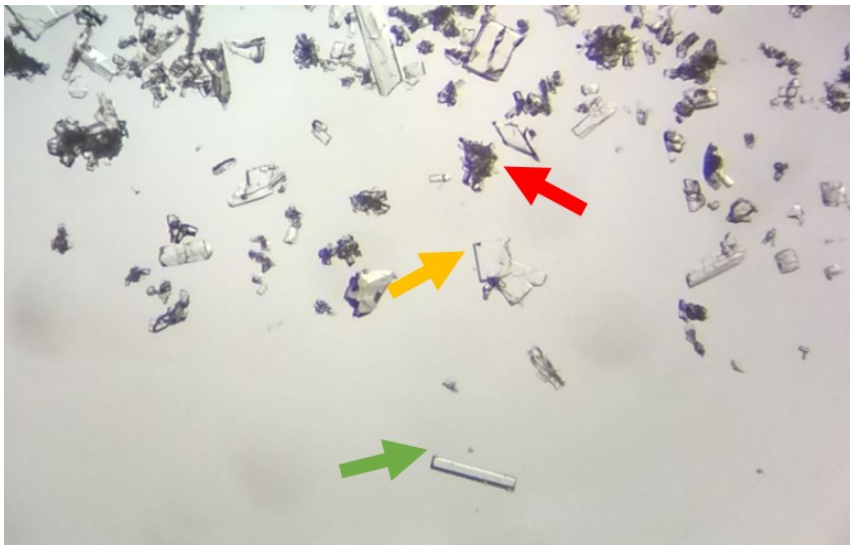

Figure 3.3: Micrograph image of one of the first batches of **1** by method **A**. The desired rods (green), damaged blocks (orange) and microcrystals (red) products are highlighted by arrows.

3.3.1.3 *Solvent Exchange*

As synthesised crystals from method **A** contain the solvent nitrobenzene in the pores. Due to its strong interaction with the framework of **1** nitrobenzene must be exchanged for another solvent before guest encapsulation experiments can proceed. Crystals of

1($C_6H_5NO_2$) were incubated at 45°C washed with cyclohexane every day until full exchange had taken place. The progress of exchange was monitored by IR spectroscopy, as recommended in the literature.[1] The FTIR spectrum of as synthesised crystals of **1($C_6H_5NO_2$)** is shown in Figure 3.4. Two strong absorption bands at 1344 cm^{-1} and 1517 cm^{-1} are characteristic of an N-O stretching. Other peaks annotated relate to C-H stretching (2845 - 3000 cm^{-1}). After 6 cycles of washing with cyclohexane (over a total of 8 days) the total exchange of nitrobenzene from the pores was confirmed by IR analysis with the disappearance of peaks at 1344 cm^{-1} and 1517 cm^{-1} (Figure 3.5). This was a similar time scale to that reported in the literature however, subsequent repetition of the procedure 3 times showed variation between batches taking between 5 - 10 days to complete the exchange. Unfortunately, the success of the solvent exchange came at the price of the crystals' integrity, which was gradually lost over the course of the solvent exchange making them unusable for SCXRD studies.

3.3.1.4 *Comparison of synthetic methods*

In total method **A** required 7 days for the initial synthesis of the sponge crystals and a further 5 - 8 days for solvent exchange. In contrast, within three days of setting up the experiment method **B** consistently yielded crystals of **1** suitable for guest encapsulation. In addition, those synthesised *via* method **A** were of poor quality; high quality single-crystals of **1($C_6H_5NO_2$)** were difficult to obtain (even after the analysis of >20 crystals), and post-solvent exchange **1(C_6H_{12})** lost single crystallinity. The average yield of each method was similar based on TPT at 72% and 68% for methods **A** and **B** respectively.

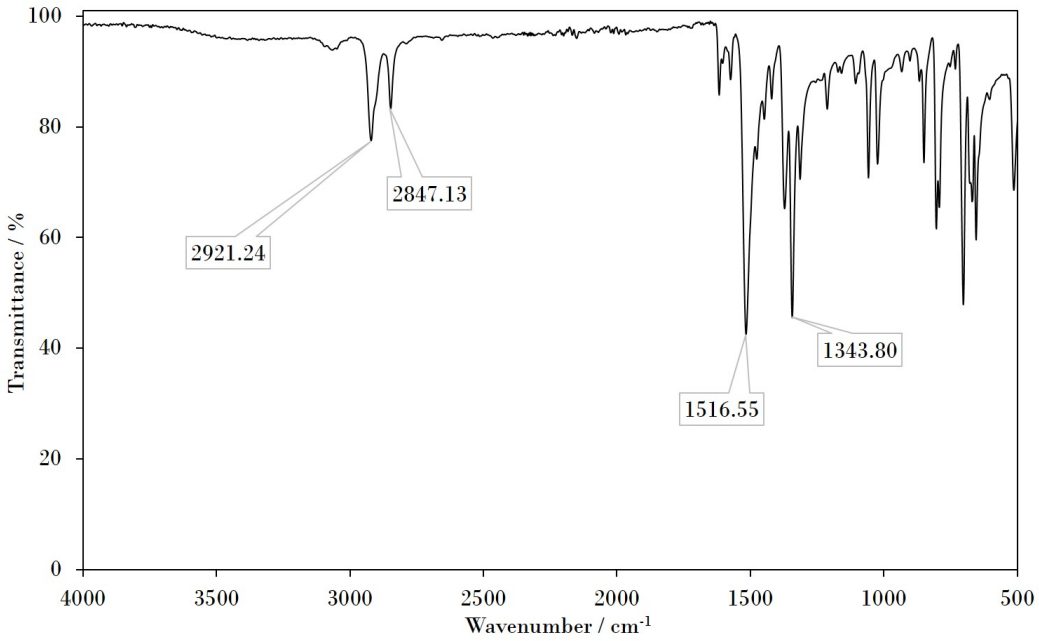

Figure 3.4: FTIR spectrum of as synthesied **1($C_6H_5NO_2$)**.

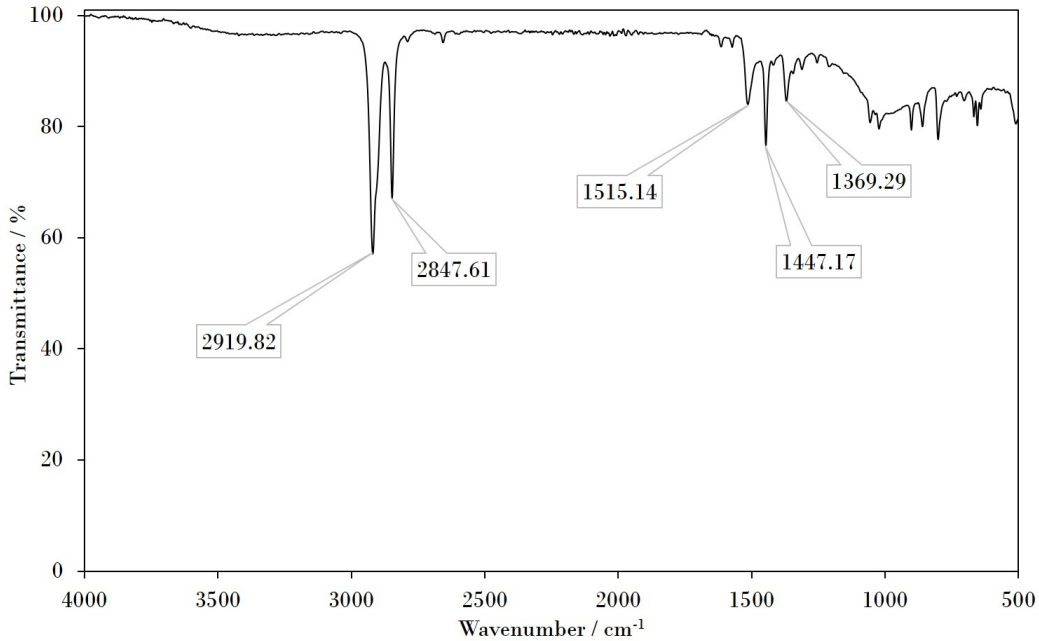

Figure 3.5: IR spectrum of **1(C_6H_{12})** indicating the sucessful removal of nitrobenzene from the pores of **1** after 8 days of washing with cyclohexane.

3.3.2 *Side Products*

After completion of the study detailed above in Section 3.3.1 method **B** was used routinely to produce the crystalline sponge for use in encapsulation experiments. During the course of these studies (detailed in the following three chapters) crystal morphologies contrary to that expected of the desired phase **1** (Form **I**) were noted, and found to be of insufficient pore size to encapsulate guest molecules. The first to be observed, Form **II**, was easily identified by its bunched obelisk-like morphology, as shown in Figure 3.6. Unit cell determination experiments of 10 such crystal from the same batch confirmed the new morphology related to a new crystal structure belonging to the orthorhombic space group *Fdd2* (Table 3.2).

Latterly, a third form, Form **III**, was identified with a second distinct morphology - bunched dagger-like crystals (Figure 3.6). Again, multiple unit cell checks showed crystal morphology was a reliable indicator of Form **III**, which was found to crystallise in the monoclinic space group $P2_1/m$ (Table 3.2). The fortuitously distinct crystal morphologies of Forms **II** and **III** would allow them to be easily identified and discarded before the guest encapsulation step. As a result their formation would not stand to impede implementation of the crystalline sponge technique, especially as only low level growth was observed (see Section 3.3.2.1).

Some months later a fourth form was discovered having a morphology indistinguishable from the desired Form **I** whilst consistently giving a unique set of unit cell parameters, crystallising in the monoclinic space group $P2_1/n$ (Table 3.2). The framework of **1**, regardless of solvent occupying the pores, was found to be fragile and after completion of SCXRD experiments some cracks would appear in the crystal. Although this did not demonstrably affect the quality of data obtained over the period of data collection, it did prevent the same crystal being reused for encapsulation experiments due to unavoidable exposure to air in processing (resulting in drying and cracking). Therefore, crystals that were chosen by eye based on their morphology (following the criteria discussed in Section 3.3.1.2) could be either Form **I** or **IV**. As a result Form **IV** caused reasonable

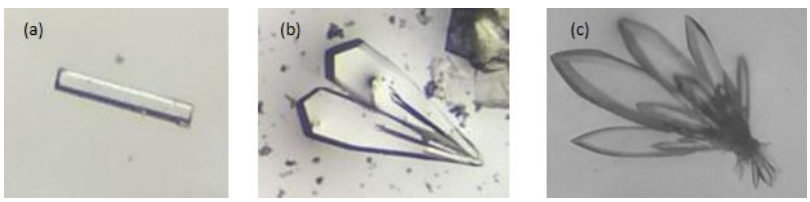

Figure 3.6: Micrographs of (a) a standard rod shaped crystal of desired Zn-TPT Form **I** compared to (b) novel Form **II** showing characteristic conjoined-beak morphology and (c) Form **III**.

inconvenience experimentally as imposter crystals were selected and used for encapsulation experiments were only unmasked at the point of data collection on the SCXRD. Fortuitously however, over time the frequency of Form **IV** formation greatly reduced with no clear indication of why. It is possible the transition to a new batch of test tubes used as synthetic vessel may have had an effect if contaminants were present. Equally, minor changes in temperature, humidity and variations in initial mixing during the layering process of crystal synthesis may have had an effect.

3.3.2.1 *Phase purity*

Attempts to determine the phase purity of the bulk product by powder X-ray diffraction (PXRD) was unsuccessful. Due to the size of crystals, samples had to be ground before analysis but this caused severe degradation of the structure such than discrete diffraction peaks were not observed.

Form	**I**	**II**	**III**	**IV**
Crystal system	monoclinic	orthorhombic	monoclinic	monoclinic
Space group	*C*2/*c*	*Fdd*2	$P2_1/m$	$P2_1/n$
a/Å	35.2913(7)	39.7112(4)	6.26012(6)	7.43196(13)
b/Å	14.7032(2)	34.5319(4)	33.0659(3)	21.5610(3)
c/Å	31.2290(6)	8.26132	12.84156(11)	12.7277(2)
α /°	90	90	90	90
β/°	101.5328(18)	90	99.7620(9)	103.38
γ /°	90	90	90	90
Volume/^{3}	15877.4(5)	11328.8(2)	2619.67(4)	1984.10(6)

Table 3.2: Crystal data for the four Zn-TPT forms obtained *via* method **B** at 150 K.

3.3.3 *Crystal Structure of Form I*

Form **I** is the 'original' MOF introduced by Fujita *et al* as a crystalline sponge,[1] developed and optimised over the preceding years as discussed in Section 1.4.2. As discussed above two synthetic methods may be used with resultant crystals sharing the same framework structure and differing only in the solvent occupying the pores. However, no single crystals of sufficient quality to run a full diffraction experiment were obtained from method **A**. Although the expected unit cell parameters were routinely observed, crystals were only poorly or moderately diffracting. It is not clear why this should be the case given the success reported in the literature. In the hands of the author, in the particular lab environment, this synthetic method was unreliable, with a very low margin for error. Therefore, crystal structure analysis of the as-synthesised MOFs is limited to the structure $[\{(ZnI_2)_3(TPT)_2 \cdot 3.95(CHCl_3)\}_n]$ obtained *via* method **B**. The asymmetric unit, shown in Figure 3.7, contains three ZnI_2 units, two TPT molecules and five partially occupied $CHCl_3$ molecules. The packing diagram of Form **I** shown in Figure 3.8, highlights the void space of over 4095 $Å^3$, 25.8% of unit cell volume.

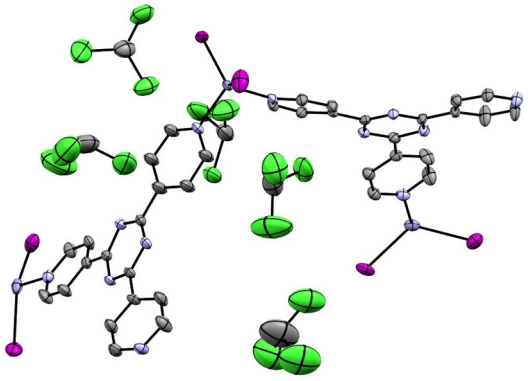

Figure 3.7: The asymmetric unit of Form **I**.

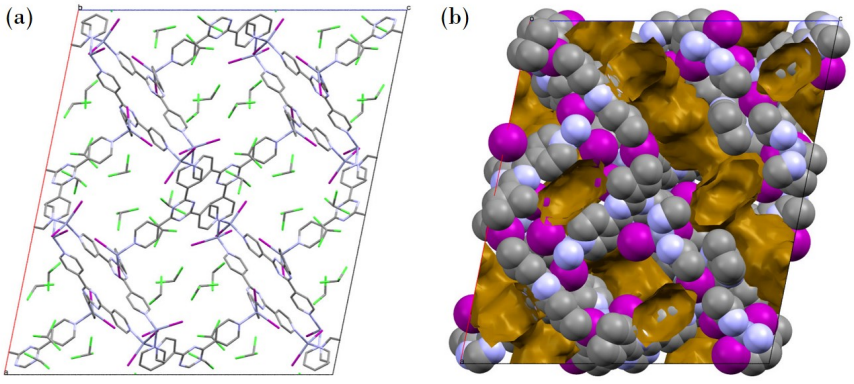

Figure 3.8: Packing diagrams of Form **I** as viewed down the *c-axis*. (a) Capped stick model (b) spacefilling model showing voids space in orange.

3.3.4 *Crystal Structure of Form II*

The asymmetric unit of $[\{(ZnI_2)_3(TPT)_2 \cdot CHCl_3\}_n]$ (**2**) contains one and a half zinc atoms, three iodine atoms and one TPT linker. Within the asymmetric unit one chloroform molecule is disordered over two sites with occupancies of 75% and 25%. In this structure there are two environments of the zinc metal centre (Figure 3.9). Each is four fold coordinate, coordinating to two iodine atoms and two nitrogen atoms of pyridyl rings in two separate TPT molecules. The structure extends in three dimensions exhibiting channels down the *c-axis*, as shown in Figure 3.10a. The overall solvent-accessible volume is 206 $Å^3$, equivalent to only 1.8% of the unit cell volume, illustrated in Figure 3.10b. Therefore, this form is unsuitable for use as a crystalline sponge.

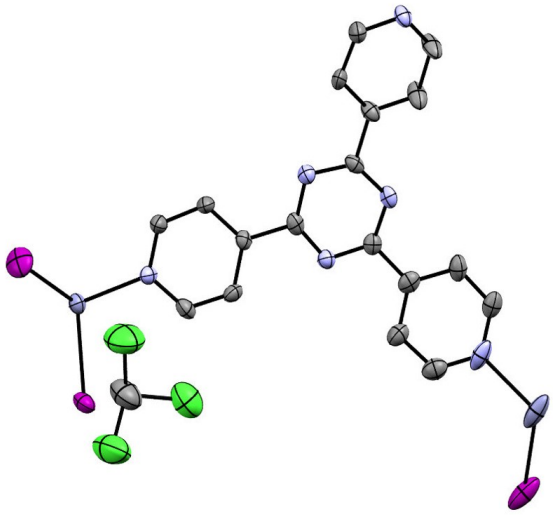

Figure 3.9: The asymmetric unit of Form **II**.

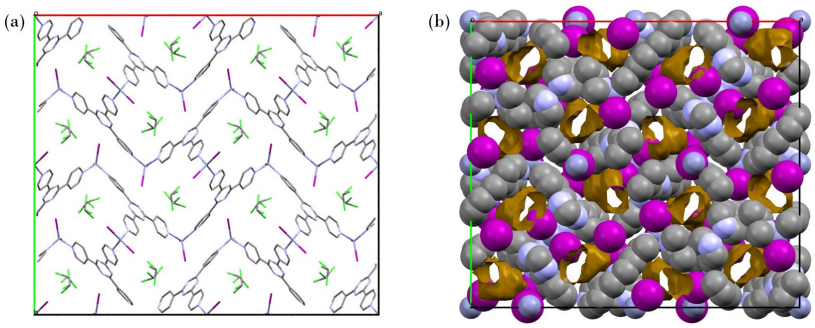

Figure 3.10: Packing diagrams of Form **II** as viewed down the *c-axis*.(a) Capped stick model (b) spacefilling model showing voids space in orange.

3.3.5 *Crystal Structure of Form III*

The third form discovered was $[\{(ZnI_2)_3(TPT)_2\}_n]$ (Form **III**). The asymmetric unit of **3** consists of two crystallographically unique zinc atoms, with one fully occupied and other at half occupancy. Each zinc is coordinated to two TPT linkers and two iodine atoms, with one TPT molecule and three iodine atoms present in the asymmetric unit, as shown in Figure 3.11. The two-dimensional MOF structure is made up of pairs of extended Zn-TPT chains cross linked by ZnI_2 units. These double-strand chains run in parallel to each other over the extended structure and do not interlink (Figure 3.12a). **3** displays a two dimensional metal-organic framework structure with solvent accessible void space of 160.86 $Å^3$ (6.1% of unit cell volume, illustrated by orange fill in Figure 3.12b. Therefore this form is not suitable for use as host framework.

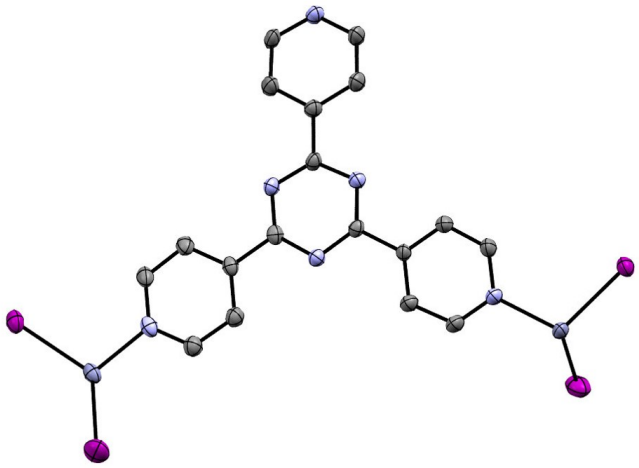

Figure 3.11: The asymmetric unit of Form **III**.

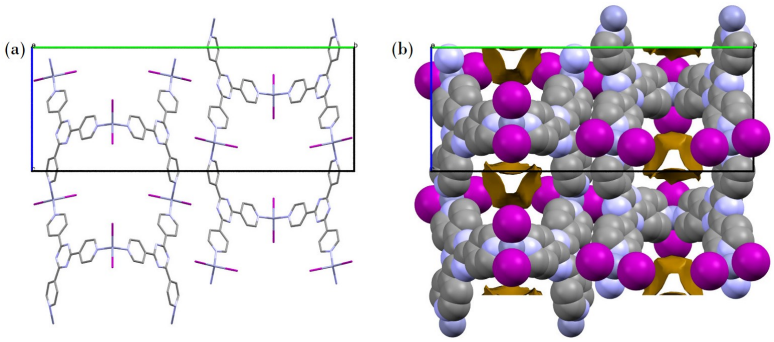

Figure 3.12: Packing diagrams of Form **III** as viewed down the *c-axis*.(a) Capped stick model (b) spacefilling model showing voids space in orange.

3.3.6 *Crystal Structure of Form IV*

The asymmetric unit of $[\{(ZnI_2)(TPT)\}_n]$ (Form **IV**) consists of one fully occupied ZnI_2 unit and TPT molecule (Figure 3.13). The zinc atom is four fold coordinated to two iodine atoms and two nitrogen atoms from separate TPT linker molecules. One of the three pyridyl nitrogen atoms in each TPT is uncoordinated. This creates infinite zig-zag Zn-TPT chains with no interlinking that extend to form a one dimensional MOF structure (Figure 3.14). Chains are interconnected by $\pi \cdots \pi$ stacking interactions at alternating distances of 3.62 Å and 4.05 Å . It displays a condensed structure with no solvent accessible voids.

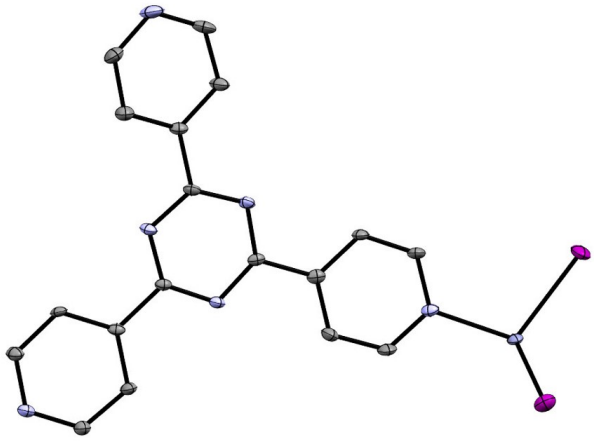

Figure 3.13: The asymmetric unit of Form **IV**.

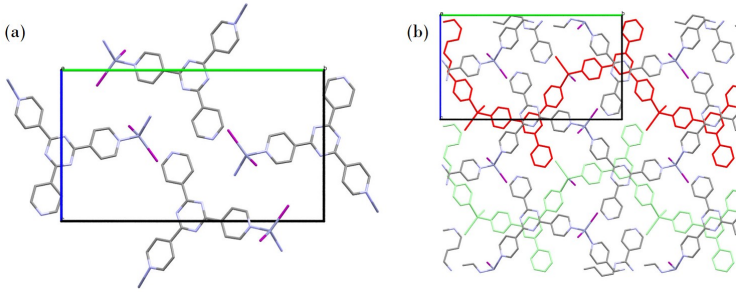

Figure 3.14: Packing diagrams of Form **IV** as viewed down the *c-axis*. (a) Capped stick model of the unit cell (b) the extended structure with two zig-zagging Zn-TPT highlights in red and green.

3.4 CONCLUSIONS

Initial worked focused on replicating the experimental procedure reported in Nature Protocols[118] as a follow up to the original Fujita paper.[1] This synthesis was carried out by diffusion of a methanol solution of ZnI_2 into a nitrobenzene/methanol solution of the 2,4,6-tri(4-pyridyl)-1,3,5-triazine (TPT) linker. The resulting MOF crystals contain nitrobenzene which must be exchanged for cyclohexane, an inert and labile solvent. This required week-long daily solvent refreshment and elevated temperature (50°C). Any crystals remaining after complete exchange were of poor quality (contrary to the report in the paper) and exhibited poor quality X-ray diffraction patterns. Many of the synthetic problems encountered were resolved subsequently, with success reported in the use of chloroform in place of nitrobenzene/methanol solution.[119]

Work in this chapter has confirmed the reliability and efficiency of this method and demonstrated it comparative advantages. These include reduced preparative time and the elimination of the solvent exchange step. Overall, after this analysis there is no doubt that crystals of sufficiently high quality may be obtain reliably in sufficient quantities *via* method **B** for guest encapsulation experiments. Furthermore, method **B** was expedient as the conditions reported were not marginal, i.e. they offered a crystallisation window broad enough to be successful in varied lab/operator conditions.

During the course of the study into the chloroform method three previously unknown forms of Zn-TPT (Forms **II**, **III** and **IV**) were observed as side products and their crystal structures determined. Whilst Form **IV** displays a condensed structure, Forms **II** and **III** display some limited solvent-accessible volume (206 and 160.86 $Å^3$ respectively). This porosity is greatly reduced from that in the desired phase Form **I** (3800 $Å^3$) and none display crystalline sponge capabilities. Their formation is evidence for the sensitivity of the experimental method and the challenge of its application.

3.5 EXPERIMENTAL

3.5.1 *Method **A**: [{$(ZnI_2)_3(TPT)_2$•x(cyclohexane)}$_n$]*

A schematic of experimental procedures is illustrated in Figure 3.15, following the path labelled with Roman numerals. The synthesis of [{$(ZnI_2)_3(TPT)_2$•x(cyclohexane)}$_n$] was carried out following the method from[118] with minor alterations.

*Framework Synthesis: **1($C_6H_5NO_2$)***

TPT (6.3 mg, 0.02 mmol) was dissolved in a nitrobenzene/methanol mixture (5 cm^3, 4:1) and left to stir for 1 hour. If the solid was not then fully dissolved the mixture was placed in an ultrasonic bath for 10 minutes or until fully dissolved. A 0.03M methanol solution of ZnI_2 was prepared by dissolving ZnI_2 (9.6 mg, 0.03 mmol) in methanol (1 cm^3). The TPT solution was transferred to a borosilicate test tube (13×1 cm) and the methanol solution layered carefully on top to ensure a clear interface between the layers. The tube was covered with a double layer of parafilm and left in an incubator at 25°c. After 7 days yellow crystals were harvested using a plastic Eppendorph pipette tip and transferred to a sealed glass vial.

*Solvent Exchange: **1(C_6H_{12})***

The yellow crystals were stored in cyclohexane (~8 cm^3) for 1 week in an incubator at 45°C. During this time the crystals were washed with cyclohexane (3 x 5 cm^3) every day for 5 days, and then once on the 8th day. Care was taken not to allow the crystals to dry out. In early experiments crystals were broken when cyclohexane was pipetted too firmly into the vial. Latterly, care was taken to smoothly add cyclohexane by pipetting it slowly down the inside wall of the vial. Progress of the solvent exchange was monitored IR analysis with the N-O streches 1374 cm^{-1} and 1516 cm^{-1} disappearing after complete replacement by cyclohexane. Crystals were then stored in cyclohexane (10 cm^3) at 25°C until needed.

3.5.2 *Method **B**: [{$(ZnI_2)_3(TPT)_2$•x(chloroform)}$_n$]*

A schematic of experimental procedures is illustrated in Figure 3.15, following the path labelled using western arabic numerals. The synthesis of [{$(ZnI_2)_3(TPT)_2$•x($CHCl_3$)}$_n$] was carried out following the method from[119] with minor alterations.

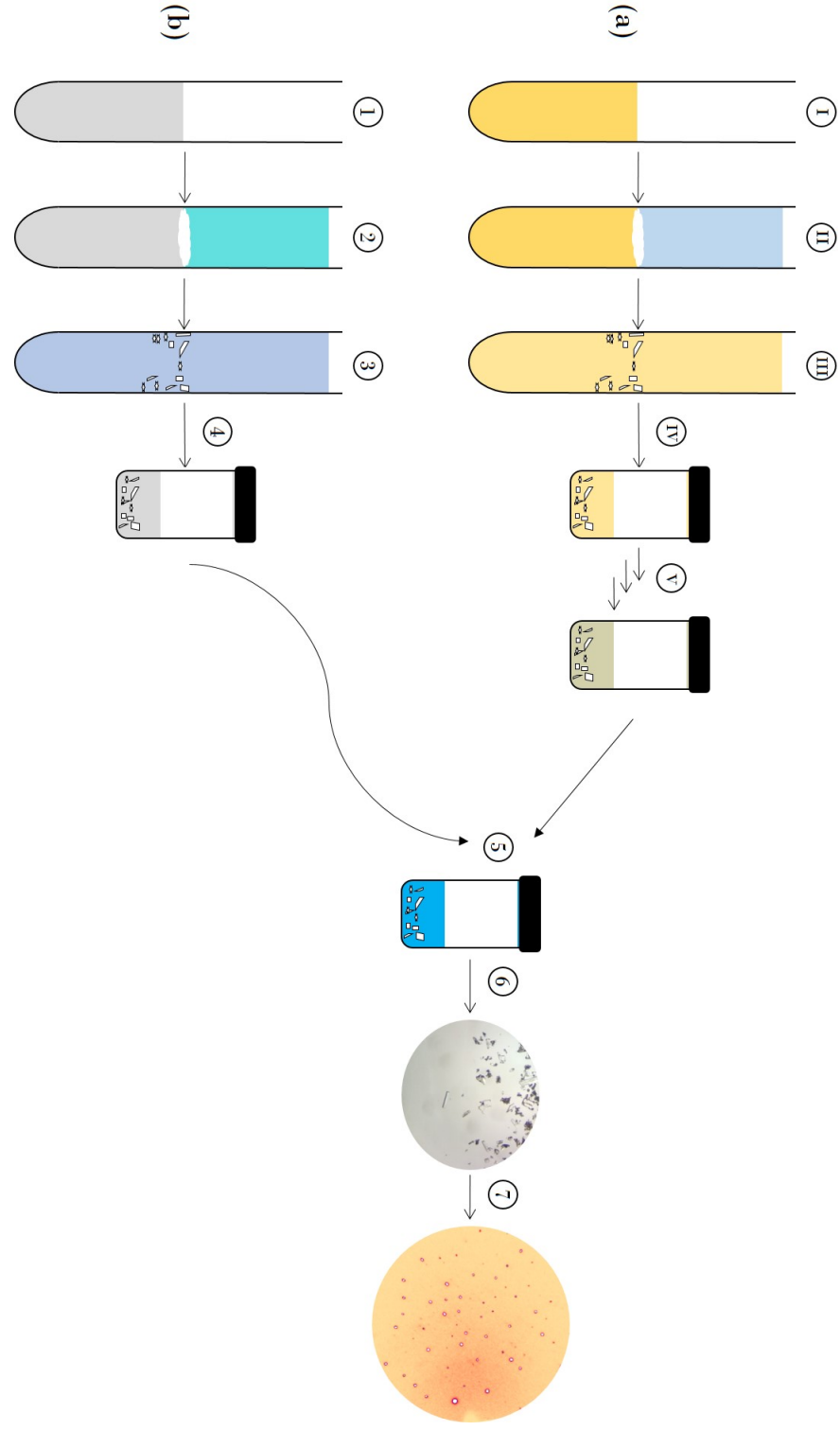

Figure 3.15: Sketch of the synthetic protocol for the synthesis of the crystalline sponge $[(ZnI_2)_3(tris(4\text{-pyridyl})\text{-}1,3,5\text{-triazine})_2]_x(CHCl_3)\}_n]$ **(1)** and subsequent guest encapsulation.

Framework Synthesis: ***1(CHCl$_3$)***

A vial containing TPT (6.3 mg, 0.020 mmol) and chloroform (4 cm^3) mixture was placed in a ultrasoninc bath until dissolved (~5 minutes). A 0.03M methanol solution of ZnI_2 was prepared by dissolving ZnI_2 (9.6 mg, 0.03 mmol) in methanol (1 cm^3). The TPT solution was transferred to a borosilicate test tube (13 x 1 cm) and the methanol solution layered carefully on top to ensure a clean interface between the layers. The tube was covered with a double layer of parafilm and left in an incubator at 25°C for 3 days. After this time colourless crystals were harvested using a plastic Eppendorph pipette tip to detached crystals from the test tube surface. Collected crystals were washed with chloroform (3 x 5 cm^3) and stored in chloroform (~8 cm^3) at 25°C in a screw cap vial.

3.5.3 *Crystallography*

A number of crystals were pipetted with mother liquor onto a glass slide and immediately covered in Fomblin to prevent evaporation of solvent and degradation of the crystal. A well formed single-crystal was selected, mounted onto a nylon loop and rapidly transferred to the diffractometer mount into the cryojet stream. X-ray diffraction data were recorded on an Agilent Super Nova Dual Diffractometer (Agilent Technologies Inc, Santa Clara CA) with Cu-K α radiation (λ = 1.5418 Å) at 150K. Unit cell determination, data reduction and absorption corrections were carried out using CrysAlisPro.[126] The structures were solved with the Sir2004[127] structure solution program by Direct Methods and refined by full matrix least squares on the basis of F^2 using SHELX 2013[128] within the OELX2 GUI[129]. Unless otherwise stated, non-hydrogen atoms were refined anisotropically without the use of restraints or constraints. Hydrogen atoms were included using a riding model.

3.5.3.1 *Crystal Structure Refinement*

The checkcif results for the crystal structures of **Form I** and **Form III** contain some level A and B alerts. Alerts for residual electron density associated with atoms in $CHCl_3$ molecules and for solvent accessible voids must be noted. These are a result of the porous nature of the structures and disorder of solvent molecules that cannot be stably refined.

4

REPRODUCIBILITY OF ENCAPSULATION

4.1 AIMS

For the crystalline sponge technique to be reliable it must be reproducible. Therefore, experiments described in this chapter aim to develop an understanding of the reproducibility of guest uptake and position within the pores of $[\{(ZnI_2)_3(TPT)_2.x(solvent)\}_n]$ (**1**). A series of simple aromatic molecules with a range of functionality will be tested and any guest-host structures obtained through successful repeat encapsulation experiments analysed. In the longer term, this study aims to lay the foundation for work to investigate the nature of guest-host interactions formed in the pores of **1** (see Chapter 5 and Chapter 6).

4.2 INTRODUCTION

At the time of study, the crystalline sponge technique was new and little work outside the Fujita group at the University of Tokyo had been published. A corrigendum published shortly after the original Nature paper stirred questions of the technique's reliability.[1] Although the error had occurred in the assignment of absolute stereochemistry of a natural product (see Section 1.7.2), this was a blow to the perceived utility of a method which was ground breaking yet barely tested. Therefore, a systematic study of the methods reproducibility would be timely.

4.2.1 *Selection of Guests*

The potential guests were chosen for their aromaticity, range of functionality and simplicity. A further requirement was that the guest was a liquid at room temperature or readily soluble in a suitable solvent (*e.g.* chloroform, cyclohexane, dichloromethane or dichloroethane). Therefore the following compounds were chosen for encapsulation experiments: benzene (**1i**); 4-fluorobenzaldehyde (**1ii**); 1,3-dichlorobenzene (**1iii**); benzonitrile (**1iv**); naphthalene (**1v**); and 1,2-dibromobenzene (**1vi**), shown in Figure 4.1. *N.B.* When solvent molecules are present from synthesis they are not referred to as guests - this title is reserved only for those molecules purposefully encapsulated.

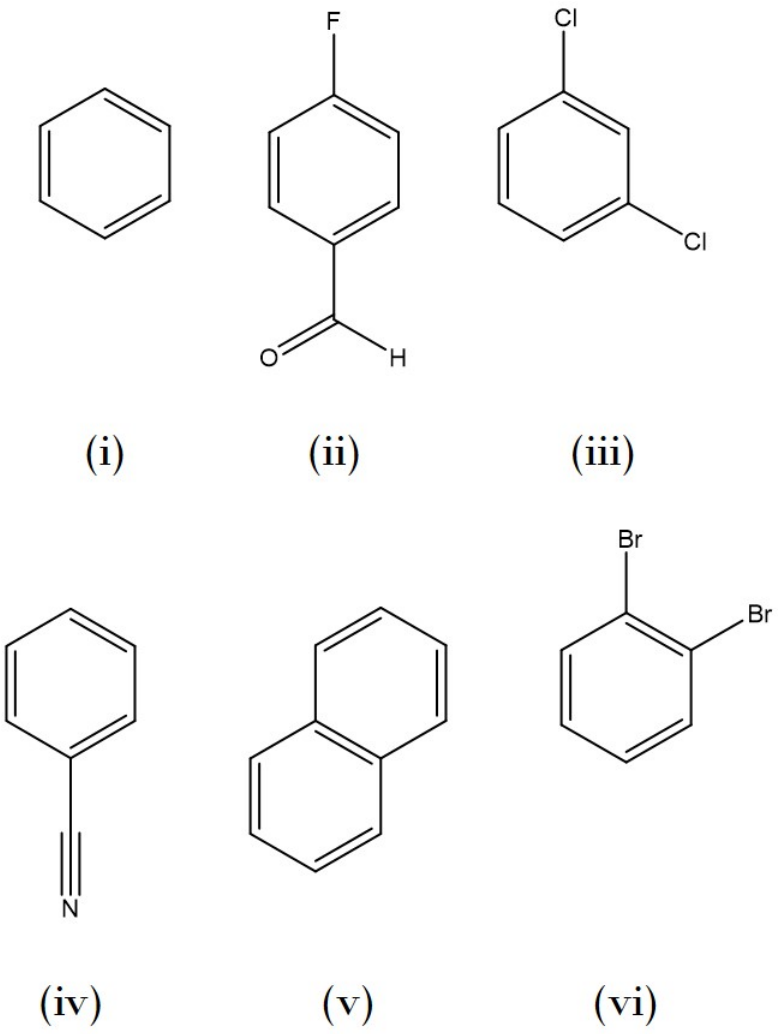

Figure 4.1: Guest compounds chosen for the reproducibility study: (**i**) benzene ; (**ii**) 4-fluorobenzaldehyde ; (**iii**) 1,3-dichlorobenzene ; (**iv**) benzonitrile ; (**1v**) naphthalene ; and (**vi**) 1,2-dibromobenzene .

4.3 RESULTS

4.3.1 *Successful Encapsulation Experiments*

Synthesis of the crystalline sponge proved successful and high quality single crystals were obtained consistently. Successful encapsulation experiments were carried out yielding novel inclusion complexes with the following guest molecules, with repeat experiments denoted by ':

- **1i and 1i'** Benzene
- **1ii and 1ii'** 4-Fluorbenzaldehyde
- **1iii and 1iii'** 1,3-Dichlorobenzene
- **1iv and 1iv'** Benzonitrile
- **1v and 1v'** Naphthalene

All crystallise in the centrosymmetric *C*2/c monoclinic space group for which full crystallographic data is shown in Table 4.1 and Table 4.2. There are modest variations in cell dimensions from the as prepared crystalline sponge **1**, as expected from specific interactions and steric demands of the range of guest within the host structure. (The effect of guest size on unit cell dimensions is discussed further in Section 6.3.3.) Ease of identification of the guest within the refined host framework varied according to the extent of disorder, all display significant thermal motion compared to the framework and in some cases additional static and/or dynamic disorder.

	1i	**1i'**	**1ii**	**1ii'**	**1iii**	**1iii'**
Crystal system	monoclinic	monoclinic	monoclinic	monoclinic	monoclinic	monoclinic
Space group	*C*2/*c*	*C*2/*c*	*C*2/*c*	*C*2/*c*	*C*2/*c*	*C*2/*c*
a/Å	35.1590(5)	35.1502(3)	35.4351(6)	35.7936(3)	35.1763(3)	35.0087(9)
b/Å	14.62744(13)	14.61392(12)	14.9537(2)	14.89081(10)	14.96705(11)	14.9458(6)
c/Å	31.1596(4)	31.0655(3)	31.1920(4)	31.3707(3)	30.2349(2)	30.6949(8)
α /°	90	90	90	90	90	90
β/°	101.4862(12)	101.3004(8)	102.4161(15)	102.6729(10)	100.7593(7)	100.800(2)
γ /°	90	90	90	90	90	90
Volume/Å^3	15704.0(3)	15648.4(2)	16141.6(4)	16313.1(3)	15638.4(2)	15776.0(9)

Table 4.1: Crystal data for **1i**, **1i'**, **1ii**, **1ii'**, **1iii** and **1iii'** at 150 K.

	1iv	**1iv'**	**1v**	**1v'**
Crystal system	monoclinic	monoclinic	monoclinic	monoclinic
Space group	*C*2/*c*	*C*2/*c*	*C*2/*c*	*C*2/*c*
a/Å	35.2839(3)	35.2654(6)	35.0571(7)	35.0715(2)
b/Å	15.15918(11)	15.1124(2)	14.6495(2)	14.62670(10)
c/Å	30.6904(2)	30.9140(5)	31.1547(6)	31.2347(2)
α /°	90	90	90	90
β/°	102.2220(8)	102.1276(16)	100.846(2)	100.5410(10)
γ /°	90	90	90	90
Volume/Å^3	16043.5(2)	16107.7(4)	15714.2(5)	15752.39(18)

Table 4.2: Crystal data for **1iv**, **1iv'**, **1v** and **1v'** at 150 K.

4.3.2 *Unsuccessful Encapsulation Experiments*

Experiments with 1,2-dibromobenzene (**vi**) were unsuccessful. Well diffracting crystals with the expected unit cell parameters were identified after guest soaking by unit cell checks and full data collections performed. In the two crystal structures obtained the framework was well ordered and well refined. Some guest fragments were evident (some anisotropically refined) but a great deal of disorder prevented full structure solution with acceptable chemical sense. The asymmetric units of the working structures are shown in Figure 4.2 with unassigned electron density peaks >3e^{-}. Attempts to assign this electron density lead to unstable refinements and no improvements of the model. Full crystallographic tables are shown in Appendix A. Such was the poor quality of the refinement that no further analysis of the structures was performed.

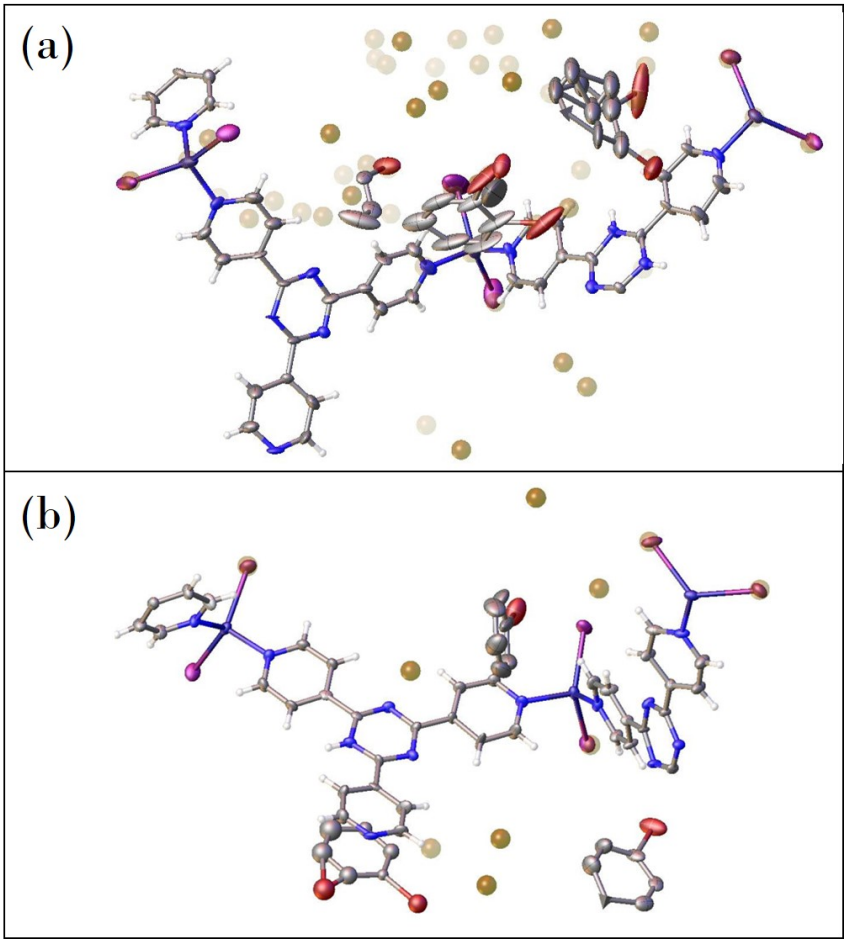

Figure 4.2: Asymmetric units of the structures obtained from repeat encapsulation experiments with 1,2-dibromobenzene (**1vi**). The large amount of disorder prevented satisfactory refinement of guest molecules. All electron density peaks >3 e^{-} Å^{-3} shown as brown spheres.

4.3.3 *Reproducibility of Liquid Guest Encapsulation*

Evaluating the crystallographic data from the successful repeat encapsulation experiments by viewing the crystal structures down the *b*-axis (Figure 4.3) allows clear visualisation of the different sites taken up by the guests within the infinite networks of solvent-accessible channels. Guest molecules have been coloured by symmetry equivalence, and by positional equivalence to guests in the other structures. Visual analysis of the eight structures shows certain sites are favourable for uptake, with guest molecules consistently taking up favourable positions and orientations, specific (but not exclusive) to their type.

4.3.3.1 *Encapsulation of benzene*

Encapsulation experiments with benzene produced two structures: $[\{(ZnI_2)_3(TPT)_2 \cdot 4.25(C_6H_6).0.5(CHCl_3)\}_n]$ **1i** and $[\{(ZnI_2)_3(TPT)_2 \cdot 4.3(C_6H_6).0.65(CHCl_3)\}_n]$ **1i'**. The number and position of benzene guest molecules occupying the crystalline sponge shows complete reproducibility (Figure 4.3a and b), with five guest molecules (green, orange, blue, purple and pink) taking up identical specific sites in each structure, along with one residual chloroform molecule (grey). There is a small variation in guest occupancy, with a marginally larger total in **1i'**. Interestingly, of the other six encapsulation complexes obtained only one other, benzonitrile (**1iv**), shows incomplete exchange of $CHCl_3$ by the intended guest molecules. This suggests the duration of soaking **1** in benzene especially was insufficient, even though this was more than double the duration of the other repeat encapsulation experiments (see Section 4.5.2).

4.3.3.2 *Encapsulation of 4-fluorobenzaldehyde*

The number and position of 4-fluorobenzaldehyde molecules occupying the crystal structures $[\{(ZnI_2)_3(TPT)_2 \cdot 1.5(C_7H_5FO)\}_n]$ **1ii** and $[\{(ZnI_2)_3(TPT)_2 \cdot 1.5(C_7H_5FO)\}_n]$ **1ii'** shows complete reproducibility in both guest position and total occupancy (Figure 4.3c and d). Three guest molecules (red, blue and green) took up identical specific sites in each structure.

4.3.3.3 *Encapsulations of 1,3-dichlorobenzene*

Repeat experiments with 1,3-dichlorobenzene yielded the encapsulation complexes $[\{(ZnI_2)_3(TPT)_2 \cdot 4.5(C_6H_4Cl_2)\}_n]$ **1iii** and $[\{(ZnI_2)_3(TPT)_2 \cdot 4.5(C_6H_4Cl_2)\}_n]$ **1iii'**. Five equivalent guest molecules were present in each crystal structure (Figure 4.3e and f), and there was complete reproducibility in total guest occupancy. The two structures were only distinguishable by the behaviour of the 'blue'

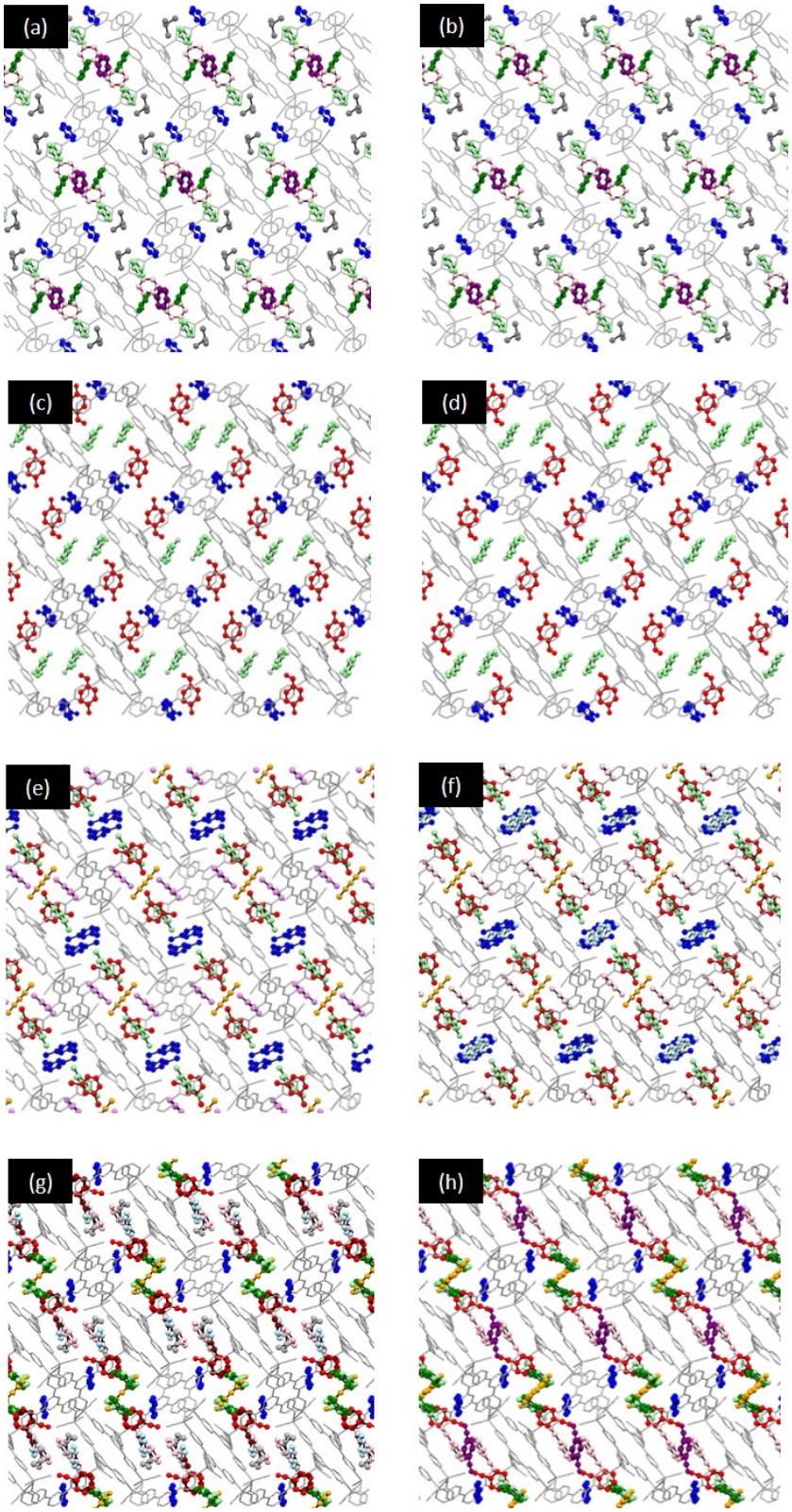

Figure 4.3: Unit cells of encapsulation complexes (a) **1i** and (b) **1i'** (benzene), (c) **1ii** and (d) **1ii'** (4-fluorobenzaldehyde), (e) **1iii** and (f) **1iii'** (1,3-dichlorobenzene), and (g) **1iv** and (h) **1iv'** (benzonitrile) viewed down the *b*-axis. Guest molecules shown as ball and stick models with the framework shown as grey wireframe. Hydrogen atoms omitted for clarity.

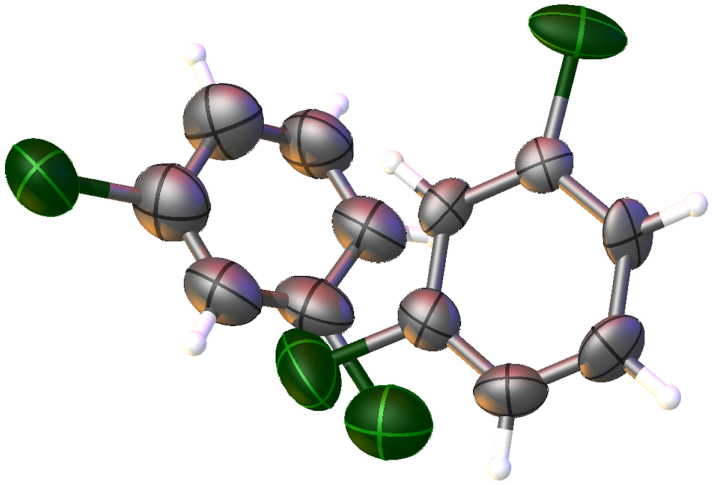

Figure 4.4: Disorder of the guest 1,3-dichlorobenzene in **1iii'**. Atoms are show as thermal ellipsoids at 50% probability.

guest molecule which is well ordered in **1iii** but disordered in **1iii'**. This is shown in Figure 4.4, with 50% occupancy of each of the parts overlapping by their chlorine atoms.

4.3.3.4 *Encapsulation of benzonitrile*

In the final comparison crystal structures $[\{(ZnI_2)_3(TPT)_2 \cdot 4.11(C_7H_5N).0.5(CHCl_3)\}_n]$ **1iv** and $[\{(ZnI_2)_3(TPT)_2 \cdot 3.95(C_7H_5N)\}_n]$ **1iv'** distinct similarities are present along with some variation in benzonitrile position. As shown in Figure 4.3g and h, each structure contains 6 guest sites, with one extra residual $CHCl_3$ solvent in **1iv**. The majority of guests sit in sites common to both structures and can be identified by blue, green, pink, red, and yellow colouration. Within this subset two instances of minor rotational disorder were observed involving rotation of the aromatic ring which resulted in variable positioning of the nitrile group, shown clearly in Figure 4.5a. One disordered molecule was observed in both **1iv** and **1iv'** as the light and dark green guest molecules in Figure 4.3g and h. In contrast the second instance of disorder was confined to **1iv'**, highlighted as red and burgundy in Figure 4.3g. This leads to the most significant findings for this study; variations between structures **1iv** and **1iv'** that relate to occupation of unique sites.

Firstly, there are instances of guest molecule disorder that results in the occupation of two overlapping sites. One instance is consistent between the two structures and involves the two disordered parts sharing only the terminal nitrogen atom of their nitrile group Figure 4.5a. The significant disorder between the two parts results in significant displacement of the aromatic ring suggesting weak π-π

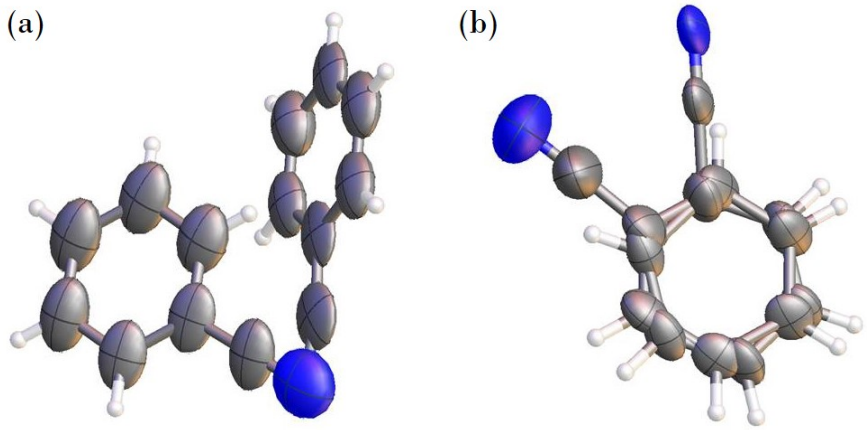

Figure 4.5: Two instances of benzonitrile disorder observed in **1iv**. (a) Significant displacement about the nitrile nitrogen atom; (b) rotational disorder resulting in variable orientation of the nitrile group. Atoms are show as thermal ellipsoids at 50% probability.

interactions. The second instance, confined to **1iv**, is characterised as rotational disorder about the aromatic ring resulting in variable orientation of the nitrile group (Figure 4.5a). The second significant difference between the structures is the presence of a molecule unique to **1iv'**, identified by its purple colouration in Figure 4.3h. Its occupancy (freely refined to 25%) is low, in fact the lowest of all guests in this study. Indeed, the position of the residual $CHCl_3$ present in **1iv** overlaps with this site. This suggests a small variation in the guest soaking conditions may have affected the rate of exchange. For example, variation in the concentration of the guest may have occurred between repeat experiments originating in the small volume of $CHCl_3$ (~0.2 cm^3) used to transfer crystals of **1** to the neat guest solution. Another, more pronounced, example of the effect variable soaking conditions have on guest uptake is discussed in Section 4.3.4.1.

4.3.4 *Reproducibility of Solid Guest Encapsulation*

4.3.4.1 *Encapsulation of naphthalene*

Near saturated chloroform solutions of naphthalene were used for guest encapsulation experiments. After three weeks of soaking a crystal was selected and the structure $[\{(ZnI_2)_3(TPT)_2 \cdot 2.5(C_{10}H_8).2(CHCl_3)\}_n]$ (**1v**) obtained. Attempts to obtain a repeat encapsulation complex were unsuccessful, although the structure $[\{(ZnI_2)_3(TPT)_2 \cdot 1.72(C_{10}H_8).2.42(CHCl_3)\}_n]$ (**1v'**) was obtained from a crystal after 2 weeks of soaking. Although not allowing the direct comparison performed above with liquid guests, interesting discussion may still be had. Figure 4.6 shows the unit cells of **1v** and **1v'**. The light green and yellow coloured molecules are in equivalent sites in both structures, with the yellow molecules disordered over a crystallographic 2-fold rotation axis. The first contrast to note is the additional guest molecule present in **1v**, coloured dark green. By overlaying the asymmetric units of each structure this difference can be clearly visualised (Figure 4.7). This shows the positional overlap of the additional naphthalene molecule in **1v** with a chloroform molecule in **1v'**. Given the additional time available for guest diffusion in **1v** this result is not surprising. It suggests there are sites within the unit cell that may be sequentially filled, perhaps due to more favourable guest-host interactions. In **1v'** there is some evidence from the residual electron density map of a low occupancy naphthalene molecule, although all ten carbon atoms are not visible (Figure 4.8) and no refinement was possible. Viewing the differential electron density map of **1v'** there is some evidence for the presence of a low occupancy naphthalene molecule, disordered over a $CHCl_3$ molecule of 62% occupancy. However not all 10 carbon atoms are visible and no refinement was possible.

4.3.5 *Guest Occupancy*

Whilst the reproducibility of guest position within repeat encapsulation compounds has been confirmed, the occupancy of equivalent guest molecules does vary in some cases. The occupancies of all the guest molecules in compounds **1i**-**1v** and their repeats are listed in Table 4.3. These were obtained by freely refining each molecule separately and only fixing the occupancy in the latter stages of refinement once stable. The figures for complexes with 1,3-dichlorobenzne, taking into account positional disorder, is completely reproducible. In contrast, occupancies of naphthlene molecules vary for each guest comparing **1v** and **1v'**. However, in general where guest occupancies were $\leqslant$50%, they were also $\leqslant$50% in the repeat if not the same value, as for $\geqslant$50%.

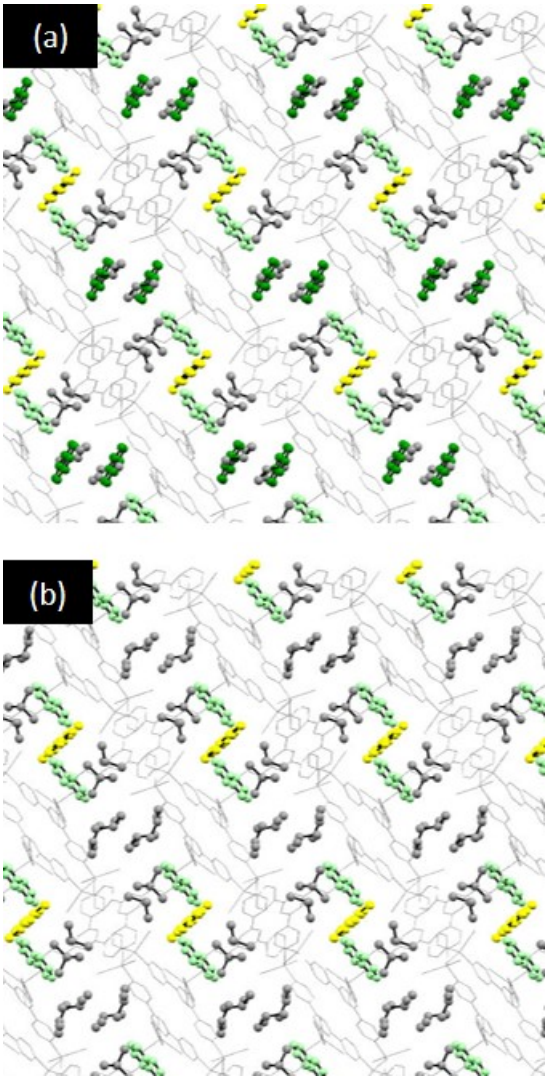

Figure 4.6: Unit cells of encapsulation complexes (a) **1v** and (b) **1v'** with naphthalene, viewed down the *b*-axis. Guest molecules shown as ball and stick models with colours corresponding to equivalent sites, framework shown as grey wireframe. Hydrogen atoms omitted for clarity.

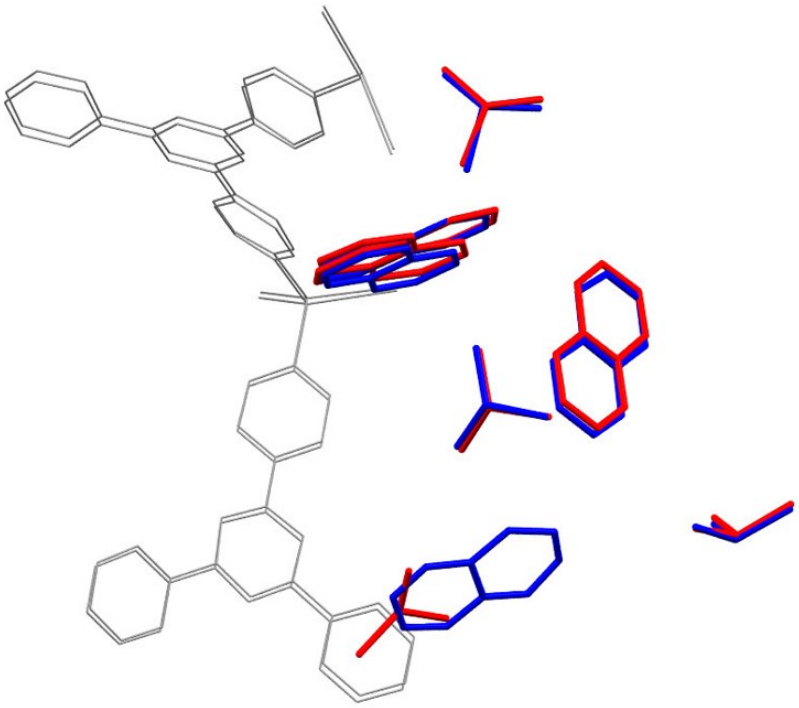

Figure 4.7: Overlaid structures of **1v** (blue) and **1v'** (red) showing equivalent uptake at all but one site. Framework show in grey.

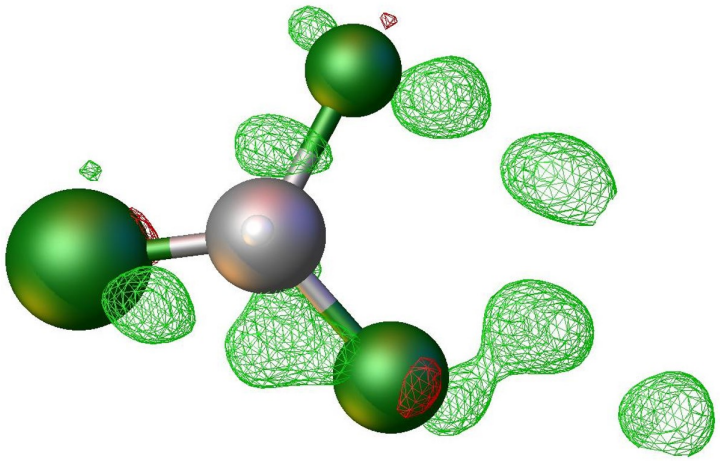

Figure 4.8: Differential electron density map superimposed on the additional $CHCl_3$ molecule found in **1v'** (σ = 0.54). The location of 7 carbon atoms in naphthalene are clear.

	Red	Burgundy	Dark Blue	Light Blue	Dark Green	Light Green	Pink	Yellow	Purple
1i	-	-	75	-	100	100	100	-	100
1i'	-	-	100	-	100	50	90	-	100
1ii	55	-	45	-	-	50	-	-	-
1ii'	35	-	25	-	-	90	-	-	-
1iii	100	-	100	-	-	100	100	100	-
1iii'	100	-	50	50	-	100	100	100	-
1iv	50	50	86	30	44	32	51	68	-
1iv'	60	-	100	-	70	30	50	60	25
1v	-	-	-	-	100	50	-	100	-
1v'	-	-	-	-	-	100	-	72	-

Table 4.3: Occupancies of each guest molecule, initially freely refined and fixed in the final stages of refinement. Colours refer to images of unit cells shown in Figure 4.3.

4.4 CONCLUSIONS

From these five studies it is clear that there is reproducibility in the uptake of guests to specific sites within the unit cell of **1** whether they be solid or liquid. Experiments with naphthalene were not directly comparable due to the difference in crystal soaking duration, but provided interesting insight into the preferential uptake of guests at different sites in the unit cell. Small variations that were observed between repeat encapsulation experiments with liquid guests are likely to stem from marginal differences in external conditions. These are many variables to contend with and even with the utmost care minor variations in experimental procedure must be expected such is the delicacy of the method. Only in a situation whereby experiments were automated might complete reproducibility be obtained. Many factors must be considered. These may be environmental resulting in slight variations in crystal quality that may lead to refinement challenges. However, overall we can be confident guest molecules preferentially take up specific sites within the unit cell of **1** and that repetition of the encapsulation procedure is not routinely required for every new encapsulation complex. This was as expected from a guest encapsulation mechanism under thermodynamic control, allowing guest molecules to reach equilibrated regularly ordered positions and thus capable of creating Bragg peaks and contributing to the diffraction pattern.

4.5 EXPERIMENTAL

4.5.1 *Crystalline Sponge Synthesis*

Crystals of **1** were synthesised according to the adapted literature procedure labelled 'method **B**' in Chapter 3. Crystals harvested from one test tube were split roughly equally between three vials. Crystals used for repeat experiments came from different batches.

4.5.2 *Guest Encapsulation Protocol*

The reaction liquor or crystal storing solution for **1** was reduced to the minimum volume whilst still covering the crystals and the guest solution ($\sim$1 cm^3) pipetted in. Liquid samples (benzene, 4-fluorobenzene, 1,3-dichlorobenzene, benzonitrile and 1,3-dibromobenzene) were used neat and solid samples (naphthalene) as near saturated $CHCl_3$ solutions. If a saturated solution was used the naphthalene was prone to crystallising out. Samples were incubated at 22 °C and guest exchange allowed to proceed for the specific length of time detailed in Table 4.4. Experiments with naphthalene were attempted on both two and three week time scales, a repeat of each of which was attempted. Suitable rod or block shaped crystals were selected (step 6) and subjected to SCXRD.

Complex	Guest molecules	Incubation time /Days
1i and **1i'**	benzene	15
1ii and **1ii'**	4-fluorobenzaldehyde	7
1iii and **1iii'**	1,3-dichlorobenzene	5
1iv and **1iv'**	benzonitrile	7
1v	naphthalene	14
1v'	naphthalene	21

Table 4.4: Specific duration of incubation time of guest soaking.

4.5.3 *Crystallography*

Following the procedure described in Section 3.5.3.

4.5.3.1 *Crystal structure refinement*

Structure refinement began with construction of the rigid MOF framework which proved straightforward and once anisotropically refined any guests and/or solvent molecules present were identified.

This often required up to 200 electron density peaks. The guests were observed in one of three conditions with either (i) 100% occupancy, (ii) partial occupancy (all around ~80%), and/or (iii) statically disordered with two molecules sharing the same site. Soft restraints (such as SIMU, DELU and SADI) were often required to aid the modelling of highly distorted and disordered guest molecules. Hard restraints (such as the DFIX command) were used sparingly and only with caution. If ADP restraints were necessary they were applied only to individual guest molecules – not globally. Where required the aromatic rings of guests were constrained using the AFIX 66 command. Additionally, molecules severely disordered on special positions fragments with idealised geometry were inserted, derived either from structures produced in ChemDraw or from an online library.[130]

For **1i** (Figure 4.9), anisotropic refinements were performed using SIMU on four of the five guest molecules, one of which required the addition of DELU to achieve stable refinement.

For **1i'** (Figure 4.10) anisotropic refinements were performed using SIMU on two of the five guest molecules, one of which required the addition of DELU to achieve stable refinement.

For **1ii** (Figure 4.11) C_{arom}-C=O bond lengths were restrained with SADI. Anisotropic refinement of two of two the guests was performed using SIMU and DELU and for the third using DELU and RIGU, along with FLAT commands.

For **1ii'** (Figure 4.12) C_{arom}-F and C_{arom}-C=O bond lengths restrained using DFIX command. One guest molecule required the use of FLAT. Anisotropic refinements were performed using a combination of DELU, SIMU and/or RIGU.

For **1iii** (Figure 4.13) most guest molecules were anisotropically refined without further constraint/restraint, with only one requiring a combination of DELU and RIGU.

For **1iii'** (Figure 4.14) anisotropic refinements performed using SIMU and DELU displacement parameter restraints.

For **1iv** (Figure 4.15) Anisotropic refinements performed with a combination of DELU, SIMU and/or RIGU. Additional geometric restraints of DFIX and FLAT were required to successfully refine two disordered molecules. A residual $CHCl_3$ solvent molecule was successfully refined anisotropically without restrain/constraint.

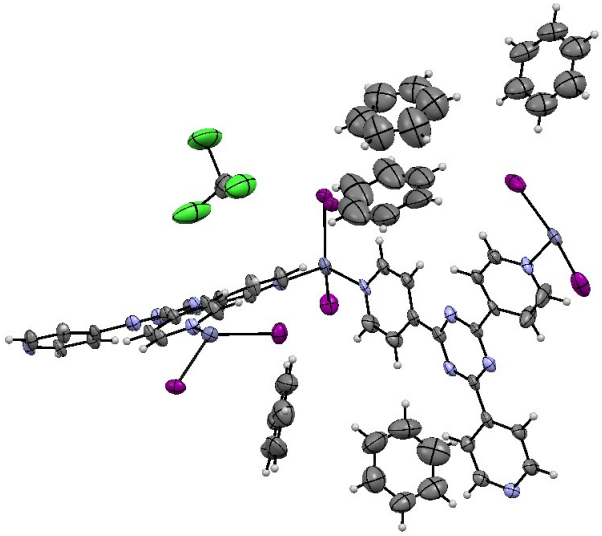

Figure 4.9: Asymmetric unit of **1i**

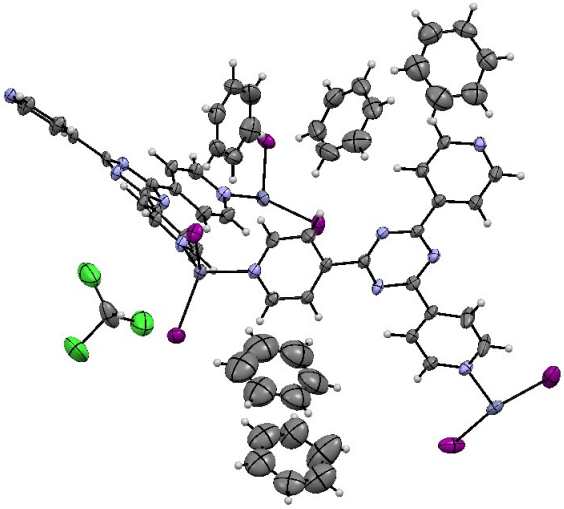

Figure 4.10: Asymmetric unit of **1i'**

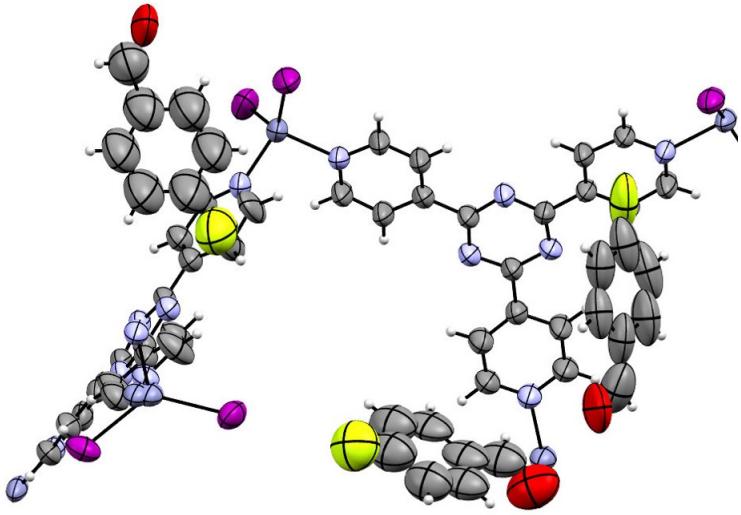

Figure 4.11: Asymmetric unit of **1ii**

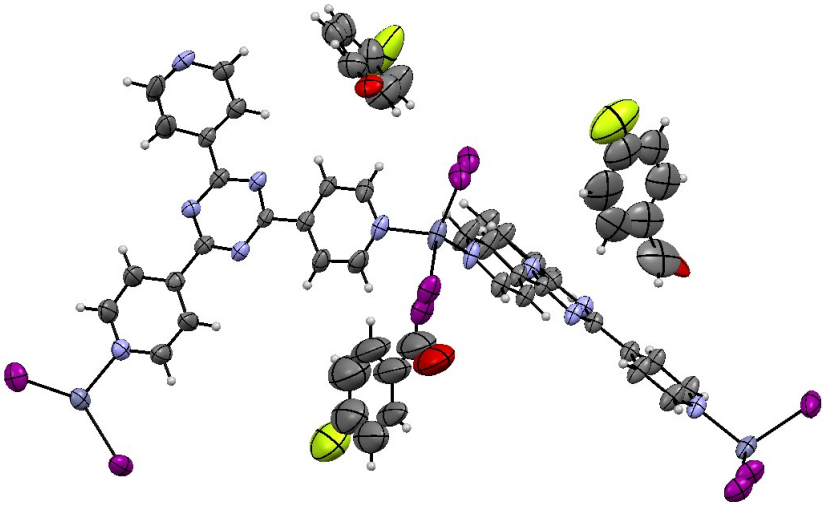

Figure 4.12: Asymmetric unit of **1ii'**

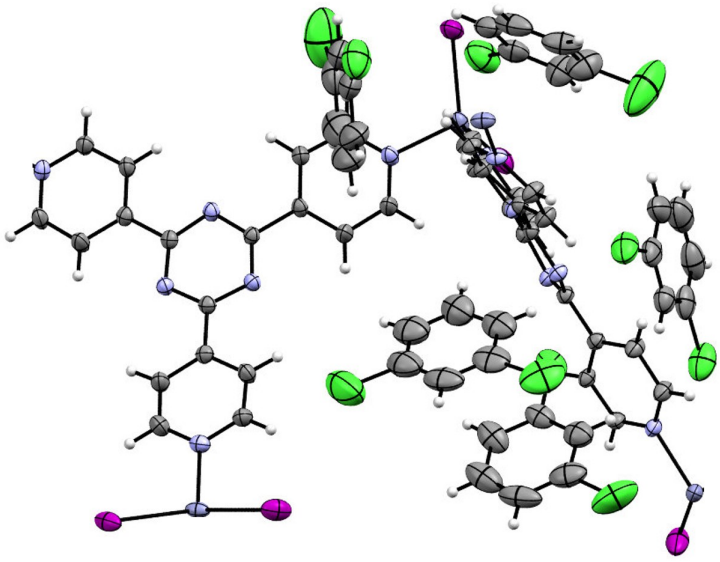

Figure 4.13: Asymmetric unit of **1iii**.

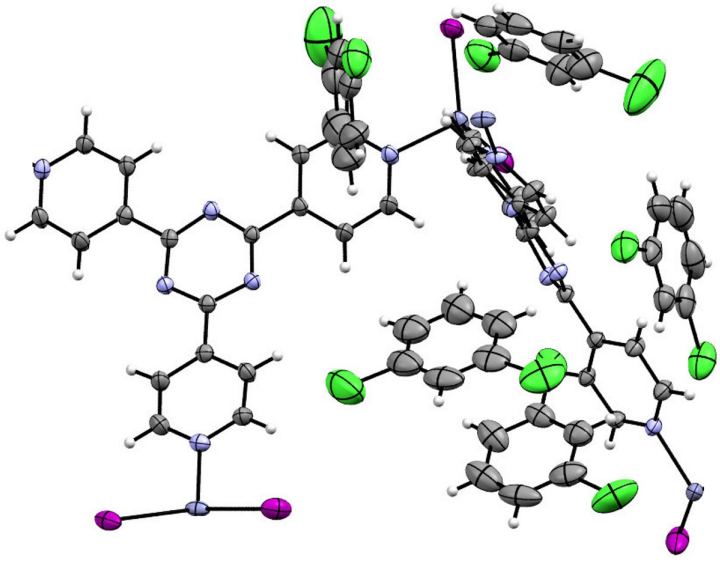

Figure 4.14: Asymmetric unit of **1iii'**.

For **1iv'** (Figure 4.16) anisotropic refinements performed with a combination of DELU, SIMU and/or RIGU. Additional geometric restraints of DFIX and FLAT were required to successfully refined one molecule disordered across two positions.

For **1v** (Figure 4.17) anisotropic refinements performed with a combination of DELU, SIMU and/or RIGU. Additionally two C-C bond lengths in one guest molecule were constrained using the DFIX command. The similarity restraint SADI was used for all C-C bonds lengths in a second guest molecule. One $CHCl_3$ molecule was stable to anisotropic refinement.

For **1v'** (Figure 4.18) anisotropic refinements performed with a combination of DELU, SIMU and/or RIGU. The similarity restraint SADI was used for C-Cl bonds lengths. $CHCl_3$ molecules were partially stable to anisotropic refinement, with some chlorine atoms remaining isotropic resulting in residual electron density in close proximity to Cl atoms.

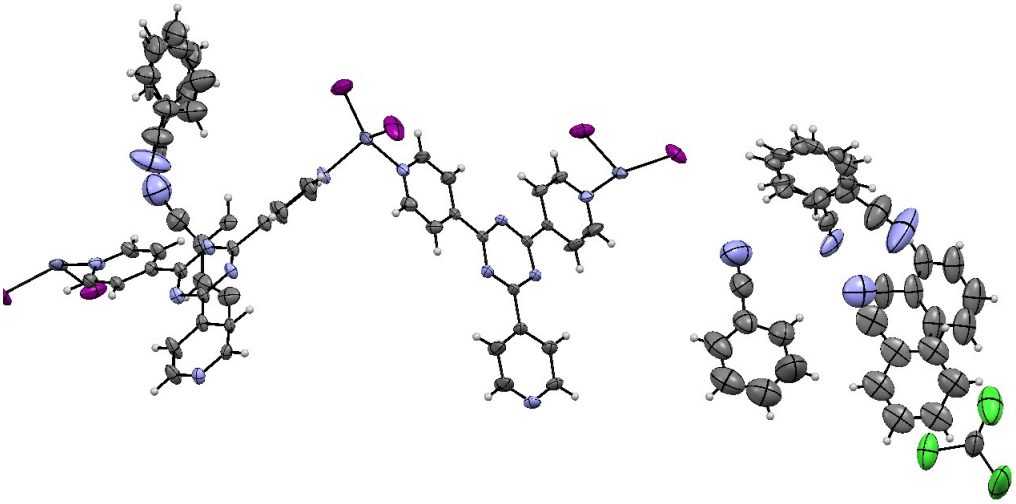

Figure 4.15: Asymmetric unit of **1iv**

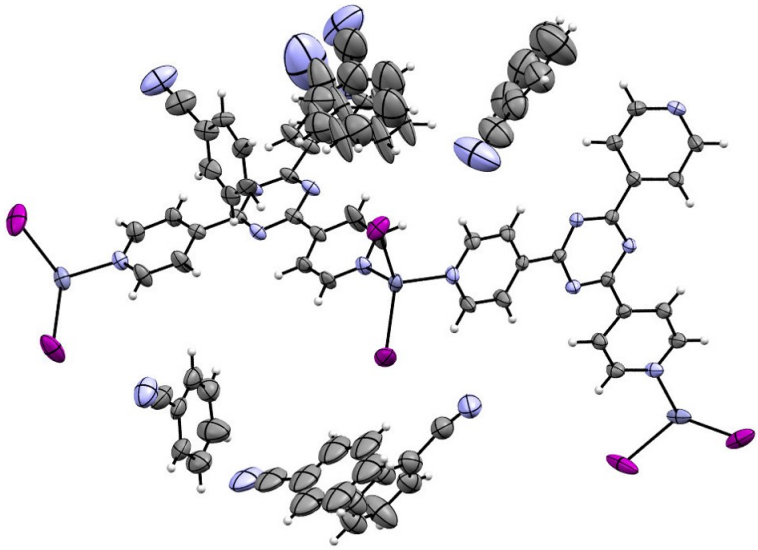

Figure 4.16: Asymmetric unit of **1iv'**

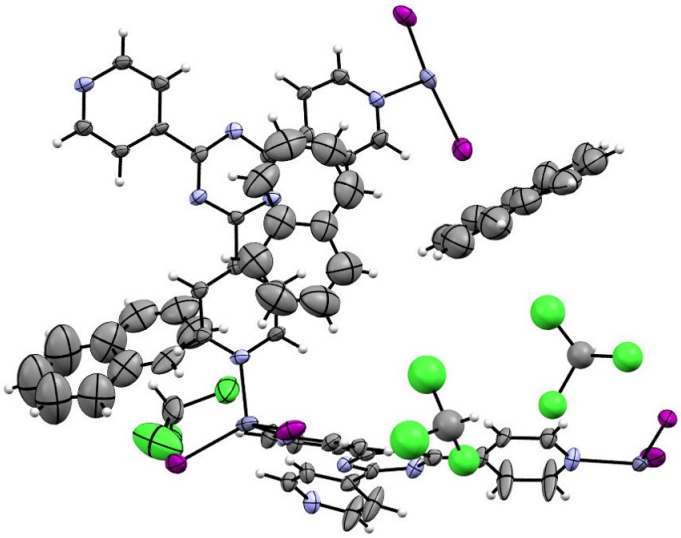

Figure 4.17: Asymmetric unit of **1v**

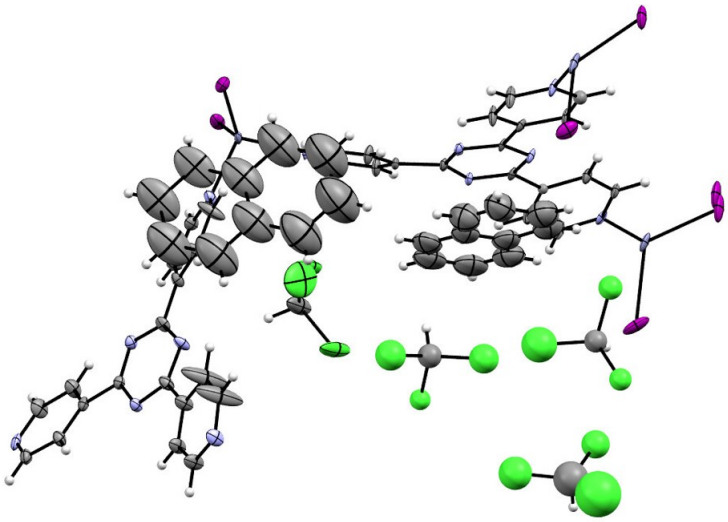

Figure 4.18: Asymmetric unit of **1v'**

5

THE EFFECT OF GUEST FUNCTIONALITY ON UPTAKE

5.1 AIMS

Having reliably determined the reproducibility of guest position in Chapter 4, the aim of this chapter is to detail the uptake and specific locations of a series of chemically related simple functionalized aromatic guest molecules within the pores of $[\{(ZnI_2)_3(TPT)_2 \cdot x(solvent)\}_n]$ (**1**). As no systematic study had been reported previously, the aim is to develop an understanding of the currently used crystalline sponge, its scope, and why it displays such unique properties. Experiments aimed to determine the manner in which guest molecules interact through their aromatic rings and varied functional groups and determine the extent to which guest functionality determines interaction with the host framework and consequential ordering.

5.2 INTRODUCTION

It is not uncommon for some solvent or other residual molecules to be crystallographically identified and refined within the voids of porous materials, but the crystalline sponge technique is designed to make this phenomenon routine.[12] There are over 70,000 metal-organic framework (MOF) structures reported in the Cambridge structural database (CSD) and only a handful of these have been shown capable of behaving as a crystalline sponge (see Section 1.8). The most successful crystalline sponge used to date is the MOF $[\{(ZnI_2)_3(TPT)_2 \cdot x(solvent)\}_n]$ (**1**) developed by Fujita *et al.*.[1]

Although the approach has already been successful (as discussed in Section 1.6) its utility is limited and not yet universally applicable and, at the time of writing, there was no definitive understanding of why these few are capable of ordering guest molecules in such a way as to make then observable by single-crystal X-ray diffraction (SCXRD). The technique is limited when the interactions the host framework is capable of forming are incompatible with the functionality of the intended guest. While this does not necessarily limit encapsulation of a guest, they may still diffuse into the pores, it does prevent the ordering of guest molecules that is intrinsic to this crystallographic method. For example, due to the nature of the organic component in **1** its pores are hydrophobic meaning hydrophillic guests cannot be analysed. Investigation of the specific guest-host interactions formed by the framework with a range of functionalised guests

would contribute directly to building an understanding of the unique properties of **1** and thus assist in the judicious design of alternative crystalline sponge structures.

5.2.1 *Guest Selection*

The following compounds were chosen to create a series of encapsulation complexes with systematic variation in guest functionality; benzene (**i**), 4-fluorobenzaldehyde (**ii**), benzaldehyde (**vii**), fluorobenzene (**viii**) and 1,4-difluorobenzene (**xi**) (Figure 5.1). Following similar reasoning to that described in Section 4.2.1 these potential guests share a common simple aromatic structure to simplify analysis, and enable direct comparison across the series. Only compounds that are liquid at room temperature and miscible with chloroform were chosen to ensure a high concentration gradient during encapsulation experiments. The selection reflects a variety of functional group and thus a potential of a broad range of guest-host interactions. *N.B.* When solvent molecules are present from synthesis they are not referred to as guests - this title is reserved only for those molecules purposefully encapsulated.

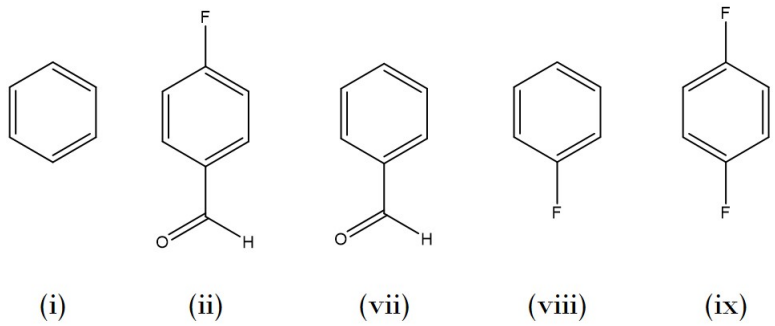

Figure 5.1: Guest compounds chosen for the functionality study are benzene, 1,4-fluorobenaldehyde, benzaldehyde, fluorobenzene, and 1,4-difluorobenzene.

5.3 RESULTS

5.3.1 *Encapsulation Complexes*

Encapsulation experiments were successful in producing the following novel encapsulation complexes:

- **1vii** benzaldehyde
- **1viii** fluorobenzene
- **1ix** 1,4-difluorobenzene

The relevant crystallographic data is reported in Table 5.1, showing all crystallise in the monoclinic space group *C*2/*c* with very similar cell parameters. The asymmetric unit of $[\{(ZnI_2)_3(TPT)_2 \cdot 2.51(C_7H_6O)\}_n]$ (**1vii**) contains benzaldehyde molecules in five unique sites, as shown in Figure 5.2. Guest occupancies were freely refined to 70%, 50%, 50%, 48% and 34%. The encapsulation complex with fluorobenzene $[\{(ZnI_2)_3(TPT)_2 \cdot 3.07(C_6H_5F).0.65(CHCl_3)\}_n]$ (**1viii**) contains four molecules in each asymmetric unit along with one residual $CHCl_3$ molecule (see Figure 5.3). Guest occupancies were freely refined to 100%, 90%, 70% and 47%. Figure 5.4 shows that the asymmetric unit of $[\{(ZnI_2)_3(TPT)_2 \cdot 3(C_6H_4F_2)\}_n]$ (**1ix**) was occupied by four molecules of 1,4-difluorobenzene with freely refine occupancies of 86%, 82%, 72% and 60%. In all three structures guest molecules display larger atomic displacement parameters than the framework signalling greater positional disorder when compared to the framework itself, although there were no instances of disorder in guest orientation.

	1vii	**1viii**	**1ix**
Crystal system	monoclinic	monoclinic	monoclinic
Space group	*C*2/*c*	*C*2/*c*	*C*2/*c*
a/Å	35.3524(4)	35.2547(8)	34.7285(10)
b/Å	14.97971(13)	14.7628(2)	14.8592(2)
c/Å	31.0275(3)	31.0405(6)	30.9411(6)
α /°	90	90	90
β/°	101.9509(10)	101.841(2)	101.514(2)
γ /°	90	90	90
Volume/Å ^{3}	16075.0(3)	15811.5(6)	15645.4(6)

Table 5.1: Crystallographic data for encapsulation complexes with benzaldehyde (**1vii**), fluorobenzene (**1viii**) and 1,4-difluorobenzene (**1ix**).

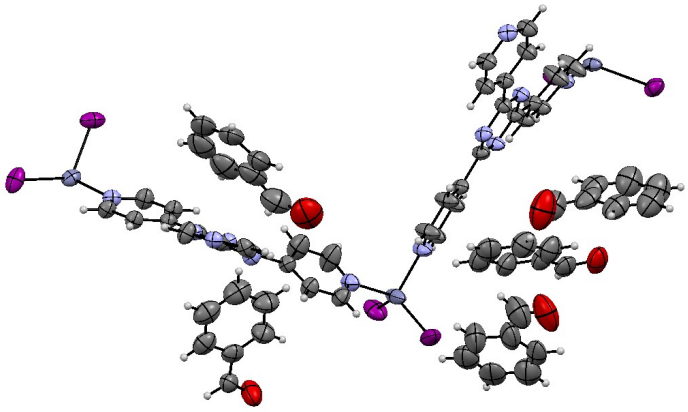

Figure 5.2: Asymmetric unit of **1vii**.

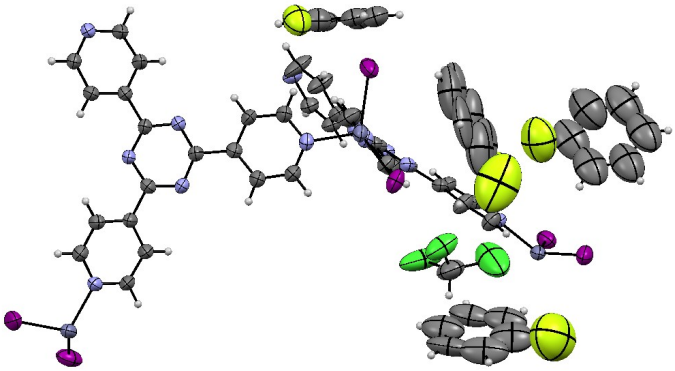

Figure 5.3: Asymmetric unit of **1viii**.

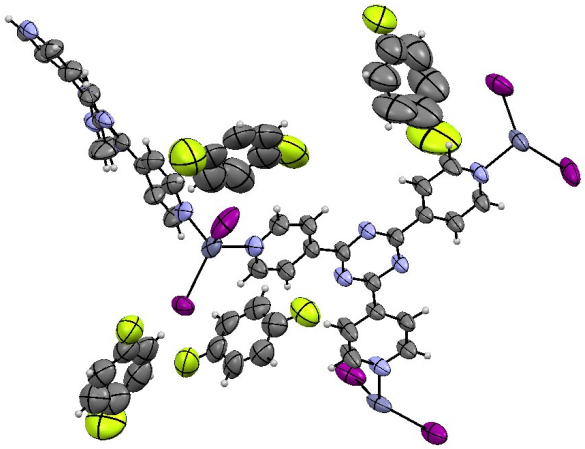

Figure 5.4: Asymmetric unit of **1ix**.

5.3.2 *Analysis of Guest-Host Interactions*

As well as the novel encapsulation complexes reported in this chapter, structures with benzene (**1i**) and 4-fluorobenzaldehyde (**1ii**) guests reported in Chapter 4 were re-analysed in the context of this study to produce the systematic series of guest-host compounds. Packing diagrams showing the unit cells of the resultant five inclusion complexes as viewed down the *b-axis* are shown in Figure 5.5. Guest molecules are coloured by their symmetry equivalence within their own inclusion complex and also positional equivalence to guests in the other four structures. It is immediately apparent that certain positions within the unit cell are particularly favourable. A detailed examination of the packing diagrams and short contacts as defined in Mercury[131] gives a clear indication of the dominant interactions. These are (i) electrostatic aromatic interactions (both CH$\cdots\pi$ and $\pi\cdots\pi$ stacking), (ii) hydrogen bonding (N$\cdots$HC(=O) 2.90 Å , F$\cdots$HC $\leqslant$2.67 Å) between the aldehyde group and fluorine atom donors, and (iii) weaker, longer range van der Waals interactions.

5.3.2.1 *Site uptake common to all crystal structures*

Comparing the encapsulation complexes across the series it is clear that systematic variation of guest functionality does not always give rise to different guest positions within the unit cell. Figure 5.5 shows the packing diagrams of all five guest-host crystal structures. As guest molecules are coloured by symmetric equivalence to other molecules in the same unit cell and also across the series, differences in site occupation are easily identified.

It is evident that one specific position is taken up commonly irrespective of functionality, observable in Figure 5.5 by the blue colouration of guest molecules. Molecules in this site adopt a perpendicular y-shaped orientation with respect to the pyridine ring of the framework through the formation of a CH$\cdots\pi$ interaction(s). The length of the interaction varied between guest molecule, as shown in Table 5.2. The effect of guest functionality appears to be minimal in this position for **1i**, **1ii**, **1vii** and **1viii**, with broadly similar intercentroid distances ranging from 4.83 - 5.46 Å. These guest molecules are orientated such that they are in proximity to interact with only one framework pyridine ring. In contrast, the orientation of 1,4-difluorobenzene molecules in **1ix** is sufficiently displaced such that it interacts with two, with intercentroid distances of 5.43 and 5.57 Å. Distances 2 and 3 quantify this orientation in terms of the inclination of the guests' ring and are reported for all guests in Table 5.2. Generally distances 2 and 3 are within ~0.5 Å of each each other except for 1,4-difluorbenzene which vary by >0.7 Å. This is visualised in Figure 5.6 showing the orientation of 1,4-difluorobenzene compared

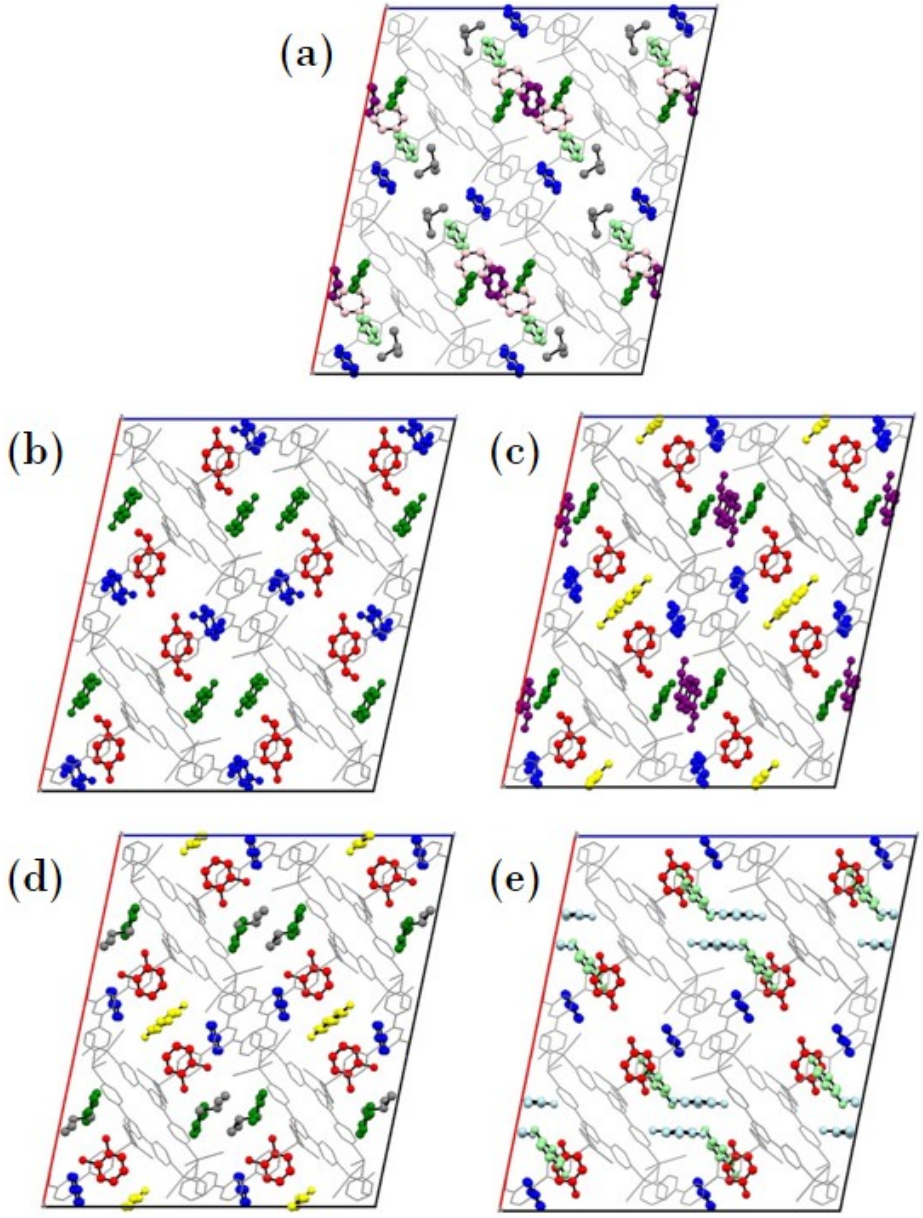

Figure 5.5: Unit cells of encapsulation complexes (a) **1i** (benzene) (b) **1ii** (4-fluorobenzaldehyde), (c) **1vi** (benzaldehyde), (d) **1vii** (fluorobenzene) and (e) **1ix** (1,4-difluorobenzene) viewed down the *b*-axis. The colouring of guest molecules indicates positional equivalence both within each structure and between the five.

Guest		Length / Å			Angle / °	
		1	2	3	α	β
Benzene	**1i**	4.83	3.28	3.16	119.69	123.91
4-fluorobenzaldehyde	**1ii**	5.46	3.86	3.56	125.18	137.91
Benzaldehyde	**1vii**	4.91	3.41	3.01	118.64	135.76
Fluorobenzene	**1viii**	5.14	3.75	3.17	116.04	141.69
1,4-difluorobenzene	**1ix**	5.57	4.36	3.54	111.28	146.97
1,4-difluorobenzene	**1ix**	5.43	4.20	3.46	110.99	140.80

Table 5.2: Four parameters defined in Figure 5.6 used to describe CH$\cdots\pi$ interactions between the hydrogen substituents of the 'blue' guest molecules in **1i**, **1ii**, **1vii**, **1viii** and **1ix**.

to 4-fluorobenzaldehyde (representative of the remainder of guests) in relation to the section of the framework with which they interact. These subtle variation in orientation reflects the substituent effect of the electron withdrawing functional groups on the nature of the aromatic ring. Additional stabilisation appears to be gained in all cases from several interactions between both hydrogen and non-hydrogen ring substituents and the triazide or pyridine rings of the host.

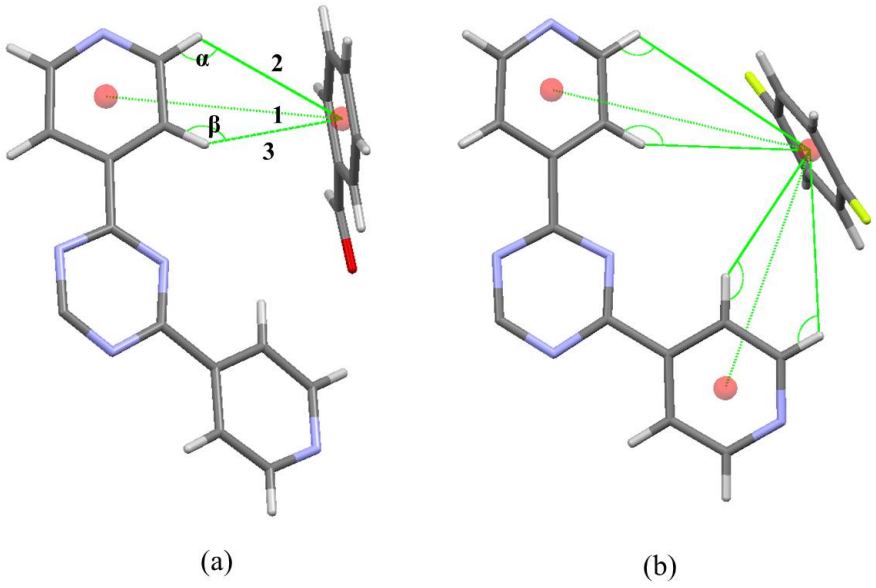

Figure 5.6: (a) Perpendicular y-shaped interaction of fluorobenzaldehyde and the host framework in **1ii**, representative of interaction in **1vii** and **1viii** (b) Offset y-shaped interaction of 1,4-difluorobenzene in **1ix**. Both in the 'blue'site. Distances and angles reported in Table 5.2.

5.3.2.2 *Site uptake common to some crystal structures*

Looking again at Figure 5.5 two sites can be identified as common to four of the five guest species. Guest molecules in these sites are coloured red (common to structures **1ii**, **1vii**, **1viii** and **1ix**) and dark green (in **1i**, **1ii**, **1vii** and **1viii**). In each site guest molecules were anchored in their general positions by aromatic interactions, whilst more subtle variation in ring inclination and functional group orientation were observed across the series.

Green Site

The interactions governing the positioning of guests coloured dark green is shown in Figure 5.7 and is broadly similar to the guest-host y-shaped CH$\cdots\pi$ interactions discussed above for the 'blue' site. Table 5.3 presents the characteristic parameters of CH$\cdots\pi$ interactions with contact distances showing that benzene and fluorobenzene in **1i** and **1viii** were positioned almost identically, as were benzaldehyde in **1ii** and fluorobenzaldehyde in **1vii**. The differences observed in orientation between these two pairs are thought to originate in the ability of those with aldehyde functionality to form additional interactions. Contact measurements reveal the presence of C(H)=O$\cdots$HC$_{\mathrm{pyridine}}$ interactions formed between **ii** and **vii** and the framework (at 2.64 and 2.89 Å, respectively).

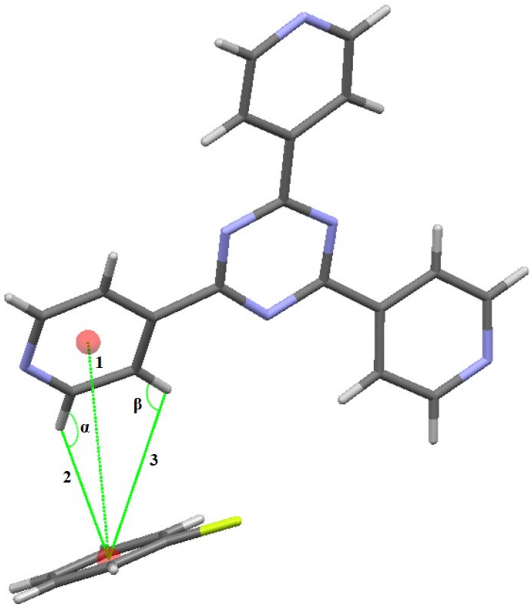

Figure 5.7: (a) Perpendicular y-shaped interaction of fluorobenzene and the host framework in **1vi**, representative of interaction in **1i**, **1v** and **1vi** at the 'green 'site.

Guest		Length /Å			Angle /°	
		1	2	3	α	β
Benzene	**1i**	4.84	2.93	3.71	135.28	105.07
Fluorobenzene	**1viii**	4.82	2.93	3.69	135.59	105.53
4-fluorobenzaldehyde	**1ii**	5.61	3.49	4.91	149.84	95.66
Benzaldehyde	**1vii**	5.38	3.28	4.49	149.35	100.35

Table 5.3: Parameters used to describe CH$\cdots\pi$ interactions between the substituents of the 'green' guest molecules in **1i**, **1ii**, **1vii** and **1viii**. Lengths and angles defined in Figure 5.7.

Red Site

Guests indicated by red colouration in structures **1ii**, **1vii**, **1viii** and **1ix** (Figure 5.5) engage in face-to-face $\pi\cdots\pi$ interactions with the pyridine ring that crosses the porous chamber of the crystalline sponge. Only benzene does not take up this position, suggesting the importance of the others guests' functional groups in facilitating this specific $\pi\cdots\pi$ interaction. The absence of benzene can be rationalised by considering the electron withdrawing nature of functional groups and how this may affect the orientation of the interaction. Relative to -H substituents in benzene, -C(O)H and -F favour a face-to-face $\pi\cdots\pi$ arrangement with the electron deficient framework.

As noted in previous cases, the intermolecular centroid-centroid distances are not obviously affected by the identity of the guests' substituent groups. Inter-centroid contact measurements give $\pi\cdots\pi$ interaction distances of 3.72, 3.69, 3.79 and 3.78 Å for **1ii**, **1vii**, **1viii** and **1ix** respectively, with all dihedral angles between mean planes of the guest and host rings found to be $<13°$. Figure 5.8a shows the 4-fluorobenzaldehyde guest in this red site, highlighting the face-to-face interaction with the pyridine ring of the framework that is common to all. Looking more closely at the subtle positioning of guest molecules within this site, highlighted in Figure 5.8b-e by observing all guests from the same crystallographic direction, it is clear that varied orientations arose due to functional groups.

Substituents involved in these guest-host interactions are orientated towards the pyridine and triazide rings of TPT, rather than into the empty void space of the pores. This enables the formation of (O=)CH$\cdots$N$_{triazide}$ hydrogen bonds by benzaldehyde and 4-fluorobenzaldehyde (short contacts 2.84 and 2.54 Å, respectively). In 4-fluorobenzaldehyde this leaves the fluorine atom substituent pointing into the void space, unable to form any significant interactions with the framework. This is unsurprising as C-F groups compete unfavourably with aldehyde groups when it comes to

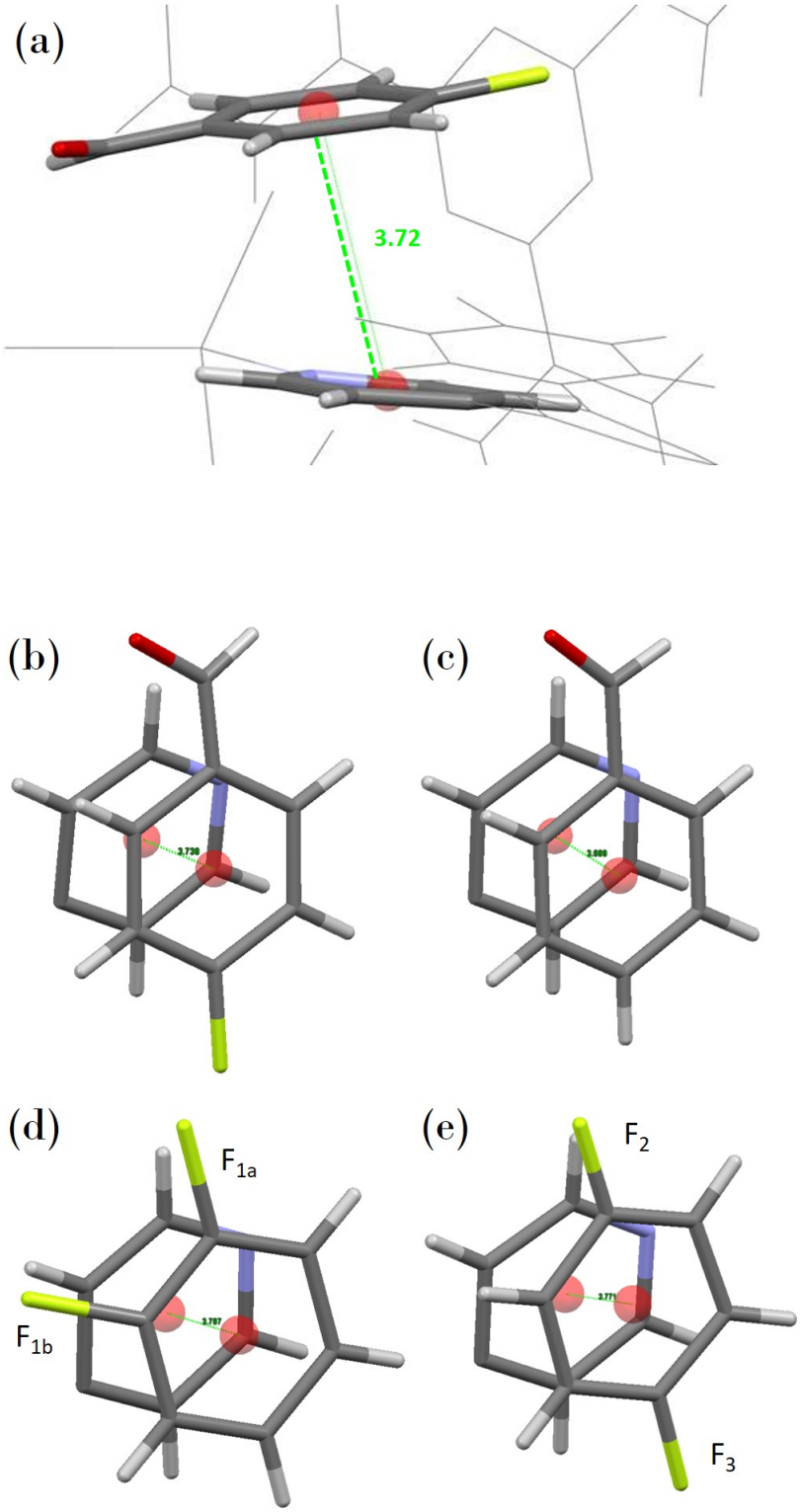

Figure 5.8: Face-to-face $\pi \cdots \pi$ interactions in the encapsulation complexes between the aromatic ring of guest molecules and a pyridine ring, at a common site within the unit cell; (a) and (b) 4-fluorobenzaldehyde **1ii** (c) benzaldehyde **1vii** (d) fluorobenzene **1viii** (rotational disorder shown, F_{1a} and F_{1b} occur with 50% occupancy each) and (e) 1,4-difluorobenzene **1ix** (fluorine atoms labelled to distinguish them). Centroids shown as red spheres and intercentroid contacts as green lines.

hydrogen bond formation. The orientation of 4-fluorobenzaldehyde therefore maximises the interaction with the framework contributing to a thermodynamically more stable position. Additionally, there is suggestion of weak $F_{red} \cdots F_{red}$ intermolecular guest-guest interactions at 3.14 Å which are likely to be a consequence of the stronger interactions that dictated overall orientation.

In the case of fluorobenzene (**1viii**, Figure 5.8d) the fluorine atom takes up a similar position to the absent aldehyde group, interacting with the equivalent part of the framework albeit with a longer contact distance. Contact measurements give these interactions as $F_{1a} \cdots N_{triazide}$ (3.11 Å) and $F_{1a} \cdots C_{triazide}$ (3.13 Å). Similarly, the closest contacts of the fluorine substituent on the equivalent 1,4-fluorobenzene guest in **1ix** are $F_2 \cdots C_{triazide}$ (3.16 Å) and $F_3 \cdots N_{triazide}$ (3.26 Å). As with 4-fuorobenzaldehyde, analysis of the para F-atom (F_3) yielded no significant short contact measurements. However, without this second substitution fluorobenzene (**1viii**) is positionally disordered, with 50:50 occupancy of two positions (Figure 5.8d). This suggests that the interaction of a single fluorine is insufficient to strongly anchor the molecule. The interaction determining this second orientation appears to be $F_{1b} \cdots HC_{pyridine}$, in the range of a weak hydrogen bond at 2.78 Å.

There are other positions within the unit cells of the encapsulation complexes that are taken up by more than one species guest. Such sites are indicated by purple coloured guests in **1i** and **1vii** (Figure 5.5a and Figure 5.5c respectively) and yellow in **1vii** and **1viii** (Figure 5.5c and Figure 5.5d respectively).

5.3.2.3 *Sites occupied by only one guest species*

There are instances where sites were taken up uniquely by certain guest species. For example, in encapsulation complex **1ix** there were two positions which were unique to 1,4-difluorobenzene, identified in Figure 5.5e as occupied by light green and light blue guest molecules. Analysis of the guest-host contacts do not show any particularly favourable interactions specific to 1,4-difluorobenzene. Instead, they were predominately aromatic in nature. Stabilising interaction for guests coloured light green appear to be a result of multiple interactions with framework pyridyl rings through both CH$\cdots\pi$ (3.43 Å, dihedral angle 74.21°) and $\pi\cdots\pi$ interactions (dihedral angle 10.24° and intercentroid distance of 3.93 Å). Similarly molecules coloured light blue display $\pi\cdots$CH interactions with a single pyridyl ring (3.48 Å, dihedral angle 56.54°). Given the importance of these aromatic interactions in determining guest position in this site, the question remains as to why these particular positions are only occupied by 1,4-difluorobenzene molecules. The answer could be the formation of CF$\cdots HC_{pyridine}$ interactions (F$\cdots$H 2.69 Å) between 1,4-difluorobenzene and the framework. However, if this interaction

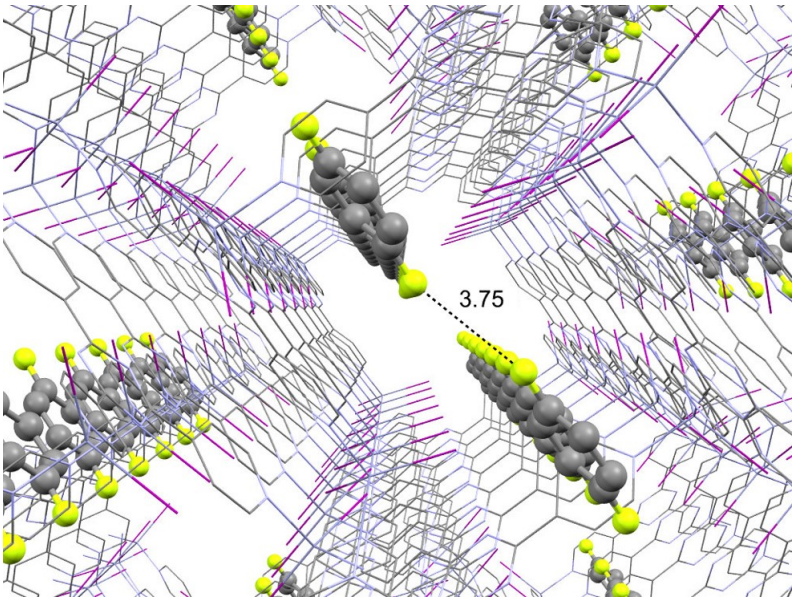

Figure 5.9: Crystal structure of **1ix** with 1,4-fluorobenzene molecules displaying a potential long range F···F interaction. Other guests and hydrogen atoms omitted for clarity.

is key it explains the absence of only 2 of the guests - those without fluoride functionality (benzene and benzaldehyde), but does not explain the absence of fluorobenzene and 4-fluorobenzaldehyde. The answer therefore may be the formation of fluorine-hydrogen bonds formed between guest molecules which may aid in the stabilisation and ordering of the guest; $F_{lightgreen}\cdots H_{red}$ interaction (2.50 Å), and two $H_{green}\cdots F_{pink}$ interaction (3.13 and 3.18 Å). Additionally, a potential long-range interaction between symmetry equivalent molecules was possible in the form $F_{lightgreen}\cdots F_{lightgreen}$ (3.75 Å) as shown in Figure 5.9. This is only facilitated by the *para* substitution of 1,4-difluorobenzene.

5.4 CONCLUSION

The crystal structure of novel encapsulation complexes with benzaldehyde (**1vii**), fluorobenzene (**1viii**) and 1,4-difluorobenzene (**1ix**) have been obtained. This has extended the scope of the crystalline sponge technique by providing more evidence for its ability to encapsulate functionalised aromatic molecules. These three structures, along with structures previously reported with benzene (**1i**) and 4-fluorobenzaldehyde (**1ii**), form a systematic series for the analysis of guest-host interactions. Comparisons of the crystal structures showed many sites within the unit cell of **1** were favourable regardless of guest functionality whilst some were taken up only by specific guests. We can be confident of the dominant role of $\pi\cdots\pi$ and CH$\cdots\pi$ interactions in dictating the position and regular ordering of the guest molecules as they persist throughout the structures. CH-π interaction were seen to take y-shape orientations, which was offset in the case of 1,4-difluorobenzene. There was further evidence for the importance of diverse interactions between functional groups and the framework. Strong and weak hydrogen bonds formed by aldehyde and fluorine groups have been observed as influencing guest ordering, specifically in determining the orientation of guest molecules.

5.5 EXPERIMENTAL

5.5.1 *Crystalline Sponge Synthesis*

Crystals of **1** were synthesised according to the adapted literature procedure labelled 'method **B**' in Chapter 3, in the form **1•(CHCl$_3$)**.

5.5.2 *Guest Encapsulation Protocol*

The crystal storing solution for **1•(CHCl$_3$)** was reduced to the minimum volume whilst still covering the crystals and the guest solution ($\sim$1 cm^3) pipetted in. As the guests investigated in this chapter are all liquid at room temperature they were used neat. Samples were incubated at 22°C and guest exchange allowed to proceed for the specific lengths of time detailed in Table 5.4.

5.5.3 *Crystallography*

Following the procedure described in Section 3.5.3.

Complex	Guest molecules	Incubation time / Days
1vi	benzaldehyde	7
1vii	fluorobenzene	5
1ix	1,4-difluorobenzene	5

Table 5.4: Specific duration of incubation time of guest soaking.

5.5.3.1 *Crystal structure refinement*

Structure refinement began with construction of the rigid MOF framework which proved straight forward and once anisotropically refined the guests and any residual solvent molecules present were identified. This often required the generation of up to 200 electron density peaks. The guests were observed in one of three conditions with either (i) 100 % occupancy, (ii) partial occupancy (all around ~80%), and/or (iii) statically disordered with two molecules sharing the same site. Soft restraints (such as SIMU, DELU and SADI) were often required to aid the modelling of highly distorted and disordered guest molecules. Hard restraints (such as DFIX) were used sparingly and with caution. Where required the aromatic rings of guests were constrained using the AFIX 66 command.

For **1vi** Anisotropic refinements performed with a combination of DELU, SIMU and/or RIGU.

For **1vii** C_{arom}-F bond lengths were restrained using SADI or DFIX commands. Anisotropic refinements were performed using a combination of DELU, SIMU and/or RIGU. A residual $CHCl_3$ solvent molecule was successfully refine anisotropically without restrain/constraint.

For **1ix** C_{arom}-F bond lengths restrained using DFIX command. One guest molecule required the use of FLAT. Anisotropic refinements were performed using a combination of DELU and SIMU.

6

THE EFFECT OF GUEST SIZE ON UPTAKE

6.1 AIMS

The aim of the experiments reported in this chapter is to further investigate novel encapsulation complexes of **1**, specifically the effect of guest size on uptake, position and orientation within the framework. By fresh analysis of the structures with benzene (**1i**), naphthalene (**1v**) and benzonitrile (**iv**) reported in Chapter 4 and Chapter 5 in the context of additional novel structures, this work sets out to create several series of encapsulation complexes with systematic increases in guest size to contrast and compare, in relation to guest position, orientation and interaction with the framework.

6.2 INTRODUCTION

The crystalline sponge method relies on the ability of the host framework to interact with introduced guest molecules and render them regularly ordered. Factors affecting the strength of these interactions are pore size (the closer the pore size correlates with guest size the higher the potential for numerous interactions, which in the van der Waals interaction quantity is of utmost importance), pore aperture (the guest must be able to access the pores[1]), and functionality of the guest. Through the encapsulation of guest molecules of systematically varying size into the pores of the most successful crystalline sponge $[\{(ZnI_2)_3(TPT)_2 \cdot x(solvent)\}_n]$ (**1**), investigation of the specific guest-host interactions formed will be facilitated and the method's scope and any limitations can be further probed.

6.2.1 *Guest Selection*

The following compounds were chosen as potential guests for investigation in this study; acetophenone (**x**), *trans*-cinnamaldehyde (**xi**), anthracene (**xii**), tetracene (**xiii**) benzylcyanide (**xiv**), phenol (**1xv**) and 2,6-diisopropylphenol (**xvi**). They were chosen for their aromaticity and simplicity and to compliment each with the aim of producing a set of guest series displaying systematic increases in guest size in combination with some previously reported

1 In the case of encapsulation by guest exchange, which is preferable to co-crystallisation (see Figure 1.12).

encapsulation complexes (Figure 6.1). A further requirement was that the guest was a liquid at room temperature or readily soluble in a suitable solvent (*e.g.* chloroform, cyclohexane, dichloromethane or dichloroethane).

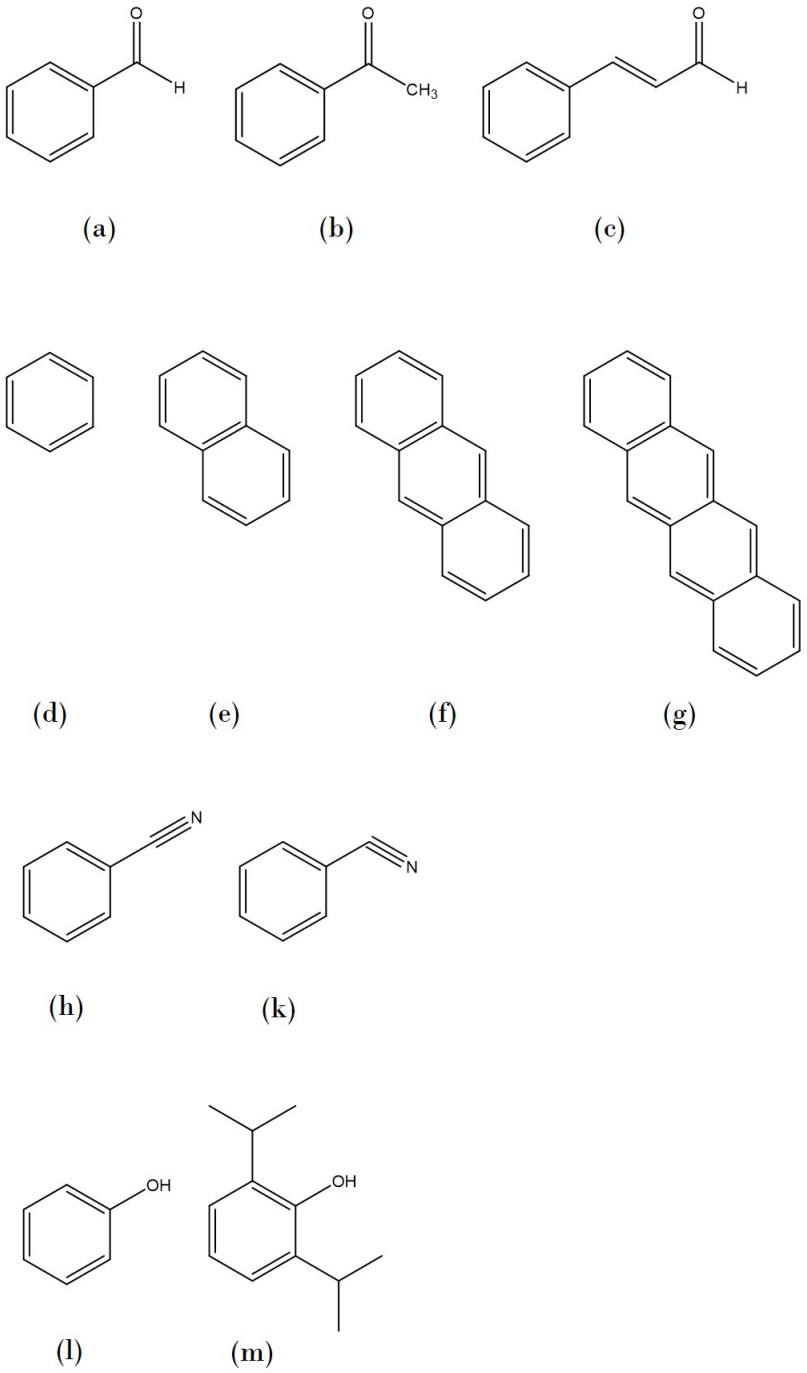

Figure 6.1: Guest molecules chosen to make up four systematic series were: (a) benzaldehyde, (b) acetophenone, (c) *trans*-cinnamaldehyde, (d) benzene, (e) naphthalene, (f) anthracene, (g) tetracene, (h) benzonitrile, (i) benzylcyanide, (j) phenol, and (k) 2,6-diisopropylphenol.

6.3 RESULTS

6.3.1 *Encapsulation Experiments*

Encapsulation experiments were performed using either the neat liquid guest (acetophenone, *trans*-cinnamaldehyde, benzylcyanide, phenol and 2,6-diisopropylphenol) or highly concentrated solutions (anthracene and tetracene). To obtain successful encapsulation complexes with anthracene and tetracene they were dissolved in $CHCl_3$ and cyclohexane, respectively. Encapsulation of phenol was tested at a range of concentrations, diluted with $CHCl_3$ and cyclohexane. However, no attempts were successful as the framework (**1**) was degraded in all cases. Synthesis of the crystalline sponge followed the preferred literature procedure.[119] The result was the preparation of new encapsulation complexes with acetophenone (**1x**), *trans*-cinnamaldehyde (**1xi**), anthracene (**1xii**), tetracene (**1xiii**), benzylcyanide (**1xiv**) and 2,6-diisopropylphenol (**1xv**). The structure with tetracene was only partially successful, whilst encapsulation experiments with phenol where unsuccessful. With the addition of previously reported structures with benzene (**1i**), naphthalene (**1v)**, benzaldehye (**1vii**), and benzonitrile (**1iv**) four systematic series were put together for facile comparison of the effect of guest size on uptake and orientation:

- **Series A**: benzaldehyde, acetophenone, *trans*-cinnamaldehyde
- **Series B**: benzene, naphthalene, anthracene and tetracene
- **Series C**: benzonitrile and benzyl cyanide
- **Series D**: phenol and 2,6-diisopropyphenol

6.3.2 *Crystal Structures*

The key refinement indicators for the new encapsulation complexes reported in this chapter are listed in Table 6.1, with full details in Appendix A. A report on specific guest uptake and occupancy is detailed in the following sections.

6.3.2.1 ***1x**: $[\{(ZnI_2)_3(TPT)_2 \cdot 1.73(C_8H_8O)\}_n]$*

Molecules of acetophenone take up three unique sites in the asymmetric unit of **1x**. Guest occupancies were freely refined to 64%, 59% and 50%.

6.3.2.2 ***1xi**: $[\{(ZnI_2)_3(TPT)_2 \cdot 9(C_9H_8O).0.85(CHCl_3)\}_n]$*

An encapsulation complex of *trans*-cinnamaldehyde has been previously reported (Cambridge Crystallographic Database refcode

REXDUV).[1] However the conditions of encapsulation were different. Cyclohexane was used as guest solvent in the literature whilst $CHCl_3$ was used here, affecting the residual solvent present in the crystal lattice. **1xi** crystallises in the triclinic space group $P\bar{1}$ rather than $C2/c$ as per the literature structure. The crystal structures also differ as the previously reported structure contained one crystallographically unique *trans*-cinnamaldehyde molecule per asymmetric unit, while the new structure contains nine, all with 100% site occupancy. Upon encapsulation of *trans*-cinnamaldehyde into the pores of **1**, the framework underwent a single crystal-single crystal transformation.

6.3.2.3 ***1xii***: *$[\{(ZnI_2)_3(TPT)_2 \cdot 0.5(C_{14}H_{10}).1.85(CHCl_3)\}_n]$*

There is one molecule of anthracene in the asymmetric unit of **1xi** at 50% occupancy along with 4 $CHCl_3$ molecules, one of which is positionally disordered. An encapsulation complex of anthracene has been previously reported (CCD refcode FARFOU).[48] As with *trans*-cinnamaldehyde the condition of encapsulation was different, with $CHCl_3$ used here rather than cyclohexane in the literature. Whilst the guest molecules in the literature were only isotropically refined, **1xii** contained a more highly ordered guest which could be stably refined anisotropically.

6.3.2.4 ***1xiii***: *$[\{(ZnI_2)_3(TPT)_2 \cdot 0.54(C_{14}H_8).0.25(C_6H_{12}).0.97(CHCl_3)\}_n]$*

Experiments for the encapsulation of tetracene were partially successful. Upon soaking in a saturated $CHCl_3$ guest solution a subtle colour change from nearly colourless to yellow was observed in crystals of **1**. After 3 weeks, a single crystal was extracted and subjected to SCXRD. The framework was anisotrophically refined and two molecules of $CHCl_3$ identified (40% and 57% occupancy) and one molecule of cyclohexane (25%) in the asymmetric unit. A partially complete molecule of tetracene (occupancy 54%) was observed with electron density assignable to three of the four rings making up tetracene. Figure 6.2 shows the asymmetric unit of **1xiii** along all three crystallographic axis along with unassigned electron density peaks shown as brown spheres. It is clear no electron density exists which is assignable to the missing carbon atoms. Overall, the refinement indicators were not satisfactory and this structure was not used for comparison as planned in series B.

6.3.2.5 ***1xiv***: *$[\{(ZnI_2)_3(TPT)_2 \cdot 2.86(C_8H_7N)\}_n]$*

Benzylcyanide guest molecules take up 5 crystallographically unique positions in the asymmetric unit of **1xiv**. One guest molecule can be identified only by the aromatic ring carbons and the substituent position is ambiguous. Guest occupancies were refined as of 60%, 52%, 42% and 74%.

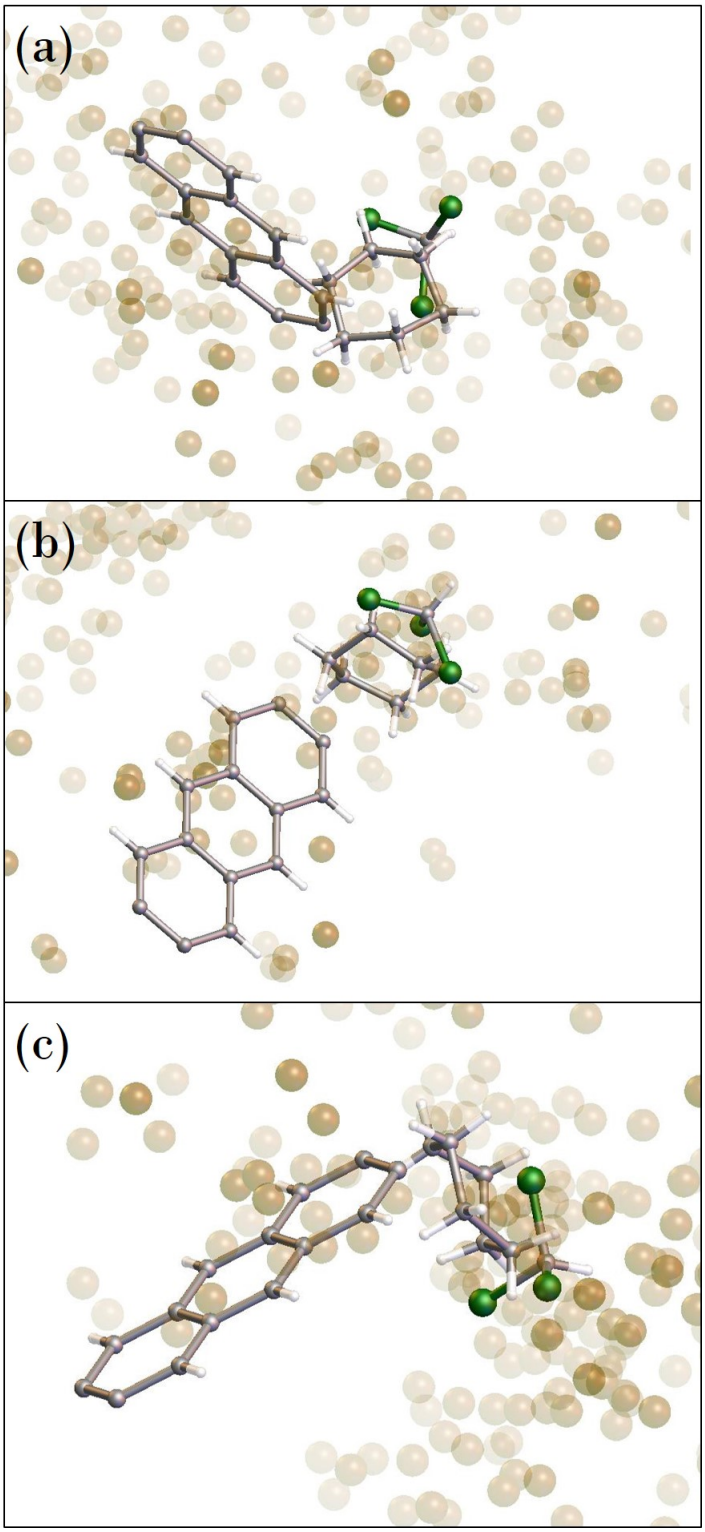

Figure 6.2: Refinement of the tetracene guest in structure **1xiii**. Electron density peaks show no final ring as view down (from top) the *a*-, *b*-, and *c-axis*. 200 electron density peaks generated, highest = 3.2 e^{-}, lowest = 0.18 e^{-}.

6.3.2.6 ***1xvi***: *[{$(ZnI_2)_3(TPT)_2$•2.24($C_{12}H_{15}OH$).0.64($CHCl_3$)}$_n$]*

Three 2,6-diisopropylbenzene molecules occupy the asymmetric unit of **1xvi** together with one disordered $CHCl_3$ molecule (65%). One guest molecule was disordered over a crystallographic two-fold axis. The guest occupancies were 100%, 80% and 45%.

6.3.3 *Effect of Guest Size on Unit Cell Dimensions*

One difficulty that arose during the preparation of encapsulation complexes was ascertaining whether the guest had successfully diffused into the pores before subjecting crystals to full SCXRD analysis. IR analysis has been used to confirm the successful exchange of nitrobenzene for cyclohexane in the pores of **1** (see Section 3.3.1.3). However, it was impractical to perform routinely as it resulted in destruction of the crystal due to solvent evaporation and consequential cracking. Therefore there was interest in determining whether any expansion or contraction of the unit cell could signify guest uptake. Indeed this was a common question encountered when discussing implementation of the technique with others during poster sessions of British and European Crystallographic Association conferences. The unit cell parameters of the structures first reported in this chapter are shown in Table 6.1. Unfortunately there does not appear to be a correlation in unit cell expansion or contraction and the size of the guest molecule encapsulated. Looking back to Table 4.1, Table 4.2 and Table 5.1 listing unit cell parameters of the structures analysed in previous chapters this conclusion is corroborated.

	1x	**1xi**	**1xii**	**1xiii**	**1xiv**	**1xv**
Crystal system	monoclinic	triclinic	monoclinic	monoclinic	monoclinic	monoclinic
Space group	*C*2/*c*	$P\bar{1}$	*C*2/*c*	*C*2/*c*	*C*2/*c*	*C*2/*c*
a/Å	35.8613(5)	14.9658(2)	35.4076(6)	35.2062(7)	35.0502(3)	35.9799(10)
b/Å	14.89535(19)	18.5746(4)	14.8501(2)	14.7703(2)	15.05034(8)	14.7798(2)
c/Å	30.8845(5)	32.5237(5)	30.9056(6)	31.9046(6)	31.3752(2)	30.8321(4)
α /°	90	81.3686(16)	90	90	90	90
β/°	101.9903(14)	89.5249(12)	101.9719(18)	103.2482(18)	102.5307(8)	101.9660(19)
γ /°	90	68.9668(17)	90	90	90	90
Volume/Å^3	16137.5(4)	8332.9(3)	15896.9(5)	16149.0(5)	16156.7(2)	16039.5(6)

Table 6.1: Crystal data for encapsulation complexes with acetophenone (**1x**), *trans*-cinnamaldehyde (**1xi**), anthracene (**1xii**), tetracene (**1xiii**, benzylcyanide (**1xiv**) and 2,6-diisopropylphenol (**1xvi**) at 150 K.

6.3.4 *Overview*

An overview of the 6 new structures presented in this chapter corroborates the conclusion from the previous two chapters that guest molecules take up certain positions within the unit cell more frequently, with a number appearing favourable to guests molecules regardless (or in spite) of their functionality. In this study, interest was focused more specifically on the effect of systematically varying the steric requirement of guest molecules across the four series, and examining the consequential site occupancy and the intermolecular interactions present.

6.3.5 *Series A*

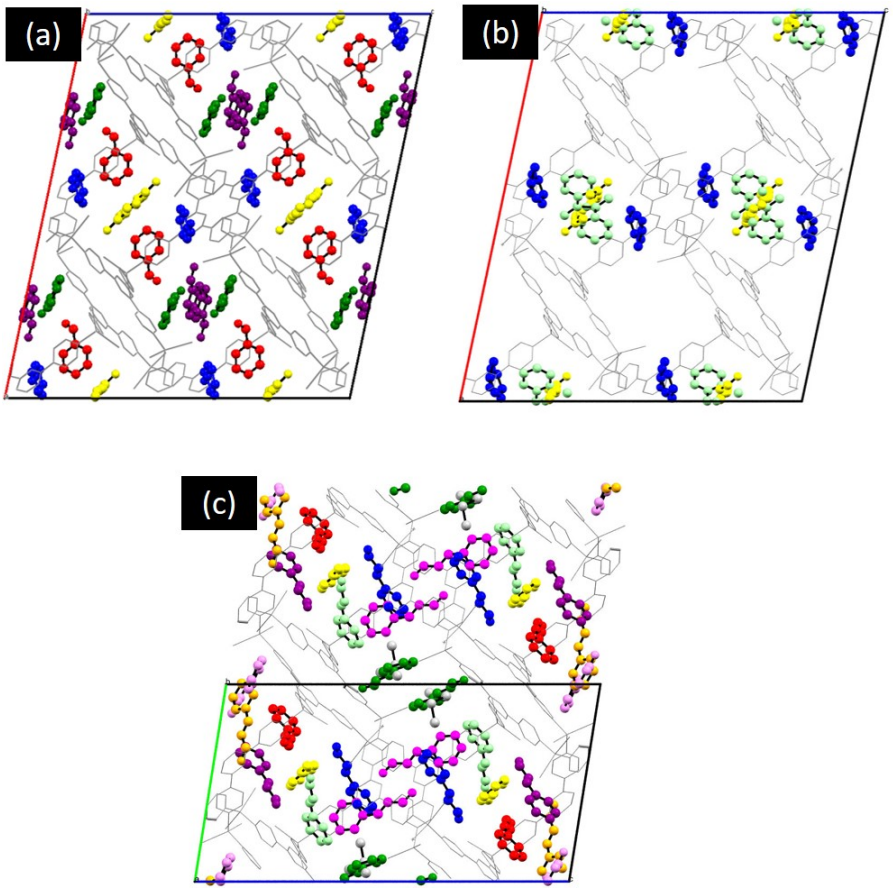

Figure 6.3: Unit cells plots of encapsulation complexes, viewed down the *b-axis* [except (c) which is viewed down the a-axis for ease of comparison]. (a) **1vii** (benzaldehyde), (b) **1x** (acetophenone), and (c) **1xi** (*trans*-cinnamaldehyde). The framework is shown as a grey wireframe and guest molecules as ball and stick models. Hydrogen atoms have been omitted for clarity.

This series compares the position of guest molecules benzaldehyde (**vii**), acetophenone (**x**) and cinnamaldehyde (**xi**). Detailed analysis of the crystal structures shows similar interactions occur in all three complexes resulting in some consistency of positioning in the pore. There are a number of sites that are occupied but all three guests in the series. For example, guest molecules in **1x** and **1xi** coloured yellow in Figure 6.3 (a) and (b) are situated in the same site relative to the tris(4-pyridyl)-1,3,5-triazine)$_2$, TPT linkers, interacting with two pyridyl rings on either side of the pore. This site is also common to the previously reported structure **1vii**. The three guests are positioned with only slight rotational differences with respect to the framework (see Figure 6.4). Each molecule formed four CH···π interactions, the average lengths of which are similar at 3.24, 3.26 and 3.27 Å in **1x**, **1xi** and **1vii** respectively showing a high degree of consistency regardless of guest size. Hydrogen bonds (C=O$\cdots$HC$_{\mathrm{pyridyl}}$) were formed by benzaldehyde and acetophenone (2.4 and 2.6 Å respectively) in these sites whilst the longer chain length in the cinnamaldehyde molecule extended too far into the pore space to allow such a strong interaction. Indeed, the closest atom is a framework iodine at a distance of 3.1 Å . This suggests that numerous longer range interactions assist in the ordering of guest molecules, specifically the chains, whilst the main body of the guest, the aromatic ring, is tethered by multiple strong CH$\cdots$ π interactions. In no instances do we see significantly greater disorder in the chains of the guest molecules compared to their aromatic rings.

Similar interactions were observed between the framework and molecules in a second site (coloured blue in Figure 6.3 a and b) albeit with the guest molecules in close enough proximity to form the CH$\cdots\pi$ interactions with only a single pyridyl ring (Figure 6.5). The CH$\cdots$centroid distances are comparable to those in the first position. Interestingly, whilst benzaldehyde and acetophenone molecules sit in this site with a common orientation forming a C=O$\cdots$HC$_{\mathrm{pyridyl}}$ bond with a pyridyl ring of the framework (at 2.44 and 2.49 Å), the equivalent cinnamaldehyde molecule is orientated in the opposite direction. This enables it to align with a different pyridyl at an appropriate distance and form a unique C=O$\cdots$HC$_{\mathrm{pyridyl}}$ hydrogen bond (2.65 Å).

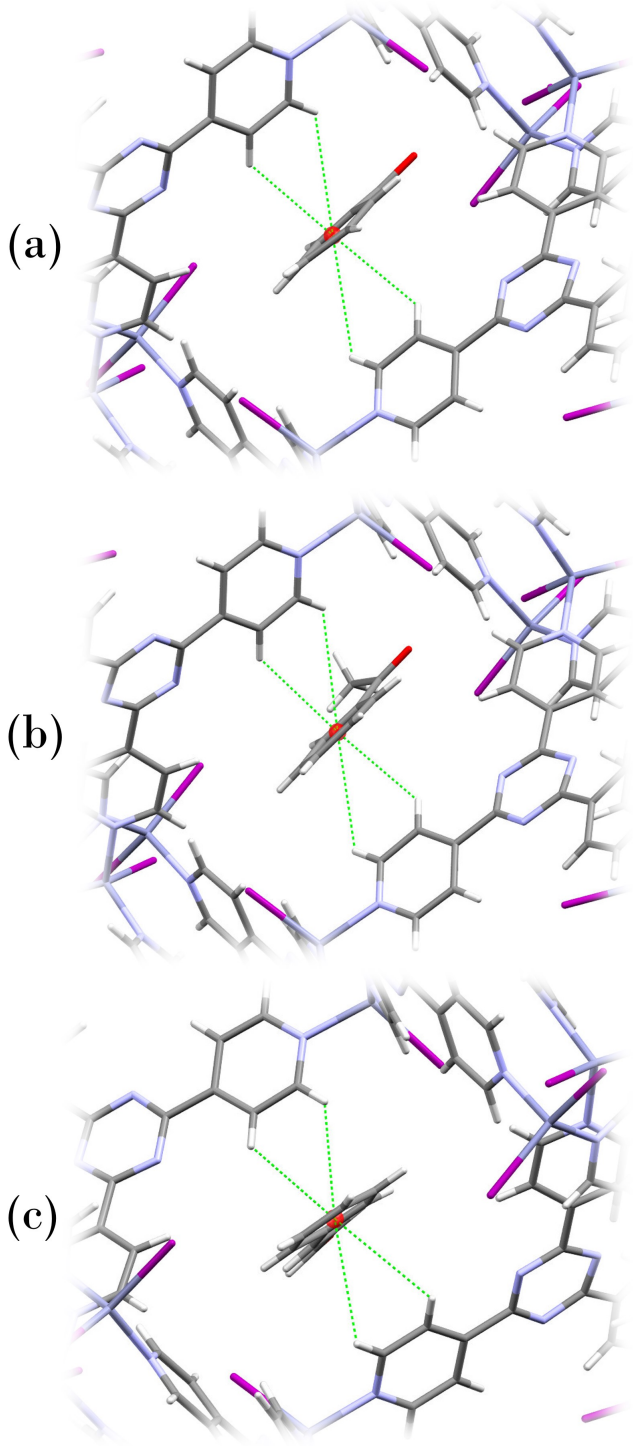

Figure 6.4: Guest molecules in the cavity of **1** (a) benzaldehyde, (b) acetophenone and (c) cinnamaldehyde. Centroids are shown as red spheres and intercentroid contacts as green lines.

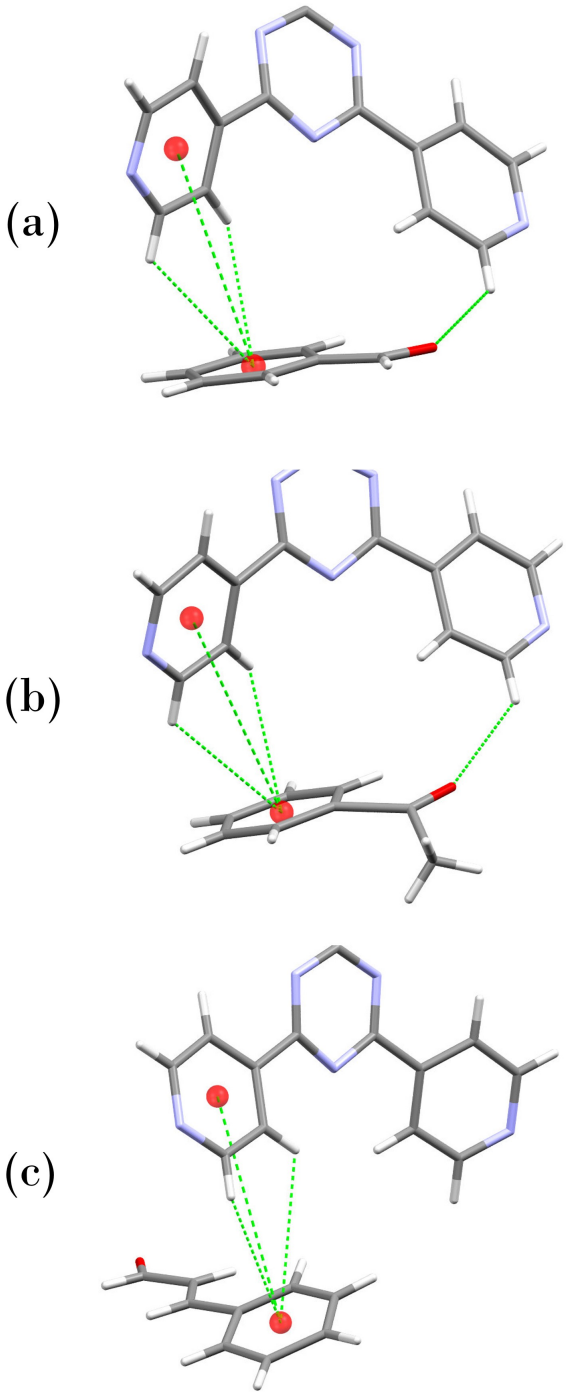

Figure 6.5: A comparison of the CH$\cdots\pi$ interaction between the framework and (a) benzaldehyde, (b) acetophenone and (c) *trans*-cinnamaldehyde at equivalent sites within their respective unit cells. Centroids are shown as red spheres and intercentroid contacts as fluorogreen lines.

6.3.6 *Series B*

In this series, all three guest molecules (benzene (**i**), naphthalene (**v**) and anthracene (**xii**)) lack functional groups and are ordered in the pores of **1** by aromatic interactions alone. Therefore, the guests' steric properties are directly responsible for any changes in positioning and extent of interaction. All three structures contain some residual solvent molecules and vary in the number of guest molecules present in the asymmetric unit. In the case of the previously established encapsulation complex with benzene there are 5 guest molecules while in the new compounds there are three in the case of naphthalene and a single guest anthracene molecule. There is no one site taken up by all three molecules but there are similarities in the sites observed for the pair of encapsulation complexes naphthalene and anthracene, and also similarities for the benzene and naphthalene pair.

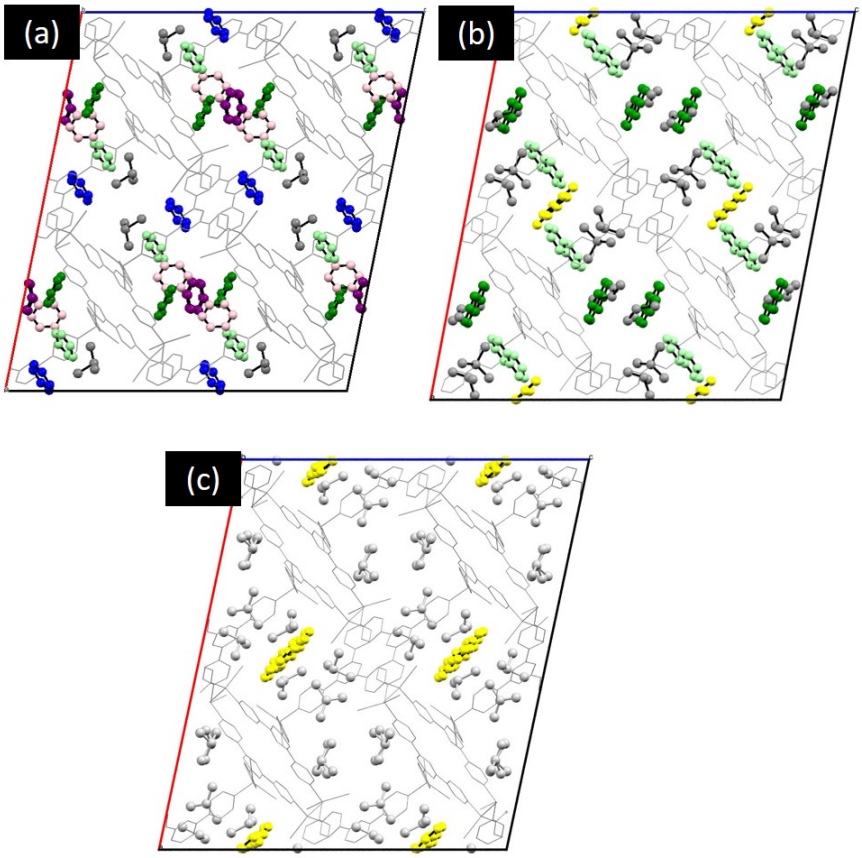

Figure 6.6: Unit cells plots of encapsulation complexes, viewed down the *b-axis*. (a) **1i** (benzene), (b) **1v** (naphthalene) and (c) **1xii** (anthracene). The framework is shown as a grey wireframe and guest molecules as ball and stick models. Hydrogen atoms have been omitted for clarity.

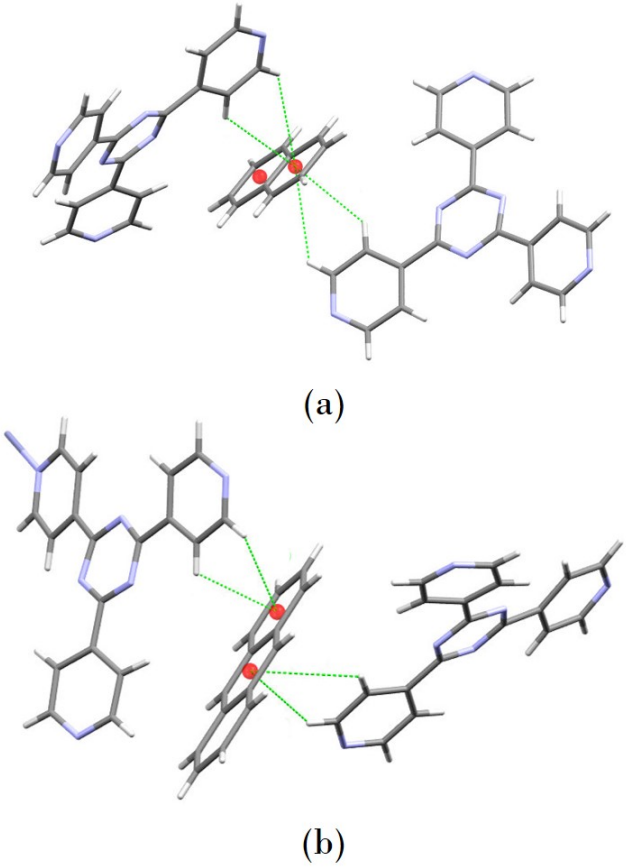

Figure 6.7: A comparison of the CH$\cdots\pi$ interaction between the framework and (a) naphthalene or (b) anthracene at equivalent sites within their respective unit cells. Centroids are shown as red spheres and intercentroid contacts as fluorogreen lines.

Comparing the structures of **1v** and **1xii** we once again see CH$\cdots\pi$ interactions governing the positioning of some guests, with molecules of naphthalene and anthracene both taking up the site signified by yellow colouration (Figure 6.6) of the guests, and as described in series A. Four significant CH$\cdots$centroid distances were observed as evidence for this interaction (see Table 1) with slight differences in orientation as shown in Figure 6.7. Benzene was observed to form similar interactions in **1i**, albeit at different sites within the unit cell.

Comparing the structure of **1v** with **1i**, similarities were seen in position and interactions formed (Figure 6.6). For example, the light green molecules of naphthalene were ordered by $\pi\cdots\pi$ interactions formed with a pyridyl group and a triazide ring (centroid$\cdots$centroid distances of 3.89 Å and 3.78 Å, respectively). In the analogous part of the unit cell of **1i**, benzene interacted with an adjacent pyridyl ring (centroid$\cdots$centroid distance 3.59 Å) of a postionally equivalent TPT

molecule. These contrasting orientations can be seen in Figure 6.8. Comparing this site to the common position taken up by naphthalene and anthracene which is defined by CH$\cdots\pi$ interactions on both faces of the molecule, these light green molecules sit asymmetrically in the pore. The framework on the opposite side lies a distant 7 Å away. However the presence of an additional benzene guest molecule in **1i** (coloured blue in Figure 6.6a) fills the otherwise empty space sitting in close enough proximity to the green site to suggest the presence of a stabilising intermolecular guest - guest interaction (centroid$\cdots$centroid distance 4.11 Å).

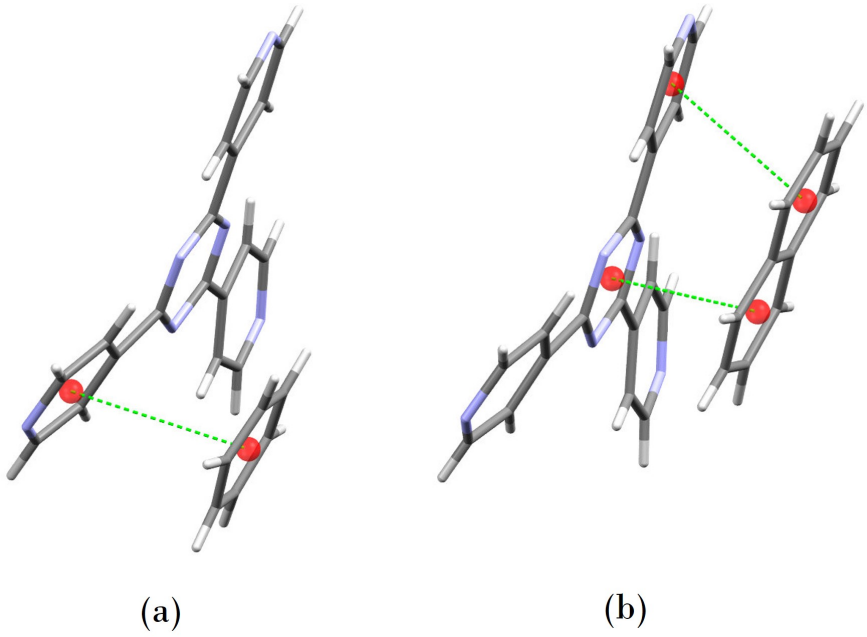

Figure 6.8: A comparison of the $\pi\cdots\pi$ interaction formed by a TPT linker in the framework of **1** with (a) benzene and (b) naphthalene at equivalent sites. Centroids are shown as red spheres and intercentroid contacts as fluorogreen lines.

6.3.7 *Series C*

In this last comparison the encapsulation complexes with benzonitrile (**iv**) and benzylcyanide (**xiv**) are studied, Figure 6.9 and the effect of even a small increase in guest size was observed. Immediately apparent from comparing their unit cell plots in Figure 6.9 is the greater disorder present in the former.

Looking at sites within the pore space common to both guests contact measurement suggest the lengthening of the functional group from **iv** (benzonitrile) to **xiv** (benzylcyanide) brings the terminal nitrogen closer in proximity to the framework enabling the formation of stronger stabilising interactions. For example, guests take up an equivalent position highlighted by orange colouration of guests in Figure 6.9. Both guests were disordered over two orientations, although the nature of the disorder was different. In the case of benzonitrile the rings were rotationally offset at an angle of 22.63° between the two positions (Figure 6.10a). In comparison, the CH_2CN group of benzylcyanide sits on a pseudo axis about which the molecule is disordered, with the phenyl rings rotated 138.25° relative to one another (Figure 6.10b).

Contact measurements show all positions were anchored by similar interactions between the guest aromatic ring and pyridyl of the framework. However, a shorter $CN\cdots H_{\mathrm{pyridiyl}}$ interaction was observed with benzylcyanide at 2.72 Å, the only crystallographically well-ordered part of the guest. In the case of benzonitrile, the two disordered components make contacts of 3.18 and 2.92 Å. This suggests differences in guest size can affect disorder by strengthening or weakening the interaction with the crystalline sponge framework, with an interplay between aromatic interaction and those associated directly with the functional group.

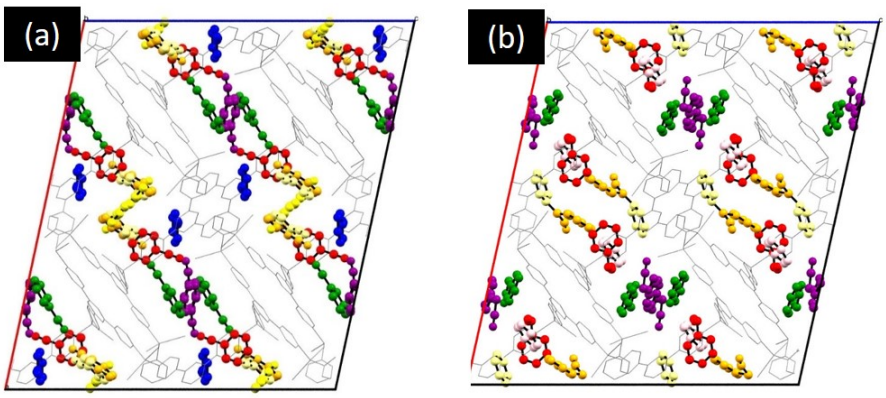

Figure 6.9: Unit cell plots of encapsulation complexes, viewed down the *b-axis*. (a) **1iv** (benzonitrile) and (b) **1xiv** (benzylcyanide). The framework is shown as a grey wireframe and guest molecules as ball and stick models. Hydrogen atoms have been omitted for clarity.

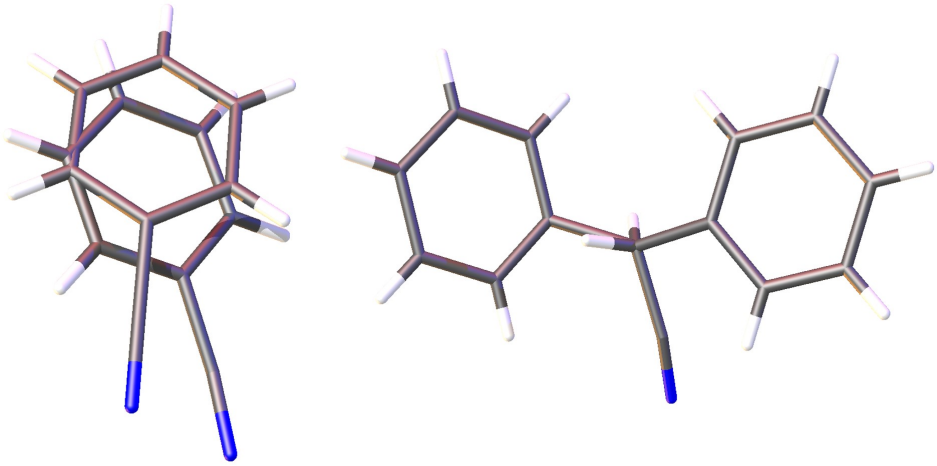

(a) (b)

Figure 6.10: The disorder observed in (a) benzonitrile **iv** (b) benzylcyanide **xiv** molecules at a specific, crystallographically equivalent site in the pore of **1**.

6.3.8 *Series D*

Of the two encapsulation complexes planned to make up series D only one, with 2,6-diisopropylphenol (**xvi**), was successfully obtained. The unit cell diagram of **1xvi** is displayed in Figure 6.11. Encapsulation experiments with phenol resulted in the degradation of **1** such that SCXRD diffraction analysis was impossible. An representative example of the resulting crystals are shown in Figure 6.12, comparing a standard as-synthesised crystal of **1** with a crystal soaked in a 0.05M solution of phenol for 24 hours. Clearly, the crystal is cracked and its edges are degraded. Therefore, no comparison in terms of steric requirement is possible for this series.

However, some interesting guest-host interactions are formed which are worth noting. Of the three 2,6-diisopropylphenol guest molecules present in asymmetric unit of **1xvi** two display unique interaction through their hydroxyl group. These are O$\cdots$N$_{\mathrm{pyridine}}$ (2.95 Å) and O$\cdots$I (3.47 Å). Both distances are shorter than the sum of the van der Waals radii of interacting atoms.

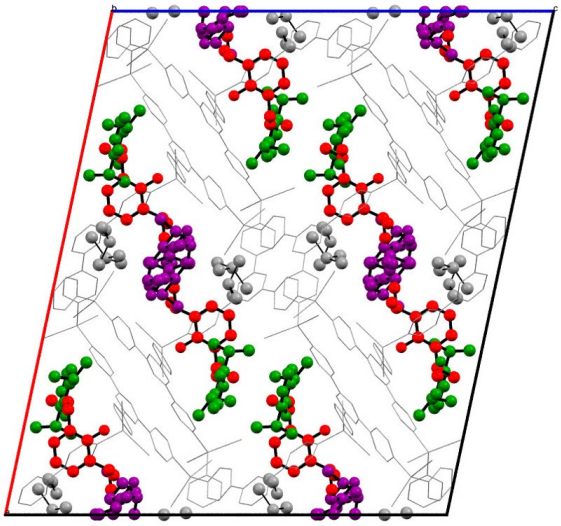

Figure 6.11: Unit cell plot of the encapsulation complexes with 2,6-diisopropylphenol (**1xvi**), viewed down the *b-axis*. The framework is shown as a grey wireframe and guest molecules as ball and stick models. Hydrogen atoms have been omitted for clarity.

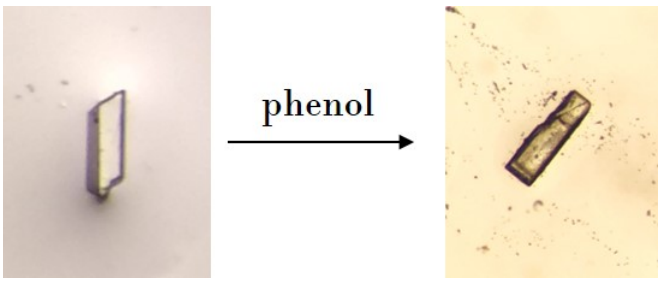

Figure 6.12: Degradation of the single-crystallinity of **1** after soaking in a 0.05M $CHCl_3$ solution of phenol for 1 day.

6.4 CONCLUSION

Five new encapsulation compounds have been reported, including 3 with guests not previously observed inside the crystalline sponge [$(ZnI_2)_3$(tris(4-pyridyl)-1,3,5-triazine)$_2$•x$(CHCl_3)_n$]. As such the methodology is validated and the scope of the technique expanded. Measurement of intermolecular interactions in relation to guest size and functionality shows the consistency with which CH$\cdots\pi$ and $\pi\cdots\pi$ interactions are formed and demonstrates that these are the most important factors in determining the location of the guest molecules within the pore structure. Due to the aromaticity of all guest molecules, many of those reported here take up similar positions within the unit cell but small changes in the functionality and size of guest molecules may affect their orientation and ordering within the sponge framework.

Complex	Guest molecules	Incubation time / Days
1x	acetophenone	3
1xi	cinnamaldehyde	3
1xii	anthracene	10
1xiii	tetracene	25
1xiv	benzylcyanide	3
1xv	phenol	1
1xvi	2,6-diisopropylphenol	2

Table 6.2: Specific duration of incubation time of guest soaking.

6.5 EXPERIMENTAL

6.5.1 *Crystalline Sponge Synthesis*

Crystals of **1** were synthesised according to the adapted literature procedure labelled 'method B' in Chapter 3, in the form **1•(CHCl$_3$)**.

6.5.2 *Guest Encapsulation Protocol*

*Acetophenone (**1ix**), trans-cinnamaldehyde (**1x**), benzylcyanide and 2,6-diisopropylphenol (**1xv**)*

These potential guests are liquid and were therefore used neat. Crystals of **1•(CHCl$_3$)** were immersed directly into 1 cm^3 of the compound in a 3 cm^3 vial. Samples were incubated at 22 °C and guest exchange was allowed to proceed for the specific length of time detailed in Table 6.2. Suitable rod or block shaped crystals were selected and subjected to SCXRD.

*Anthracene (**1xi**) and tetracene (**1xii**)*

Both anthracene and tetracene exhibit low solubilities. Of the solvents compatible with **1**, they both exhibited highest solubility in CHCl$_3$. Near-saturated solutions were obtained at concentrations of 0.066 M for anthracene and 0.013 M for tetracene. Solutions of these molarities were therefore used in encapsulation experiments, following the same procedure as in Section 6.5.2.

*Phenol (**1xiv**)*

Encapsulation experiments were attempted with phenol at variable guest concentrations. Beginning with neat phenol, the guest was diluted with CHCl$_3$ to produce concentrations of 1M, 0.5M, 0.25M, 0.1M, 0.03M and 0.003M. Soaking duration was kept to a minimum, at 1 day.

6.5.3 *Crystallography*

Following the procedure described in Section 3.5.3.

6.5.3.1 *Crystal structure refinement*

For **1x** (Figure 6.13) rigid bond restraints were required for all guest molecules. A combination of SIMU and DELU or RIGU were employed. The SADI instruction was additionally used to restraint C=O and C-CH_3 bond lengths where required. The anisotropic displacement parameters of pairs of disordered iodine atoms in the framework were constraint using EADP.

For **1xi** (Figure 4.13) anistropic refinement performed with a combination of DELU and SIMU were used for two of the eight guest molecules

For **1xii** (Figure 6.15) guest molecule anisotropic refinement was performed with a combination of SIMU and RIGU. C-Cl bond lengths were restrained using a universal SADI command for all four residual $CHCl_3$ solvent molecules. Two were successfully refined anisotropically. Additionally, one positionally disordered $CHCl_3$ molecule required EADP to constrain as equal the isotropic atomic displacement parameters of the two carbon atoms parts.

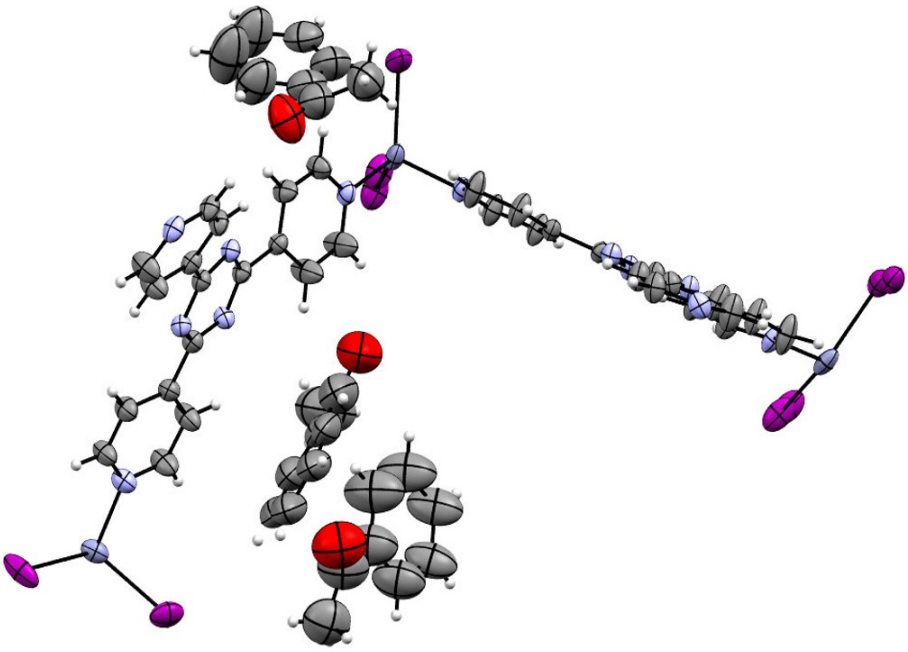

Figure 6.13: Asymmetric unit of **1x**

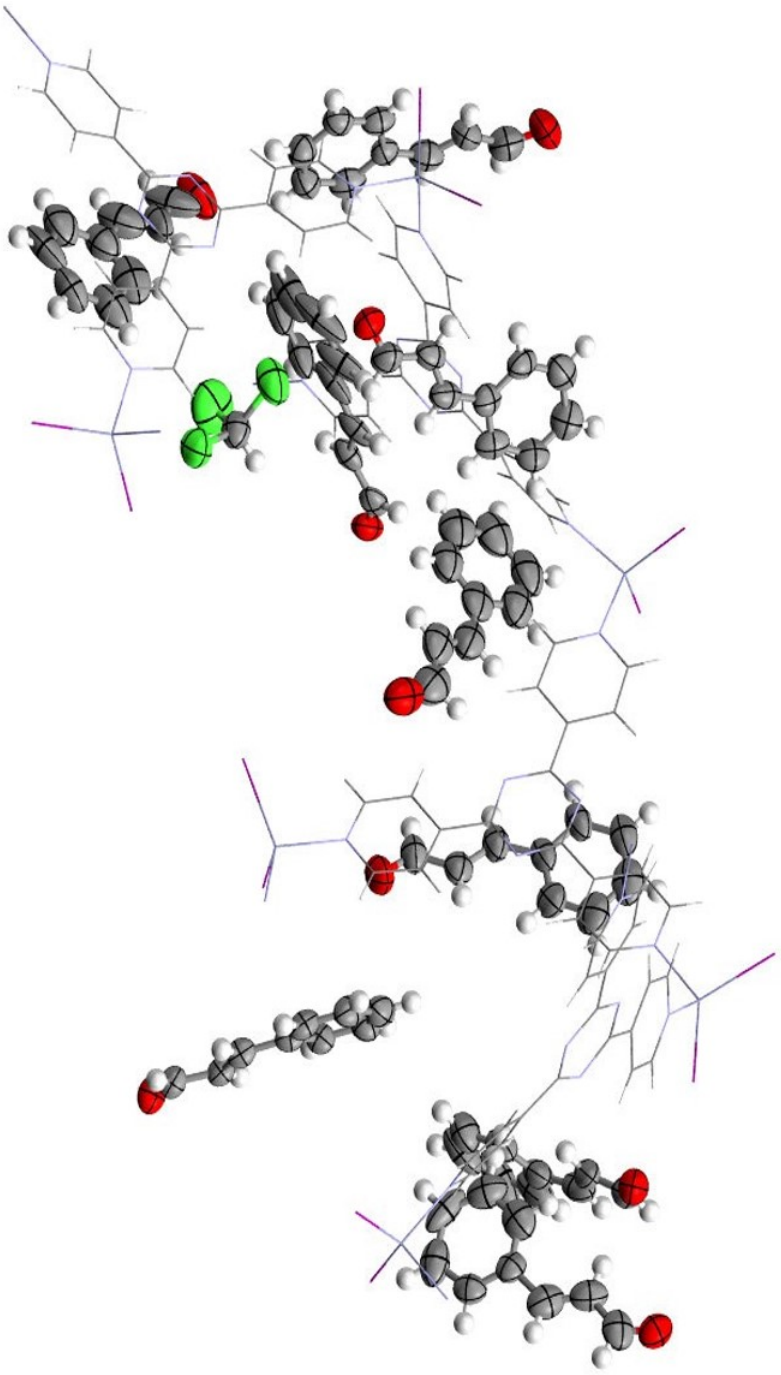

Figure 6.14: Asymmetric unit of **1xi**, framework shown in wireframe model for clarity.

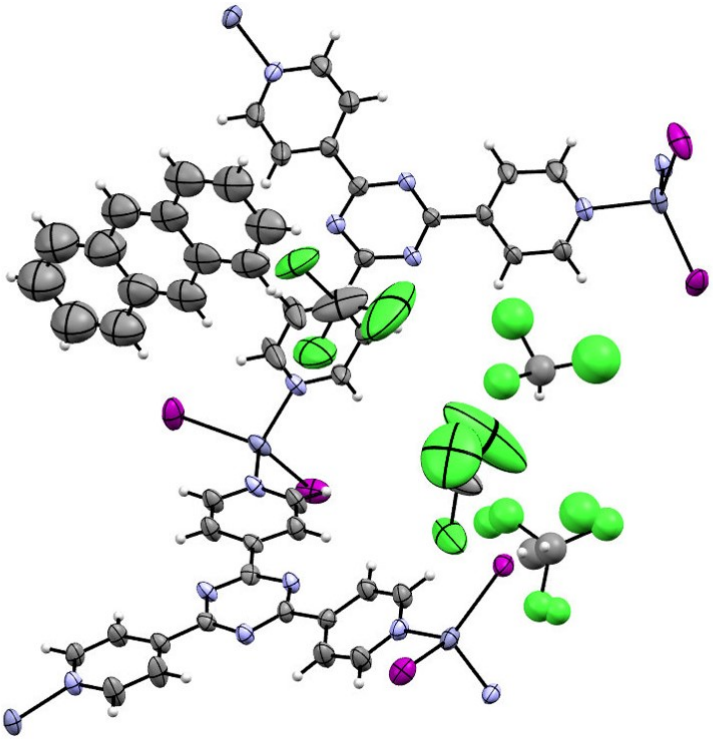

Figure 6.15: Asymmetric unit of **1xii**

For **1xiii** (Figure 6.16) anisotropic refinements performed with a combination of SIMU and DELU. C-Cl bond lengths were restrained using a universal SADI command for all four residual $CHCl_3$ solvent molecules. The anisotropic displacement parameters of pairs of disordered iodine atoms and one zinc atoms in the framework were constraint using EADP.

For **1xiv** (Figure 6.17) anisotropic refinements were performed using a combination of SIMU and DELU. DFIX was required to contrain bond lengths in C-CN groups in all cases to obtain stable anistopic refinement.

For **1xv** (Figure 6.18) anisotropic refinements were performed using SIMU, one guest molecules required the addition of RIGU to achieve stable refinement.

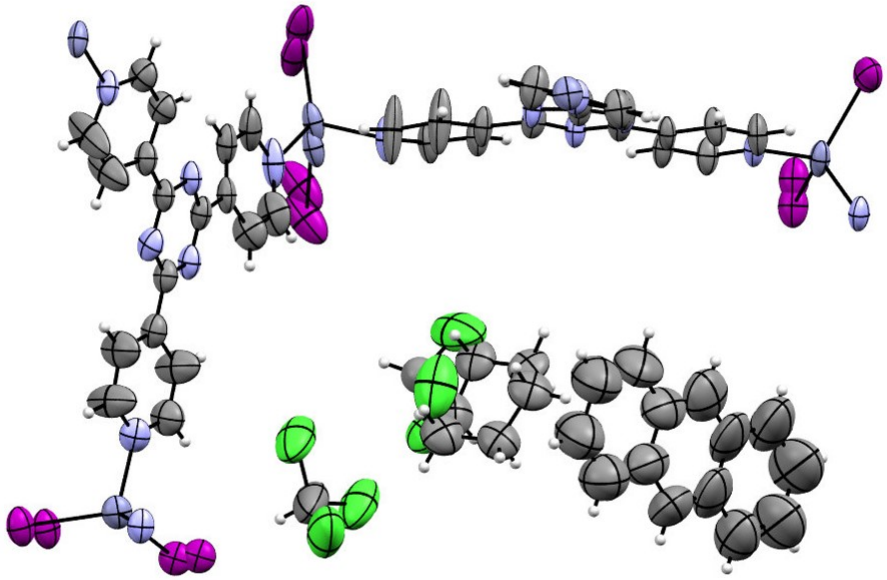

Figure 6.16: Asymmetric unit of **1xiii**

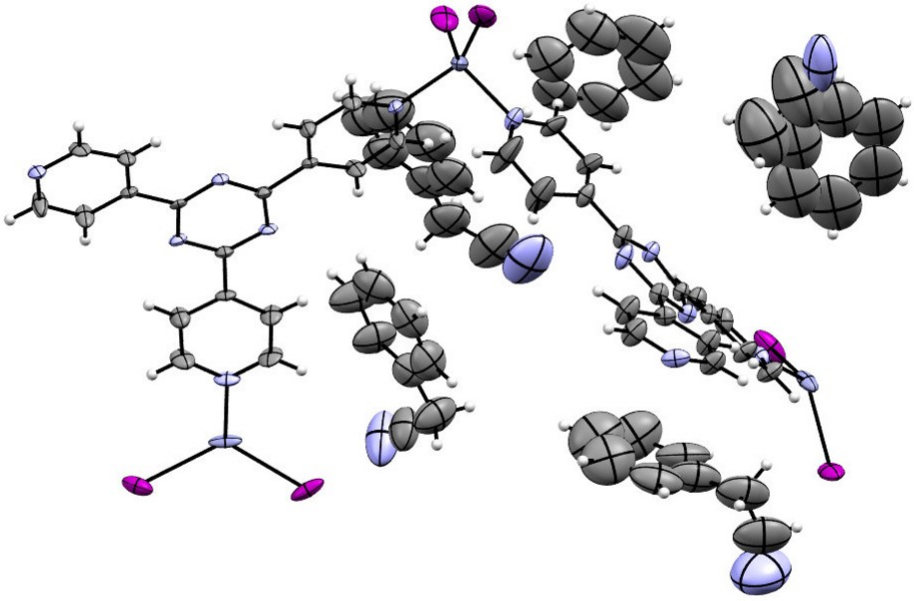

Figure 6.17: Asymmetric unit of **1xiv**

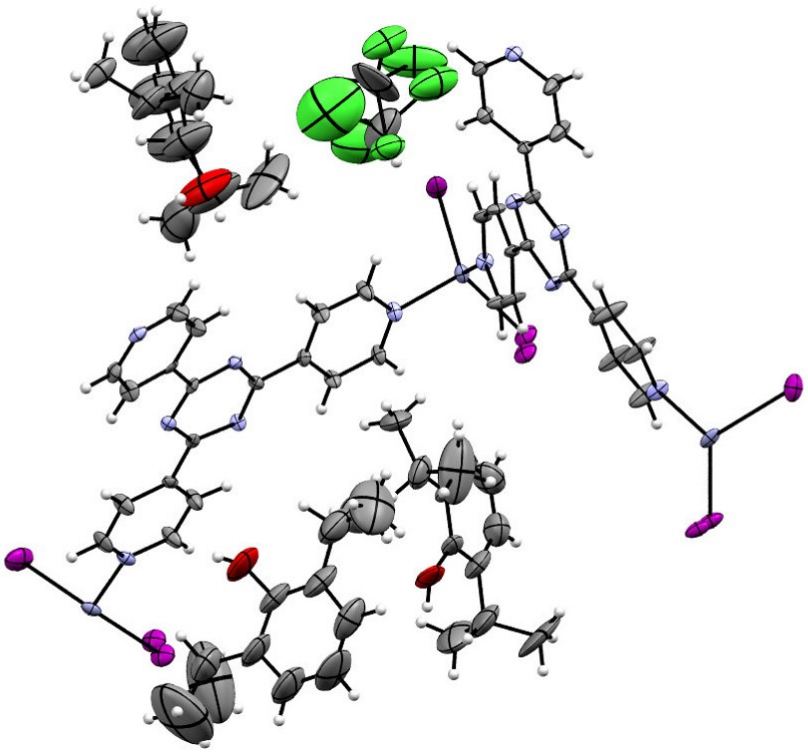

Figure 6.18: Asymmetric unit of **1xv**

7

SYNTHESIS OF NOVEL LINKER COMPOUNDS

7.1 AIMS

The aim of the work in this chapter is to synthesise chemically similar compounds for use as linkers in the synthesis of novel MOFs to expand the crystalline sponge technique. The work looks to produce a systematic series of linkers structurally similar to tris(4-pyridyl)-1,3,5-triazine (TPT) with the potential of creating an isoreticular, or structurally distinct but chemically similar, series of metal-organic frameworks (MOFs).

7.2 INTRODUCTION

The crystalline sponge technique has, in the few years since its conception, proved exceedingly useful in the structural elucidation of non-crystalline compounds (see Section 1.6). Whilst compounds with a range of functionalities have been shown compatible with the original and most successful sponge, $[\{(ZnI_2)_3(TPT)_2.x(solvent)\}_n]$ (**1**) there are limitations on its use.

The most significant of these are summarised in Figure 7.1. The framework's pore size (8 x 14 Å) limits guest size, it is reactive towards basic amines, and the hydrophobic natural of TPT precluded

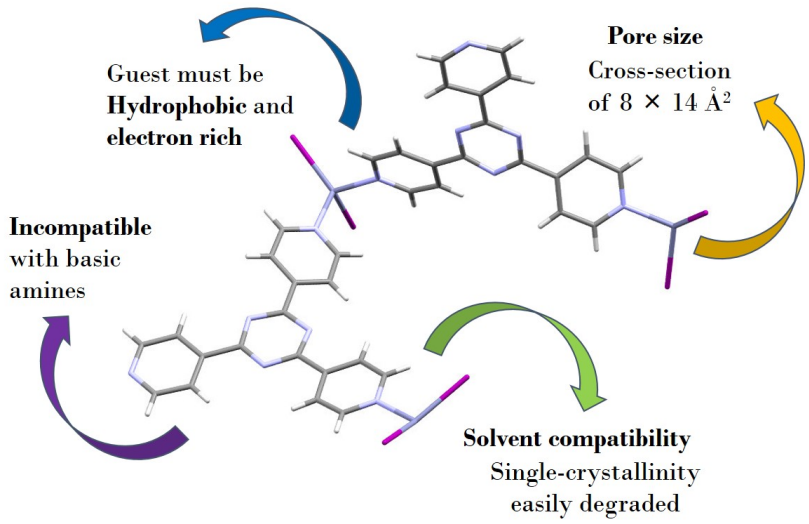

Figure 7.1: The limitations of the crystalline sponge $[\{(ZnI_2)_3(TPT)_2.x(solvent)\}_n]$.

encapsulation of hydrophilic guests. Furthermore, guests must be soluble in or miscible with inert solvents that are compatible with the host framework. Progress has been made with the development of a saccharine-based sponge that has been reported as suitable for the encapsulation of both hydrophobic and hydrophilic guests.[85]

Although other alternative crystalline sponges have been presented in the literature, none have systematically addressed the issue of pore-size. An ideal outcome would be to develop a library of MOFs with varying pore size and chemical properties, which could be accessed as required according to the nature of the non-crystalline compound of interest. Therefore, the production of a series of MOFs isoreticular to **1** could contribute to this goal.

The concept of isoreticular synthesis is detailed in Section 1.3.1 and involves the use of specific building blocks to produce structures with the same skeleton but different functionalities and/or dimensions. In this case, linkers of common functionality but different dimensions to TPT were chosen for investigation. Those compounds chosen were 2,4,6-tri(imidazol-1-yl)-1,3,5-triazine (**TIMTZ**), 2,4,6-tris(4-(pyridin-4-yl)phenyl)-1,3,5-triazine (**TPPT**) and 2,4,6-tri(4'-(pyridin-4-yl)-[1,1'-biphenyl]-4-yl)-1,3,5-triazine (**TPPPT**), shown in Figure 7.2. None of these compounds were available commercially and whilst synthetic protocols for the production of **TIMTZ** and **TPPT** are in the literautre,[132,133] **TPPPT** was a previously unreported compound. Their synthesis involves the construction of new bonds by the metal catalysed cross-coupling of two simple molecules to create a more complex product. Of specific interest here are the Suzuki-Miyaura (SMR) and Stille reactions.

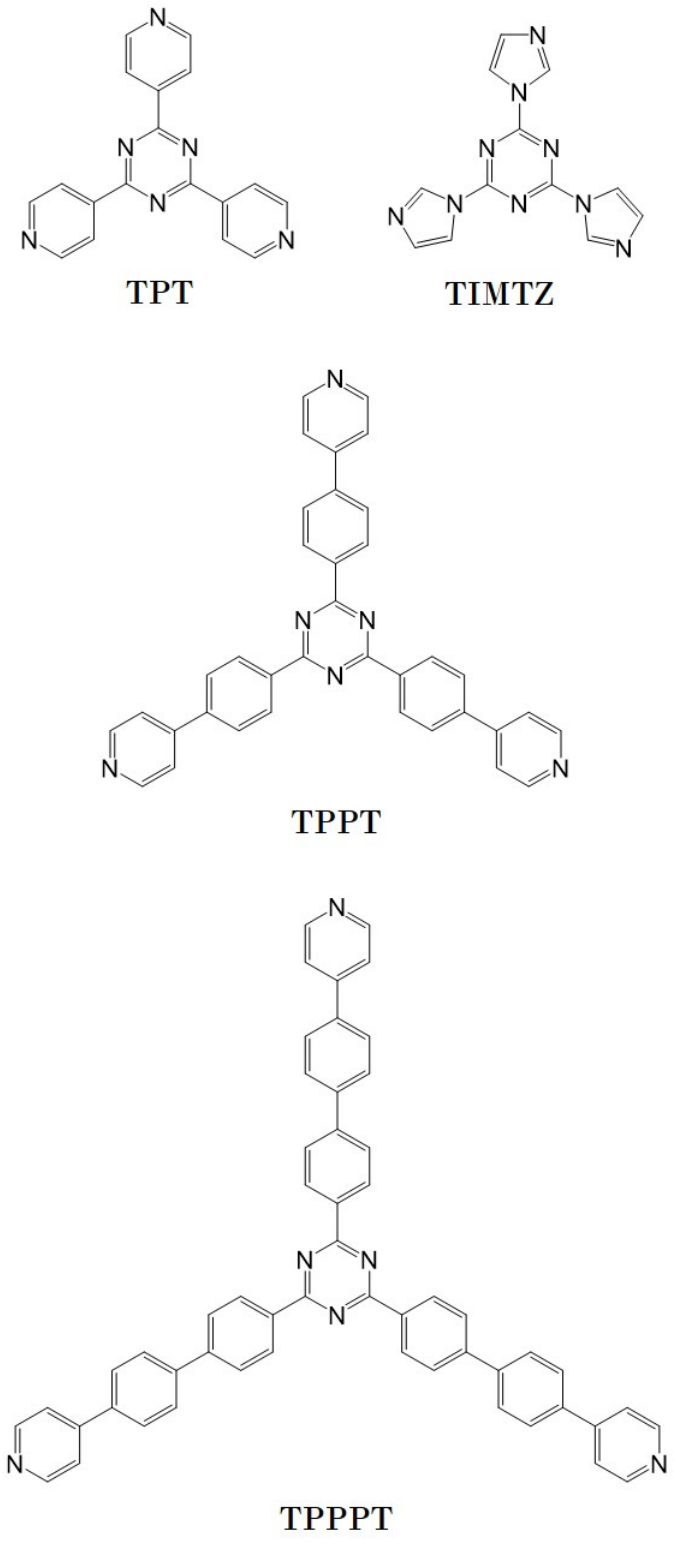

Figure 7.2: Proposed series of linkers.

7.2.1 *Suzuki-Miyaura Coupling*

First published in 1979, the Suzuki-Miyaura reaction (SMR), shown in Scheme 7.1, involves the cross-coupling of sp^2-hybridized aryl or vinyl-halides (or related electrophiles) with sp^2-hybridized aryl- or vinyl-boronic acids.[134,135] The SMR has become one of the most important transition metal catalysed carbon-carbon bond forming reactions, especially in drug discovery.[136,137]

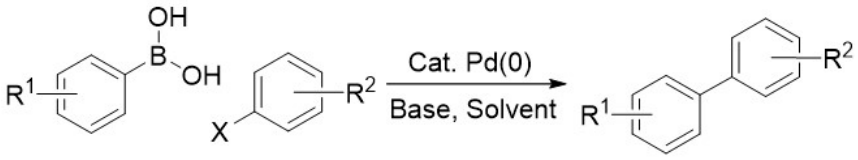

Scheme 7.1: Suzuki coupling reaction.

The reaction relies on a palladium catalyst (or strictly pre-catalyst), often with phosphine ligands, and is commonly used to synthesise styrene, substituted biphenyl and polyolefin compounds. The advantages of the SMR lies in its versatility, high functional group tolerance, non-toxic boronic acid side products and high yields. It is largely unaffected by moisture although sensitive to oxygen. However, the formation of side-products, such as self-coupling products or reaction with displaced ligands (especially with PPh_3) must be considered. Judicious selection of catalyst, solvent, base, additive and experimental conditions allows the optimisation of reactions and enables its application to a huge range of organboranes and halide substituents. The reactivity of reagents can be ordered R-I > R-OTf > R-Br » R-Cl (where R = aryl/vinyl).

Scheme 7.2 shows the major steps of the catalytic cycle.[138] It is initiated by the oxidative addition of the halide to Pd(0), forming the σ-aryl Pd(II) species [R^1-Pd(L_n)-X]. This is often the rate determining step. The displacement of the halide ion by a base gives the more reactive organopalladium alkoxide or hydroxide species (dependant on the base used). Reaction of this intermediate with the boronate *via* transmetallation forms a bi-aryl organopalladium species [R^1-Pd(L_n)-R^2]. Lastly, reductive elimination gives the desired R^1-R^2 product and regenerates the Pd(0) catalyst.

7.2.2 *Stille Coupling*

Like the Suzuki-Miyaura, the Stille reaction is a palladium-catalysed cross-coupling reaction. A generalized reaction is shown in Scheme 7.3, involving the coupling of an organostannane with one of a variety of organic electrophiles.[139] The electrophile is commonly a halide (bromide or iodide) or sulfonate (often triflates).

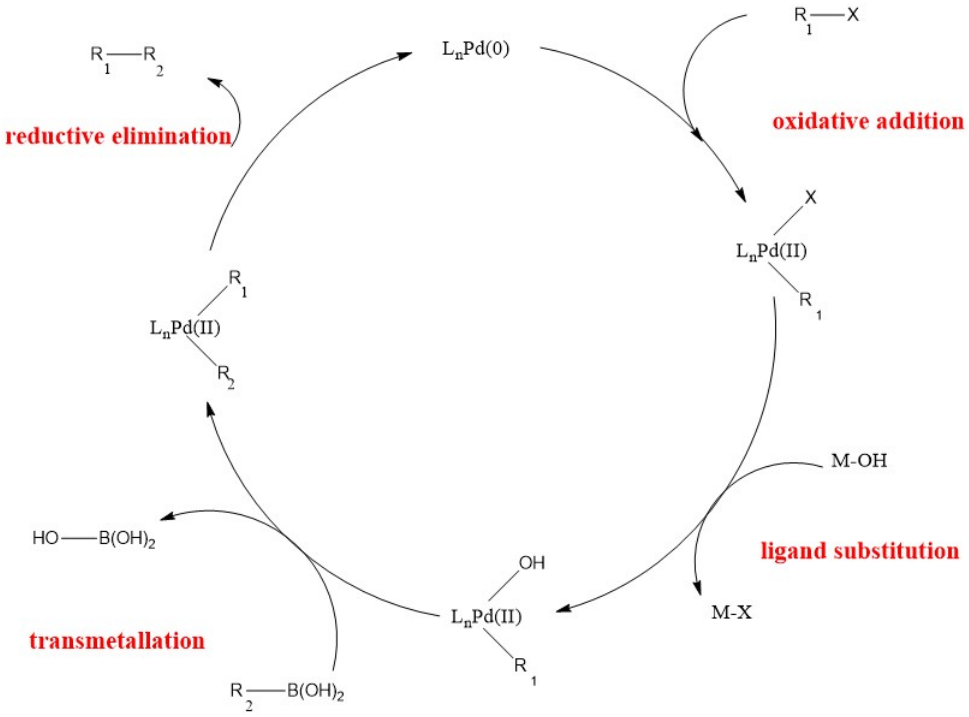

Scheme 7.2: Suzuki coupling catalytic cycle.

Its greatest advantage is that, unlike most organometallic processes, it is highly tolerant of functional groups limiting the need for protecting/deprotecting steps. These properties are mostly due to the low polarity of the C-Sn bond. Furthermore, organostannes are easy to synthesise and relatively stable, with low sensitivity to air and water. However, the drawback is high toxicity with the potential for product contamination and can lead to purification challenges.

The Stille mechanism is similar to SMR perhaps due to the similar chemical properties of tin and boron derivatives. In simple terms the catalytic cycle contains four steps; oxidative addition, transmetallation, isomerization and reductive elimination.[140] These are represented in Scheme 7.4. Oxidative addition of the vinyl or aromatic triflate or halide produces a palladium intermediate [R^1-Pd(L_n)-X]. This undergoes transmetallation with the organostannane in the rate determining step, displacing a halide ion to give the δ-coordinated organopalladium complex [R^1-Pd(L_n)-R^2]. Once *trans*/*cis* isomerization has occurred, reductive elimination gives the cross-coupled product and regenerates the catalyst. This summary provides a representative, simplified picture of the coordination envirnoments of Pd, more details of which are available in the literature.[141]

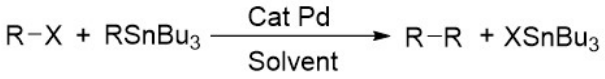

Scheme 7.3: Stille coupling reaction.

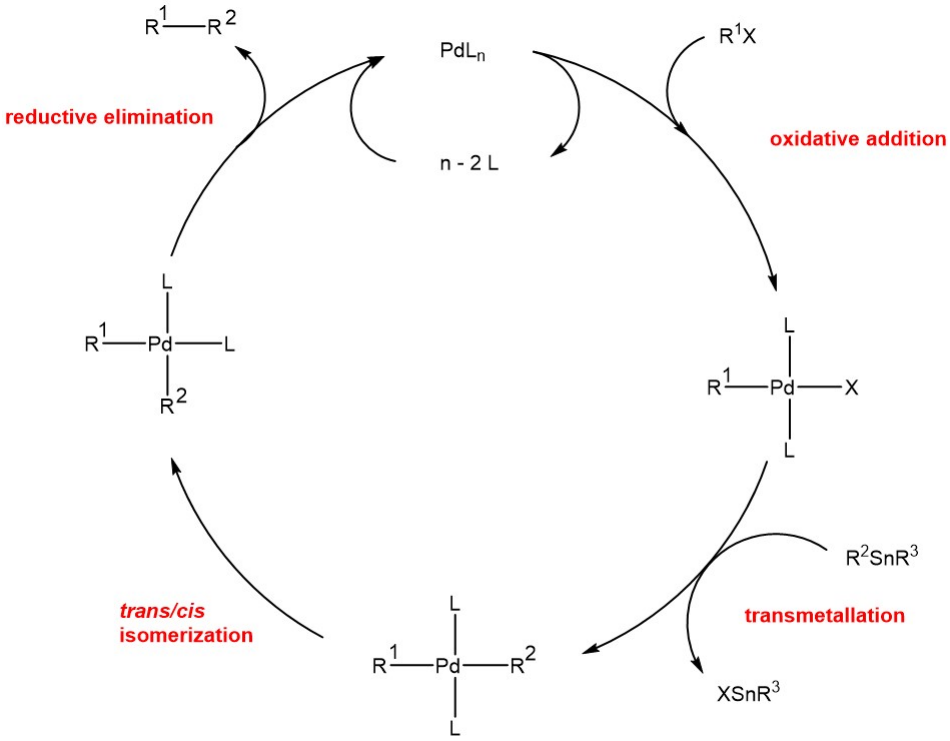

Scheme 7.4: Stille coupling catalytic cycle.

7.3 RESULTS

The results discussed here come from experiments performed over a three month period in the lab of Dr Neil Press at the Novartis Institute for BioMedical Research in Basel, Switzerland. Guidance and advice was given by Dr Press and Dr Christel Guibourdenche through out this period, both in planing and performing experiments.

7.3.1 *Synthesis of TIMTZ*

Following a modified procedure to that outlined by Mohammad *et al*, **TIMTZ** was obtained from the solvent-free nucleophilic reaction of imidazole with 2,4,6-trichloro-1,3,5-triazine (cyanuric chloride) 70°C (Scheme 7.5).[132] The first step, direct reaction of two starting materials proceeded as reported with LC-MS analysis showing conversion after heating and stirring the reaction mixture for 2 minutes. However, NMR analysis identified impurities that could not be assigned to the starting materials or partial substitution by the nucleophile on cyanuric chloride. Purification of the yellow crude product by recrystallisation from ethyl acetate (as reported in the literature) produced a white solid of higher purity. However, the yield of 32% was significantly lower than the 85% reported in the literature. This can be attributed to the hard, glassy consistency of the obtained solid preventing efficient dissolution in the recrystallisation solvent.

Subsequently, a new work up and purification procedure was developed. To increase solubility the large flakes of crude product were ground and ultrasonically dispersed in large quantities of ethyl acetate (~100 cm^3g^{-1}). After 10 minutes heating under reflux any insoluble solid was filtered off and the filtrate retained. The residual solid was re-dispersed in solvent and again heated under reflux. It was found that thrice repetition of this filtering/dispersal procedure was sufficient to extract a reasonable amount of pure product without using an unreasonably large amount of solvent. Evaporation of the solvent under reduced pressure returned a white solid at an average yield of 73%. The product was characterised by mass spectrometry

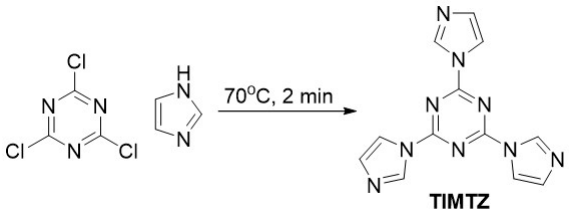

Scheme 7.5: Synthesis of **TIMTZ**.

([M+H]$^+$ 280.1055) and the ^{1}H and ^{13}C NMR spectra give peaks consistent with those reported in the literature.

Conclusive evidence for the structure of **TIMTZ** was obtained by SCXRD, Figure 7.3. **TIMTZ** was found to crystallise in the orthorhombic spacegroup *Pccn*. The asymmetric unit contains half a **TIMTZ** molecule which sits on a 2-fold rotation axis. As a consequence one imidazole ring has a disorder (50:50) of a C/N position. This disorder was modelled using the EXYZ and EADP commands to fix the coordinates and anisotropic displacement parameters of C7 and N6. The C7-N6 bond length of 1.408(5) Å is longer than expected, exceeding the C2-N2 distance of 1.386(2) Å of the equivalent bond in the complete imidazole group in the asymmetric unit.

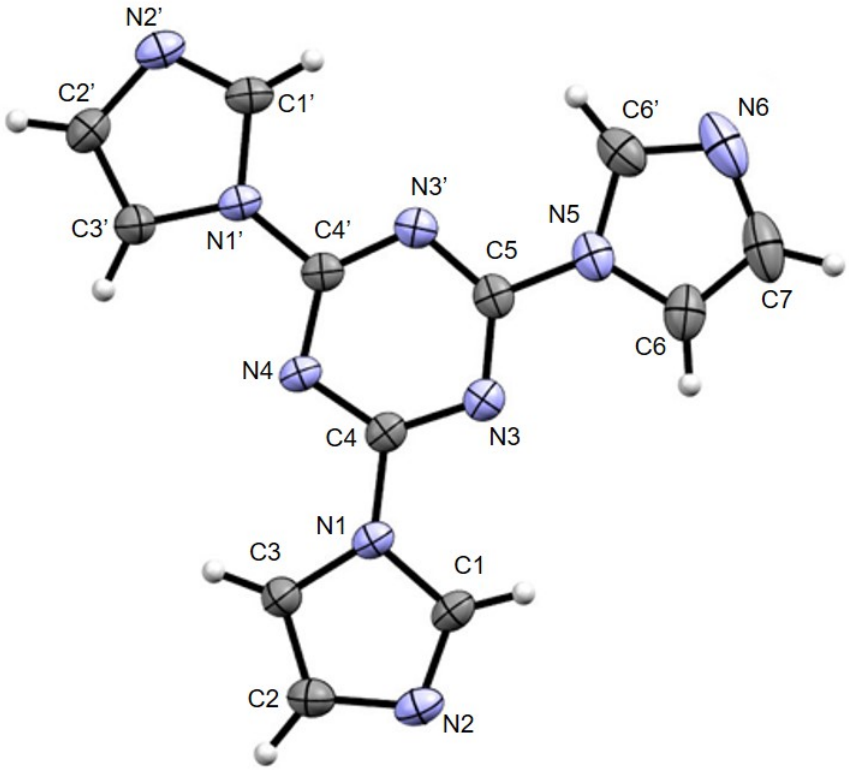

Figure 7.3: The crystal structure of 2,4,6-tri(imidazol-1-yl)-1,3,5-triazine (**TIMTZ**). Bond lengths: C6-N6/C7 = 1.311(3) Å, C7-N6 = 1.410(5) Å.

7.3.2 *Synthesis of TPPT*

TPPT was initially synthesised following a two step literature procedure.[133] Firstly, the brominated precursor **TBPT** was synthesised in 77% yield from the reaction of 4-bromobenzonitrile and triflic acid (Scheme 7.6). The second step was a [$PdCl_2(PPh_3)_2$] catalysed Stille cross-coupling reaction performed in toluene (Scheme 7.7). In the authors hands, **TPPT** was obtained in consistently lower yield to that previously reported (25% vs 66%). Therefore, in an effort to increase the yield a systematic series of experiments were performed to optimise the reaction conditions. An alternative solvent, 1,4-dioxane, and catalyst, 1,1'-bis(diphenylphosphino)ferrocene-palladium(II)dichloride [Pd(dppf)Cl_2], were investigated. Alongside yield the toxicity of reagents was considered, with the use of 4-(trimethylstannyl)pyridine far from desirable. Although Sn could not be avoided, the viability of the marginally less toxic analogue 4-(tri^{n}butylstannyl)pyridine was investigated. Experiments were performed in duplicate with both stannanes to assess their potency. Table 7.1 reports the reaction conditions tested and the analysis of the results follows.

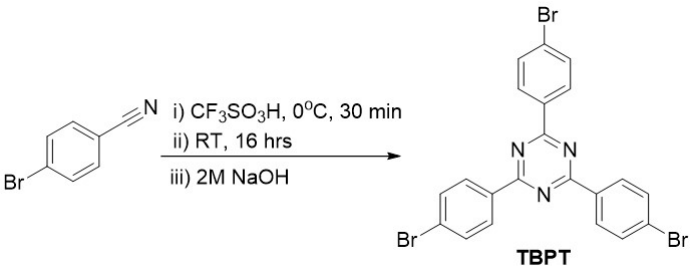

Scheme 7.6: Synthesis of precursor **TBPT**.

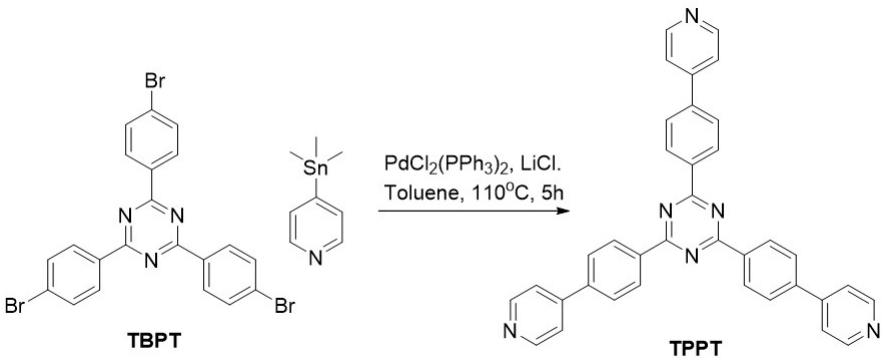

Scheme 7.7: Literature synthesis of **TPPT**.

No.	Catalyst	Sn compound	Solvent	LiCl	Yield / %
1	$PdCl_2(PPh_3)_2$	Methyl	Toluene	✓	18.8
2	$PdCl_2(PPh_3)_2$	^{n}Butyl	Toluene	✓	1.7
3	$PdCl_2(PPh_3)_2$	Methyl	1,4-dioxane	✓	55.6
4	$PdCl_2(PPh_3)_2$	^{n}Butyl	1,4-dioxane	✓	7.6
5	$PdCl_2(PPh_3)_2$	Methyl	1,4-dioxane	✗	26.2
6	$Pd(dppf)Cl_2$	Methyl	1,4-dioxane	✓	23.0
7	$Pd(dppf)_2$	^{n}Butyl	1,4-dioxane	✓	6.2
8	$Pd(dppf)_2$	Methyl	Toluene	✓	24.7
9	$Pd(dppf)_2$	^{n}Butyl	Toluene	✓	10.0
10	$Pd(dppf)_2$	Methyl	Toluene	✗	16.9

Table 7.1: Reaction conditions tested in the development of **TPPPT** synthesis and final yields.

Catalyst

The original procedure was published in 1995 using $[PdCl_2(PPh_3)_2]$ and it was hypothesised that the more recently developed catalyst $[Pd(dppf)Cl_2]$, frequently used in similar cross-coupling reactions, may prove beneficial. The relative potencies of the two palladium catalysts were assessed. Reactions were performed with the same mole percent catalyst (6.6 mol%) with different combinations of ^{n}butyl and methyl Sn compounds, solvents and LiCl. Comparing the highest yielding experiments with each catalyst (3 and 8 in Table 7.1), $[PdCl_2(PPh_3)_2]$ was over twice as effective in term of yield (55.6% vs 24.7%). Interestingly however, in the case of toluene solvated experiments, $[Pd(dppf)Cl_2]$ was marginally more effective.

Organostanne

By comparison of experiments 1 - 4 and 6 - 9 in Table 7.1 the dramatic effect of the nature of the organostannane was evident. Under all conditions the use of 4-(trimethylstannyl)pyridine resulted in significantly higher yields when compared with those of 4-(tri^{n}butylstannyl)pyridine in otherwise identical conditions. This was visually noticeable by the off-white appearance of the crude product with 4-(tri^{n}butylstannyl)pyridine compared to 4-(trimethylstannyl)pyridine (see Figure 7.4). This difference in activity was magnified when used with $[PdCl_2(PPh_3)_2]$ rather than $[Pd(dppf)Cl_2]$ catalyst. For example in 1,4-dioxane, replacing the methyl-stannane with its ^{n}butyl analogue effected a dramatic drop in yield of 48.0% with $[PdCl_2(PPh_3)_2]$ compared to 16.8% with $[Pd(dppf)Cl_2]$. This may be explained by the marginally higher steric demand of the tri^{n}butyl- compared to trimethyl-stannyl. During the

transmetallation step in the catalytic cycle the Sn species must approach the Pd(II) species to form the transmetalation transition state. With a higher steric demand on either reagent this step may be impeded. While it was hoped the affect on yield would not be so significant, it is clear the use of 4-(trimethylstannyl)pyridine is greatly preferable.

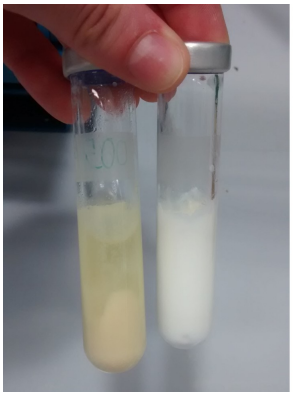

Figure 7.4: Crude products of reactions 3 and 4 in Table 7.1 varying only by stannyl compound used; (*left*) 4-(tributylstannyl)pyridine and (*right*) 4-(trimethylstannyl)pyridine.

Solvent

Comparing reactions 1 with 3, and 2 with 4 clearly shows the significant effect of solvent on the $[PdCl_2(PPh_3)_2]$ catalysed Stille coupling. With all other parameters constant the yield increased up to 7 times when 1,4-dioxane was used rather than toluene. This increase was seem for both the methyl- and butyl-organistannes. This is likely partly due to the increased solubility of the reagents in 1,4-dioxane allowing greater availability for reaction. Additionally, by comparing the LCMS-UV spectra of the crude products from reactions 1 and 3 it was clear a greater number of impurities were formed in toluene (Figure 7.5). However, for reactions catalysed by $[Pd(dppf)Cl_2]$ the effect of solvent on **TPPT** yield was negligible, if not marginally favoured by the use of toluene. This may be a result of the relative polarities of the solvents (0.164 and 0.099 for 1,4-dioxane and toluene respectively)[142] and/or their ability to stabilise catalytic intermediates by loosely coordinating and acting as labile leaving groups.

LiCl additive

According to Stille's interpretation of the effect of LiCl on cross-coupling reactions, LiCl accelerates the transmetallation step by replacing an inert Pd-O bond with an active Pd-Cl bond for

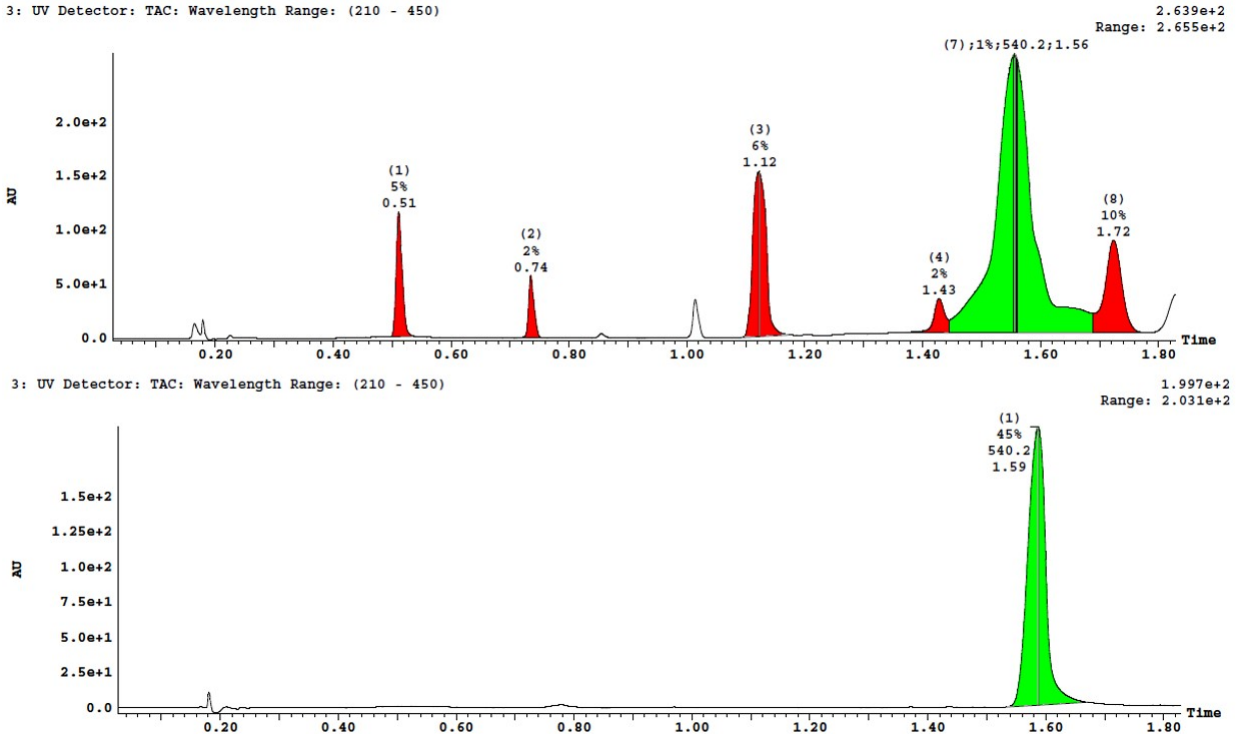

Figure 7.5: LCMS UV spectra of crude products from (*bottom*) reaction 1 in toluene and (*top*) reaction 3 in 1,4-dioxane. Product peak in green, impurities or solvent in red.

transmetallation. In this reaction however, where no Pd-O bonds are involved, it was suggested that nucleophilic attack of a chloride ion on organostannanes may produce reactive hypervalent species.[133] Having ascertained the favourability of 1,4-dioxane as a solvent over toluene, the effect of LiCl was revisited, along with its effect on reactions with the alternative catalyst Pd(dppf) in toluene. Comparing the yields from experiments numbered 3 and 5, 8 and 10 recorded in Table 7.1 there was a drop in yield in the absence of LiCl confirming its continued value.

Purification and scale up

The crude products were purified by column chromatography. The literature procedure provided no specific details of the eluent use but it was found that dichloromethane/methanol mixture at 90:10 was suitable for separating the product. However, NMR analysis showed the presence of residual impurities. A subsequent purification step of washing the product in chloroform/hexane (50 cm^3, 1:1) removed this impurity (Figure 7.6). However, this was accompanied by a large drop in yield (down to 20%) and due to the relatively low level of the original impurity this second purification step was omitted in subsequent syntheses. Furthermore, MS analysis showed the purity was acceptable and the molecular ion confirms the identity of the compound ($[M+H]^+$ at m/z = 541.20).

Summary

The optimised reaction conditions are shown in Scheme 7.8. TPPT was obtained on the 1.2 mmol scale in an average yield of 53% over 5 repeat experiments. Attempts to obtain single-crystals suitable for SCXRD analysis were unsuccessful.

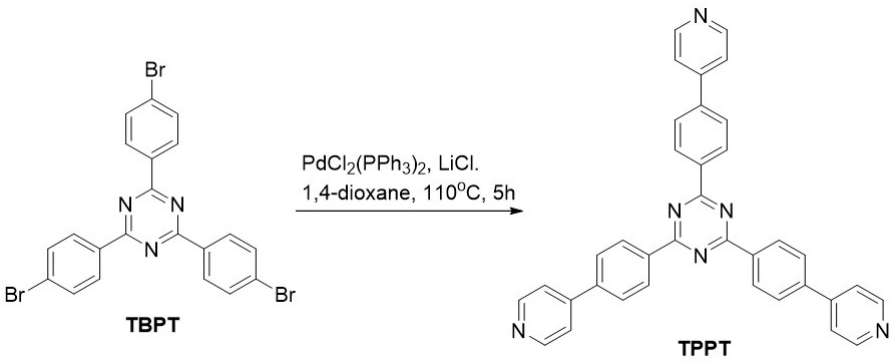

Scheme 7.8: Optimised synthesis of **TPPT**.

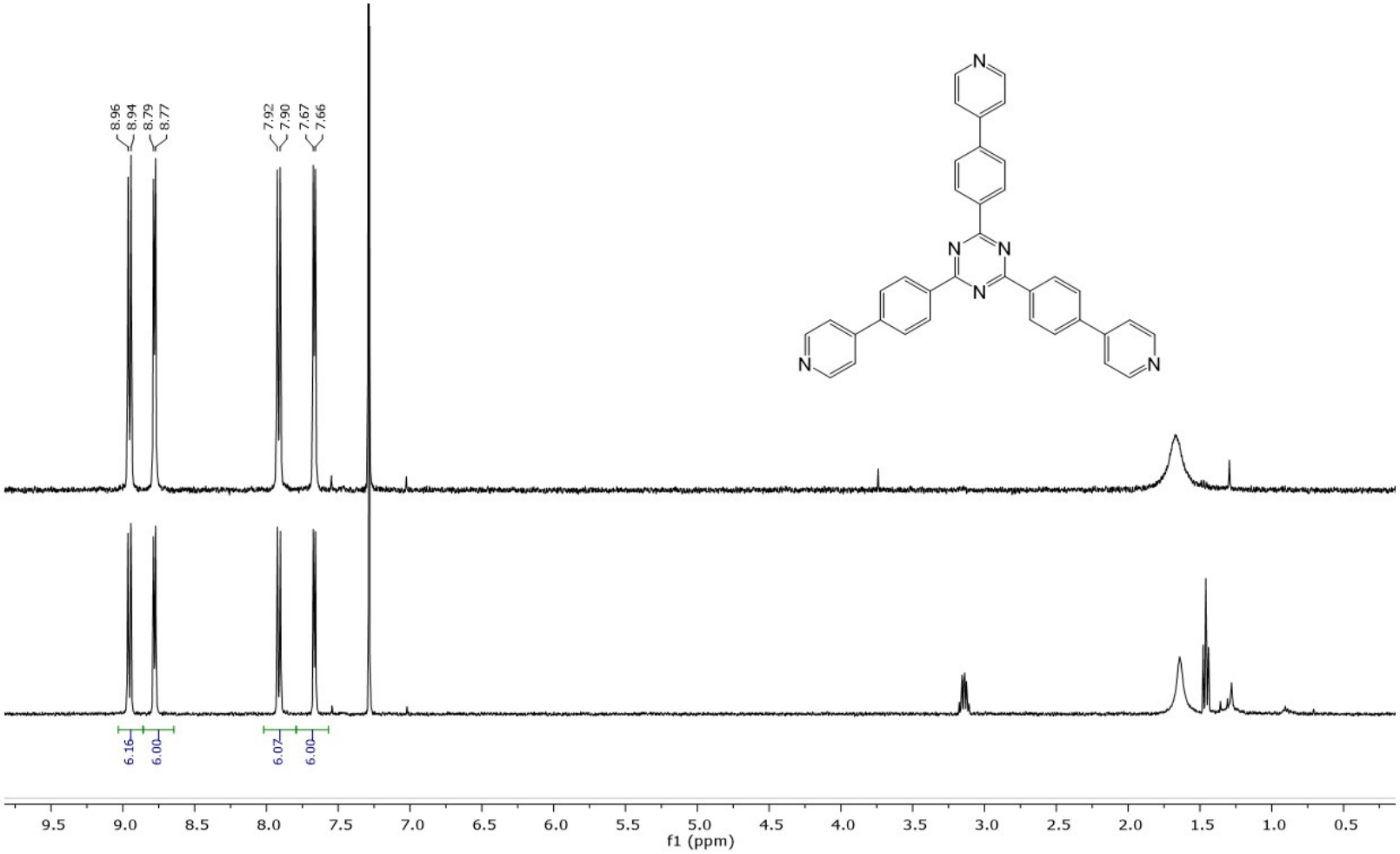

Figure 7.6: ^{1}H NMR spectrum of **TPPT** (*bottom*) after purification with column chromatography and (*top*) column chromatography and recrystallisation from hexane.

7.3.3 *Synthesis of TPPPT*

The design of this reaction was based on the use of compound **TBPT** and 4-(4-pyridyl)phenylboronic acid pinacol ester (**BAPE-PP**). **BAPE-PP** is commercially available but its high cost limited availability. Therefore, the judicious, informed selection of catalyst, solvent and base was extremely important in developing this chemistry. A search of the literature using SciFinder led to the conditions shown in Scheme 7.9 being successfully employed, with an average yield of 91%. ^{1}H NMR spectroscopy of the product revealed five peaks representing the 6 different different hydrogen environments present in **TPPPT** (distinguished as **A** - **F** in Scheme 7.9), with integrals matching the expected 36 protons. This was further supported by the expected twelve peaks in the ^{13}C NMR spectrum. Thorough analysis of the ^{1}H/^{13}C HSQC correlations enabled peak assignment. Two doublets with highest chemical shift (δ = 8.96 and 8.74 ppm) corresponded to those protons in closest proximity to nitrogen atoms (HC-N$_{pyridyl}$ (F) and HC-CC-N$_{triazine}$ respectively (A)). Those twelve protons associated with positions C and D, were observed as a multiplet at 7.96 - 7.87 ppm. Six protons relating to position B appeared as a multiplet at 7.87 - 7.78 ppm, and those at position E as a doublet at 7.65 pm. Purity was established by mass spectrometry with the molecular ion in the mass spectrum ([M+H]$^{+}$) at m/z = 541.20 further confirming the synthesis of **TPPPT**. Full NMR analysis is reported in Section 7.5.2.3. Rod-shaped crystals obtained by the slow cooling of solutions of **TPPPT** in both DMF and DMA were only weakly diffracting, preventing SCXRD analysis.

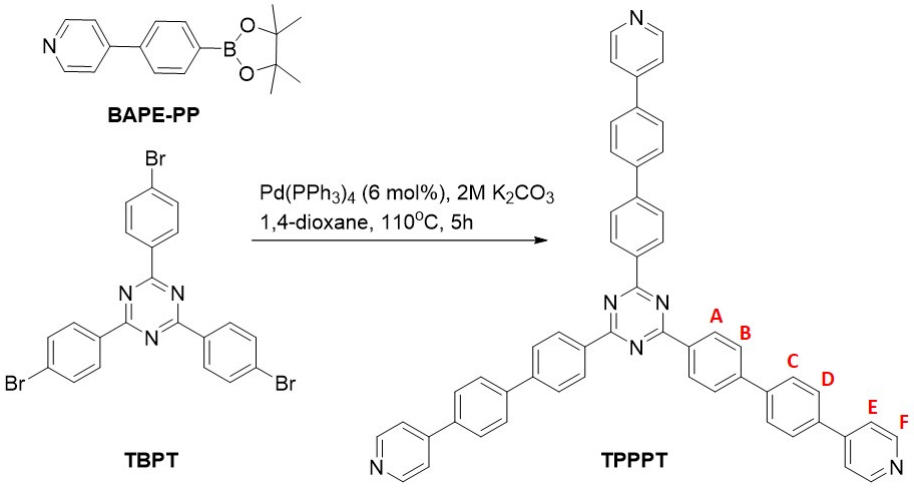

Scheme 7.9: Synthesis of **TPPPT**.

7.4 CONCLUSION

Three potential linker compounds for the synthesis of novel crystalline sponges have been synthesised. 2,4,6-tri(imidazol-1-yl)-1,3,5-triazine (**TIMTZ**) was obtained in a greatly improved yield from those obtained following the established literature procedure (rising from 32 - 73%). Furthermore, its previously unreported crystal structure was determined. The synthesis of 2,4,6-tris(4-(pyridin-4-yl)phenyl)-1,3,5-triazine (**TPPT**) was also successful, making use of a Suzuki-Miyaura reaction protocol. The literature procedure for its synthesis was found to be unreliable, but by the use of 1,4-dioxane as the reaction solvent acceptable yields of high purity product where obtained. A novel compound 2,4,6-tri(4'-(pyridin-4-yl)-[1,1'-biphenyl]-4-yl)-1,3,5-triazine (**TPPPT**) was synthesised from a boronic acid pinacol ester precursor *via* the Stille coupling reaction. This synthesis recorded extremely high yields of 91%.

7.5 EXPERIMENTAL

7.5.1 *Reagents and Materials*

Solvents and reagents were obtained from TCI and Sigma-Aldrich Co. All were of reagent grade and used without any further purification. NMR spectra were obtained on a Bruker AVANCE III HD 400 NMR spectrometer (Bruker-Biospin, Karlsruhe, Germany) equipped with TCI gradient CryoProbe. Chemical shifts (δ) are reported with respect to an internal tetramethylsilane (TMS) standard. NMR data were processed with MestReNova software. Melting points were determined on an Electrothermal IA9300 melting-point apparatus.

7.5.2 *Synthesis*

Experiments for the synthesis of **TPBT**, **TPPT** and **TPPPT** were performed in the closed environment of a sealed microwave vial to create autogenous pressure. The were performed under argon and reflux was achieved *via* a bench top hotplate with suitable insert.

7.5.2.1 *2,4,6-tri(imidazol-1-yl)-1,3,5-triazine*

2,4,6-trichloro-1,3,5-triazine (1.84 g, 10 mmol) and imidazole (4.08 g, 60 mmol) were mixed in the absence of solvent for 2 minutes at about 70 °C. Water/dichloromethane (50 cm^3, 1:1) was added to the reaction mixture which was sonicated until all solid was dispersed (5 min $\times$ 4) to allow the impurities to dissolve. The mixture was filtered and dried under vacuum to obtain the crude product (2.02 g). This was ground to a fine powder and was refluxed in ethyl acetate (100 cm^3). The insoluble components were filtered off, re-dispersed in ethyl acetate (100 cm^3) and the process repeated twice over. A white solid product was obtained from the filtrate (1.02 g, average yield 72%). Single-crystals were obtained by the slow-cooling of a saturated ethyl acetate solution of **TIMTZ**; mp 271 °C; ^{1}H NMR (400 MHz, $CDCl_3$) δ 8.73 (s, 3H), 7.95 (t, J = 1.4 Hz, 3H), 7.33 – 7.29 (m, 3H); ^{13}C NMR (101 MHz, $CDCl_3$) δ 162.16, 136.19, 131.87, 115.98; *m/z* 280.10 ($[M+H]^+$, 100%); cell parameters orthorhombic *Pccn*, a = 4.6228(2), b = 12.9308(7), c = 20.1709(10) Å, α = 90, β = 90, γ = 90°, V = 1205.75(11) $Å^3$ (full details in Appendix A).

7.5.2.2 *2,4,6-tris(4-(pyridin-4-yl)phenyl)-1,3,5-triazine*

4-bromobenzonitrile (3.64 g, 20 mmol) was added portion wise to triflic acid (6.00 cm^3, 68 mmol) at 0 °C with stirring. After 30 minutes the ice bath was removed and the yellow solution further stirred at room temperature. After 16 hrs a yellow precipitate had formed. The reaction mixture was neutralised with 2M NaOH solution (~16

cm ^{3}) and washed with chloroform and acetone (1:1, 50 cm^3). The organic layer separated and the aqueous layer extracted with chloroform/acetone (1:1, 50 cm^3). The combined organic layers were filtered and reduced under vacuum to obtain a white solid (3.43 g, 95% yield); ^{1}H NMR (400 MHz, $CDCl_3$) δ 8.63 (d, J = 8.6 Hz, 6H), 7.74 (d, J = 8.6 Hz, 6H); ^{13}C NMR (101 MHz, $CDCl_3$) 132.92, 132.17, 127.54, 117.56, 110.80; *m/z* [M•+] 545.0.

7.5.2.3 *2,4,6-tris(4-(pyridin-4-yl)phenyl)-1,3,5-triazine*

General procedure

Under argon, a dry 20 cm^3 microwave vial equipped with stirring bar was charged with **TBPT** (1.20 mmol, 1 eq.), stannyl compound (3.3 eq.), [Pd(dppf)Cl_2] or [$PdCl_2(PPh_3)_2$] catalysts (6.6 mol%) and LiCl (6.0 mmol). The vial was sealed and flushed with argon three times. Toluene or 1,4-dioxane (20 cm^3) was added through a syringe and the reaction mixture heated under reflux for 5h with continuous stirring. The reaction mixture was left to cool, filtered and the solid washed with water (3 $\times$ 10 cm^3) and toluene (3 $\times$ 10 cm^3).

Optimised reaction conditions

Under argon, a dry 20 cm^3 microwave vial equipped with stirring bar was charged with **TBPT** (655 mg, 1.20 mmol), 4-(trimeythylstannyl)pyridine (958 mg, 4.0 mmol), $Pd(PPh_3)_2Cl_2$ (56 mg, 0.08 mmol) and LiCl (254 mg, 6.0 mmol). The vial was sealed and flushed with argon three times. 1,4-dioxane (20 cm^3) was added through a syringe and the reaction mixture heated under reflux for 5 h with continuous stirring. The reaction mixture was left to cool, filtered and the solid washed with water (3 x 10 cm^3). The obtained white solid was dried under vacuum (0.35 g, 53%); mp 261 - 262 °C; ^{1}H NMR (400 MHz, $CDCl_3$) δ 8.95 (d, J = 8.2 Hz, 6H), 8.78 (d, J = 5.8 Hz, 6H), 7.91 (d, J = 8.2 Hz, 6H), 7.66 (d, J = 5.9 Hz, 6H); ^{13}C NMR (101 MHz, $CDCl_3$) δ 170.81, 149.91, 147.03, 141.74, 136.18, 129.30, 126.90, 121.22; *m/z* $[M+H]^+$ 541.20.

7.5.2.4 *2,4,6-tri(4'-(pyridin-4-yl)-[1,1'-biphenyl]-4-yl)-1,3,5-triazine*

A microwave vial equipped with a magnetic stirrer bar was dried under vacuum with a heat gun and flushed with Ar. It was charged with **TBPT** (0.1 g, 0.183 mmol), 4-(4-(4,4,5,5-tetramethyl-1,3,2-dioxaborolan-2-yl)phenyl)pyridine (0.170 g, 0.604 mmol, 3 eq.) and [$PdCl_2(PPh_3)_4$] (8.46 mg, 7.33 μmol), sealed and flushed with Ar $\times$ 3. Anhydrous 1,4-dioxane (3 cm^3) and 2M K_2CO_3 solution (0.366 cm^3, 0.733 mmol) were syringed in. The reaction mixture was heated under reflux for 5 h. After cooling the

mixture was diluted with water (20 cm^3), filtered and the filtrate washed with dichloromethane (3×20 cm^3) to separate the organic layer. The combined organic phases were concentrated to yield a light-grey solid (0.14 g, 91%); mp 286 - 288 °C; ^{1}H NMR (400 MHz, $CDCl_3$) δ 8.96 (d, J = 8.5 Hz, 6H), 8.74 (d, J = 6.1 Hz, 6H), 7.96 – 7.87 (m, 12H), 7.87 – 7.78 (m, 6H), 7.65 (d, J = 6.2 Hz, 6H); ^{13}C NMR (101 MHz, $CDCl_3$) δ 170.87, 149.62, 143.71, 140.67, 137.12, 135.46, 135.12, 129.15, 127.51, 127.10, 126.84, 121.06; m/z $[M+H]^+$ 769.3.

7.5.3 *Crystallography*

Following the procedure described in Section 3.5.3.

8

THE SYNTHESIS OF ALTERNATIVE CRYSTALLINE SPONGES

8.1 AIMS

The aim of experiments in this chapter is to produce novel porous metal-organic framework (MOF) structures of varying pore size capable of behaving as a crystalline sponge for the ordering and crystallographic analysis of non-crystalline compounds. The organic linkers used in experiments are based on the functionality of tris(4-pyridyl)-1,3,5-triazine (**TPT**) used in the established crystalline sponge $[\{(ZnI_2)_3(TPT)_2 \cdot x(\text{solvent})\}_n]$ (**1**). These include those synthesised in Chapter 7.

8.2 INTRODUCTION

> *'...it is important to first appreciate that it is difficult (although not impossible) to attempt a priori synthesis of structures...from simple metal ions and organic links because ions hold little directional information. This relative lack of directionality often results in flexibility around the metal ion, a multiplicity of possible structures and a general lack of control.'* From 'Reticular synthesis and the design of new materials' by Yaghi *et al.*[37]

As discussed in Section 1.4.1, the properties required of a potential crystalline sponge are three-fold: it must have guest-accessible pores of appropriate size; be reliably obtained as high quality single crystals; and it must be stable to the guest encapsulation processes. Designing a synthesis to achieve these targets remains a highly empirical processes requiring a 'give-it-a-go' attitude. The key experimental parameters to explore and refine can be divided into composition and process.[143] The most important of these are described in Figure 8.1. Of the established experimental methods for MOF production, layered diffusion and solvothermal techniques are most successful at producing single-crystalline products (see Section 1.3). Therefore, in a quest to discover viable synthetic protocols for the production of novel crystalline sponges, the relevant experimental parameters must be explored and refined.

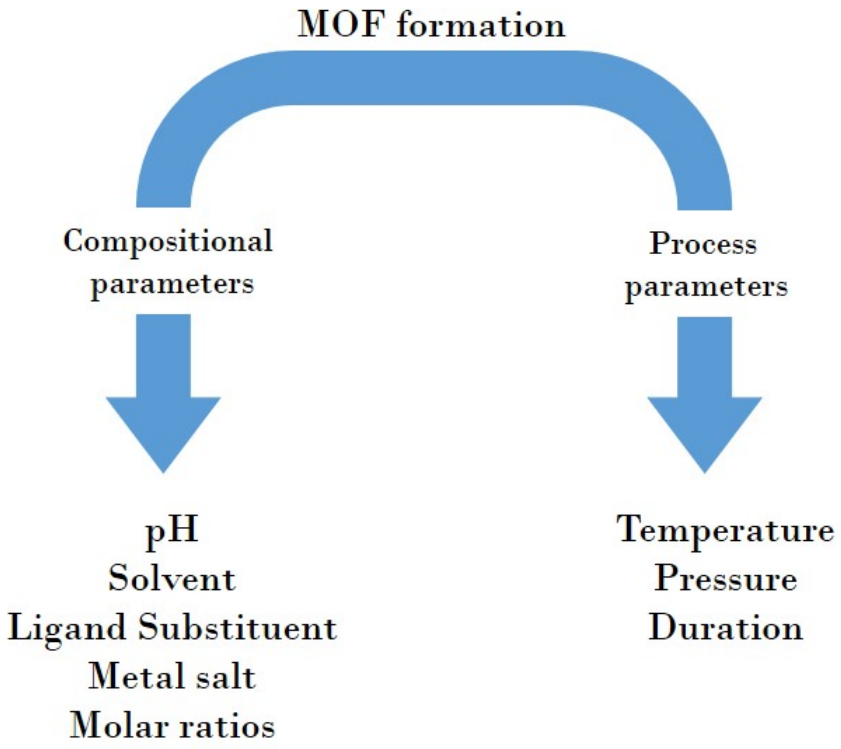

Figure 8.1: Factors effecting MOF synthesis.

8.2.1 *Chosen organic linkers*

Synthesis of alternative crystalline sponges focused on the following linkers, as shown in Figure 7.2: **TPT**, 2,4,6-tri(imidazol-1-yl)-1,3,5-triazine (**TIMTZ**), 2,4,6-tris(4-(pyridin-4-yl)phenyl)-1,3,5-triazine (**TPPT**) and 2,4,6-tri(4'-(pyridin-4-yl)-[1,1'-biphenyl]-4-yl)-1,3,5-triazine (**TPPPT**). These have the potential to form an isoreticular series of MOFs with systematic variations in pore size. Additionally, 4,4'-trimethylenedipyridine (**TMDP**), was investigated as an additional linker of interest due to its common terminal functionality (pyrdiyl group).

8.3 RESULTS

While attempts at the synthesis of novel MOFs using the linker series focused on interfacial and solvothermal methods, only the former successfully yielded characterisable solids. Searches of the literature informed experimental design, specifically in regards to solvents combinations and reagent concentrations. Discussion of the novel compounds obtained and difficulties faced in using **TPPT** and **TPPPT** linkers follows.

8.3.1 *Structures Based on TPT*

Experiments reported in the literature exploring the terminal ligand effect on Zn-**TPT** based structures yielded bromide and chloride analogs of **1**.[82] Here interest was focused on a non-halogen terminal ligand, specifically using $[Zn(OAc)_2.2H_2O]$. To this end, a single-crystalline product was obtained from the interfacial reaction of **TPT** in $CHCl_3$ and $[Zn(OAc)_2.2H_2O]$ in methanol after 37 days. SCXRD analysis reveal the formation of an extended MOF structure with the formula $[\{(Zn_4(OAc)_6)(\mathbf{TPT})\cdot 2(H_2O)\}_n]$ (**2**), crystallising in the monoclinic space group $C2/m$. The asymmetric unit of **2**, shown in Figure 8.2a, was found to contain half a TPT molecule sitting on a mirror plane and one and half $Zn(OAc)_2$ units, along with two water molecules.

In the extended structure, two symmetry equivalent Zn(II) centres of octahedral geometry and one in trigonal bipyramidal coordination were linked to a central oxygen anion in a planar environment. This cluster is surrounded by bridging acetate moieties to form a symmetrical neutral acetate trimeric cluster of formula $[Zn_3(\mu_3\text{-}O)(O_2CCH_3)_5]$ (Figure 8.2b). This is similar to the very well known class of coordination compounds $[M_3(\mu_3\text{-}O)(COO)_6]$, and an important motif in some well know MOFs.[144–147] In **2**, TPPT linkers bridge three Zn(II) centres completing their coordination sphere. The structure extends as two-dimensional sheets held together by $\pi\cdots\pi$ interactions. The structure is condensed and displayed no solvent accessible voids (Figure 8.3).

8.3.2 *Structures Based on TMDP*

Experiments with 4,4'-trimethylenedipyridine (**TMDP**) resulted in the production of two novel compounds in single-crystalline form. The first, $[\{(ZnI_2)_2(\mathbf{TMDP})\cdot C_6H_5NO_2\}_n]$ (**3**) was synthesised by the interfacial reaction of ZnI_2 in methanol with **TMDP** in nitrobenzene. The second is the mixed linker compound $[\{Co(\mathbf{TMDP})(mand)_2\}_n]$ (**4**), formed by the interfacial reaction of $[Co(NO_3)_2.6H_2O]$ and enantiopure D-mandelic acid (mand) in methanol and **TMDP** in

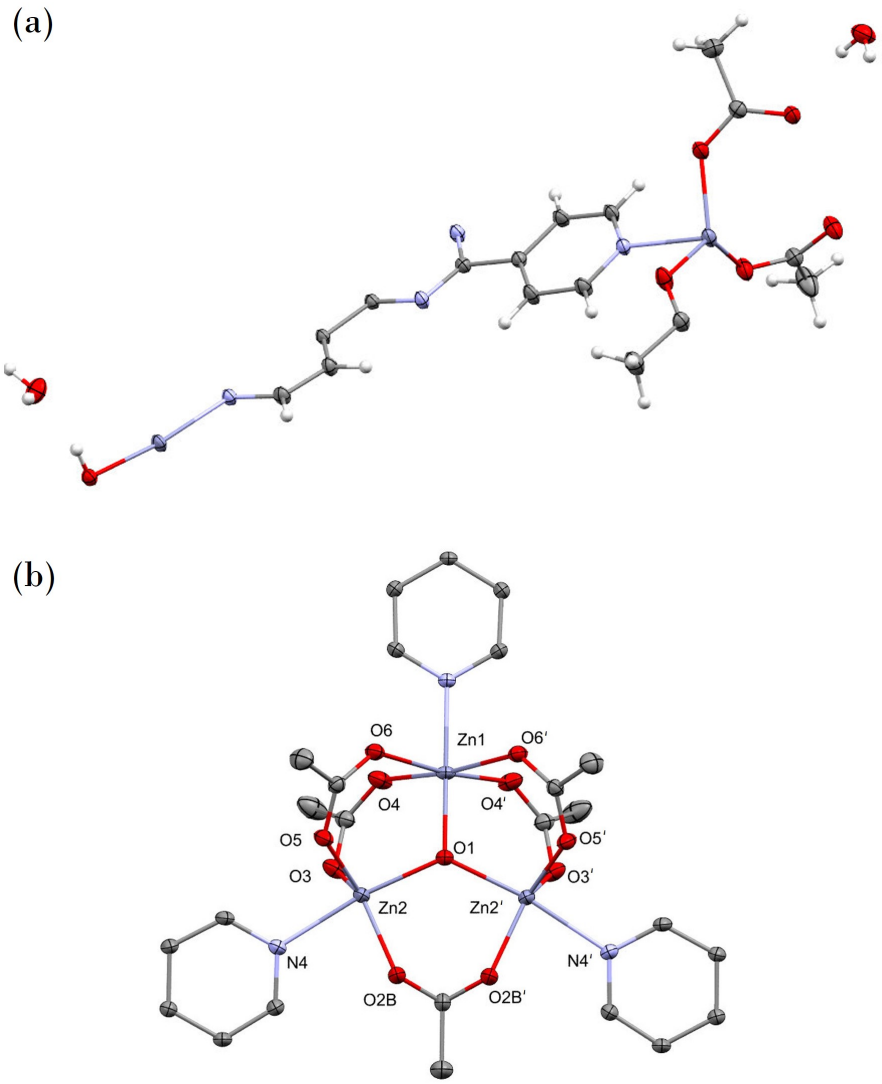

Figure 8.2: (a) Asymmetric unit of **2** and (b) the $[Zn_3(\mu_3\text{-}O)(O_2CCH_3)_5]$ cluster.

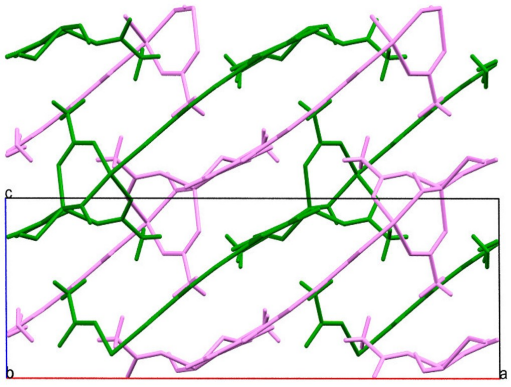

Figure 8.3: Extended structure of **2** formed of two-dimensional discrete sheets (highlighted in pink and green) extending along the *a*- and *b*-*axes*.

nitrobenzene. Crystals formed in each reaction were harvested after 8 days and subjected to SCXRD analysis.

*Crystal structure of **3***

3 was found to crystallise in the orthorhombic space group *Pnma*. The asymmetric unit (Figure 8.4a) contains half a **TMDP** molecule on a mirror plane coordinated to zinc in a ZnI_2 moiety and an uncoordinated nitrobenzene molecule. The tetrahedral geometry around Zn is shown in Figure 8.4b, the same motif as present in the four Zn-TPT forms described in Section 3.3 and those discussed in Section 1.4.2. One-dimensional Zn-**TMDP** chains form an extended structure, as shown Figure 8.5, which displays no solvent accessible voids and is therefore unsuitable as a crystalline sponge.

*Crystal structure of **4***

4 crystallised in the chiral hexagonal space group $P6_522$. The asymmetric unit contains half a **TMDP** molecule, D-mandelic acid cations and one Co(II) (Figure 8.6a). D-mandelic acid acts as a monoanionic O,O'-bidentate ligand that chelates Co^{2+} through the carboxylic and hydroxyl oxygens to form a five-membered chelate ring, with a bite angle of 77.26°. This is a well characterised coordination environment in chiral MOFs based on Co(II) and other metal centres,[148,149] although there are fewer reports of structures with N-donor auxiliary ligands.[150] Here, Co(II) exists in an octahedral environment chelated by two D-mandelic acid cations and two N atoms from separate bridging **TMDP** molecules, shown clearly in Figure 8.6b. In the extended structure, Co-TMDP-Co-TMDP chains with D-mandelic acid protrusions extend in three orientations to produce one dimensional chains with a condensed, non-porous structure. This is highlighted by colouration of symmetry equivalent chains in Figure 8.7.

8.3.3 *Structures Based on TPPT and TPPPT*

Attempts at the production of MOFs based on linkers **TPPT** and **TPPPT** were unsuccessful. The most significant difficulty experienced was the low solubility of the reagents, with only DMA and DMF found to be suitable. DMA was found to be the best solvent with solutions of 8.0 $\times 10^{-3}$ M and 8.0 $\times 10^{-4}$ M obtained for **TPPT** and **TPPPT** respectively (measured at 25°C, with dissolution aided by 10 minutes in an ultrasonic bath). This prevented significant variation in concentration and solvent, with focus instead placed on varying temperature, pressure, metal salt and experiment duration. Ultimately however, extensive interfacial and solvothermal experiments yielded no characterisable solid.

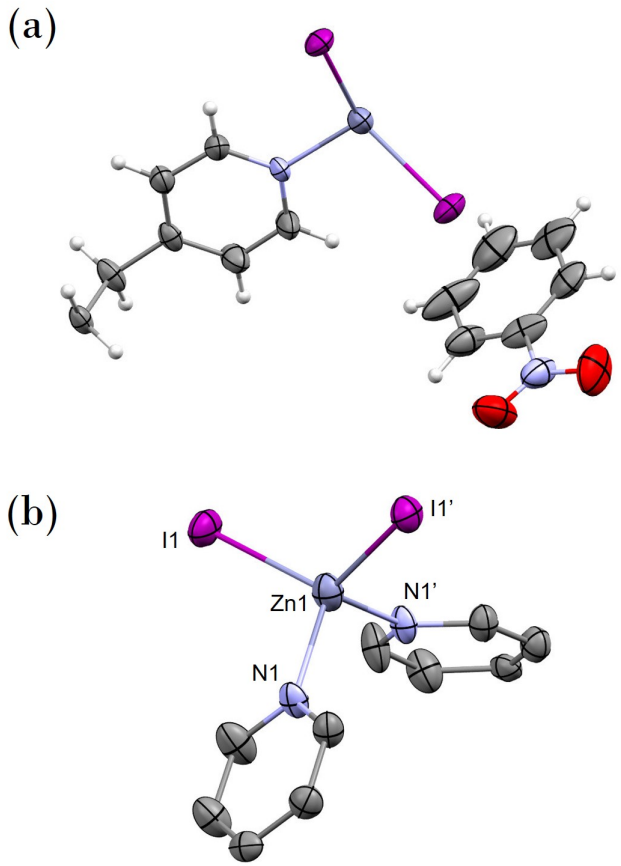

Figure 8.4: (a) Asymmetric unit of **3** and (b) the coordination environment of Zn(II)(hydrogens and nitrobenzene omitted for clarity).

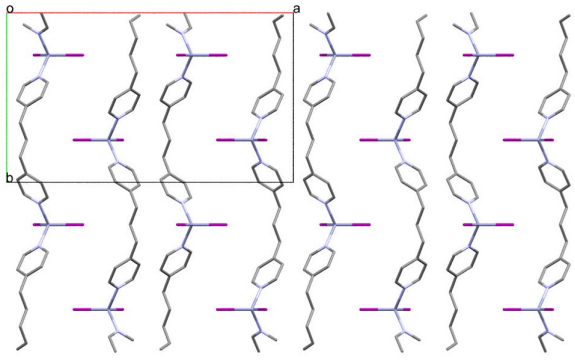

Figure 8.5: (a) Extended structure of **3** (hydrogens and nitrobenzene omitted for clarity).

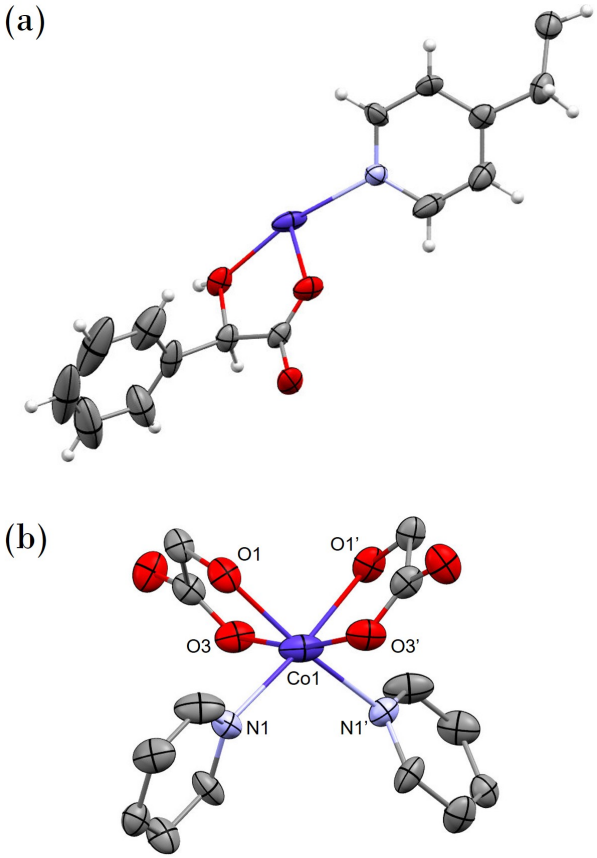

Figure 8.6: (a) Asymmetric unit of **4** and (b) extended structure (hydrogen atoms omitted for clarity).

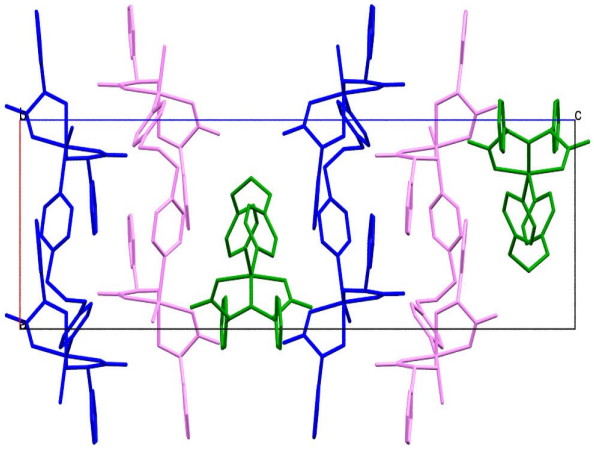

Figure 8.7: Extended structure of **4**, with chains coloured according to orientations (hydrogen atom omitted for clarity).

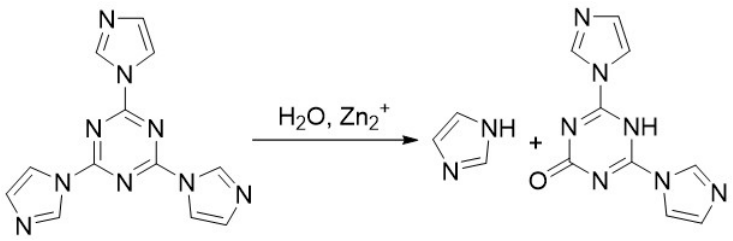

Scheme 8.1: Zinc catalysed hydrolysis of TIMTZ.

8.3.4 *Structures Based on TIMTZ*

The interfacial reaction of **TIMTZ** in wet DMF with ZnI_2 (or $Zn(OAc)_2$) in methanol yielded colourless crystals in just two days, occurring as the two morphologies shown in Figure 8.8. Only the morphology indicated by a yellow asterisk were high quality single crystals. SCXRD revealed these crystallised in the monoclininc space group $P2_1/c$ with formula $[\{Zn(C_9H_6N_7O)_2 \cdot 0.63(DMF)\}_n]$. The asymmetric unit shown in Figure 8.9 contains one zinc atom of octahedral geometry coordinated to four N-atoms from the imidazole groups along with two carbonyl oxygen atoms from the linker. It is evident that the intended linker **TIMTZ** underwent the hydrolysis reaction shown in Scheme 8.1 with the loss of one imidazole group, as has been previously reported.[151] This is thought to be a specifically zinc catalysed hydrolysis as a sample of **TIMTZ** dissolved for an equal time (2 days) in wet DMF only did not show any ^{1}H NMR peaks attributable to its hydrolysed analogue. As the zinc atom has a 2+ charge this must be balanced by a negative charge on each linker to produce an overall neutral structure. This is most likely delocalised around each triazide ring. A DMA molecule of 63% occupancy was also present in the asymmetric unit, uncoordinated to the framework. Some residual electron density was present in the asymmetric unit that could not be modelled. To complete the refinement the OLEX2 solvent mask was applied, removing 126 e^-, full details of which are given in Appendix A.

The extended crystal structure of **5**, shown in Figure 8.10, is made up of infinite criss-crossed chains which create channels extending down the *a*- and *c-axes*. After removal of residual DMF molecules in Mercury, **5** is calculated to have solvent accessible voids of 1225.58 $Å^3$ per unit cell (29.6% by volume). This is approximately a quarter the volume accessible in the pores of **1**.

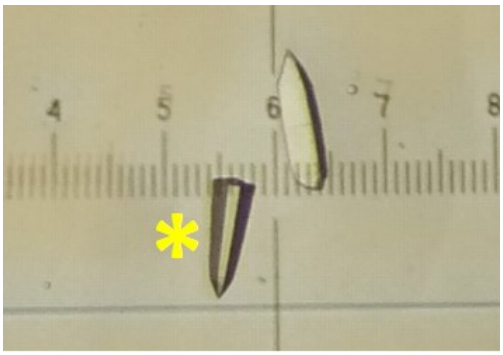

Figure 8.8: Micrograph images of the two crystal morphologies obtained from the interfacial reaction of TIMTZ and Zn.

	5	**5a**	**5b**
Crystal system	monoclinic	monoclinic	monoclinic
Space group	$P2_1/c$	$P2_1/c$	$P2_1$
a/Å	16.1806(4)	15.9810(4)	17.8789(2)
b/Å	19.7259(4)	18.9684(4)	18.5716(2)
c/Å	14.2453(4)	15.0742(4)	25.7333(3)
α/°	90	90	90
β/°	114.513(3)	111.945(3)	92.2587(11)
γ/°	90	90	90
Volume/Å^3	4137.0(2)	4238.41(18)	8536.37(18)

Table 8.1: Crystal data for **5**, **5a** and **5b** at 150 K.

8.3.5 *Encapsulation Experiments*

Experiments establish the capability of **5** to act as a crystalline sponge. Successful encapsulation experiments were carried out which yielded encapsulation complexes with the guests *trans*-cinnamaldehyde and 2,4,6-trimethylaniline (Figure 8.11), forming encapsulation complexes **5a** and **5b**, respectively. Experiments were performed using the neat liquid guest with a soaking duration of 2 days. There was no need for solvent exchange and no colour change was observed upon encapsulation. Analysis of specific quest uptake, occupancy and key intermolecular interactions is reported in the following sections.

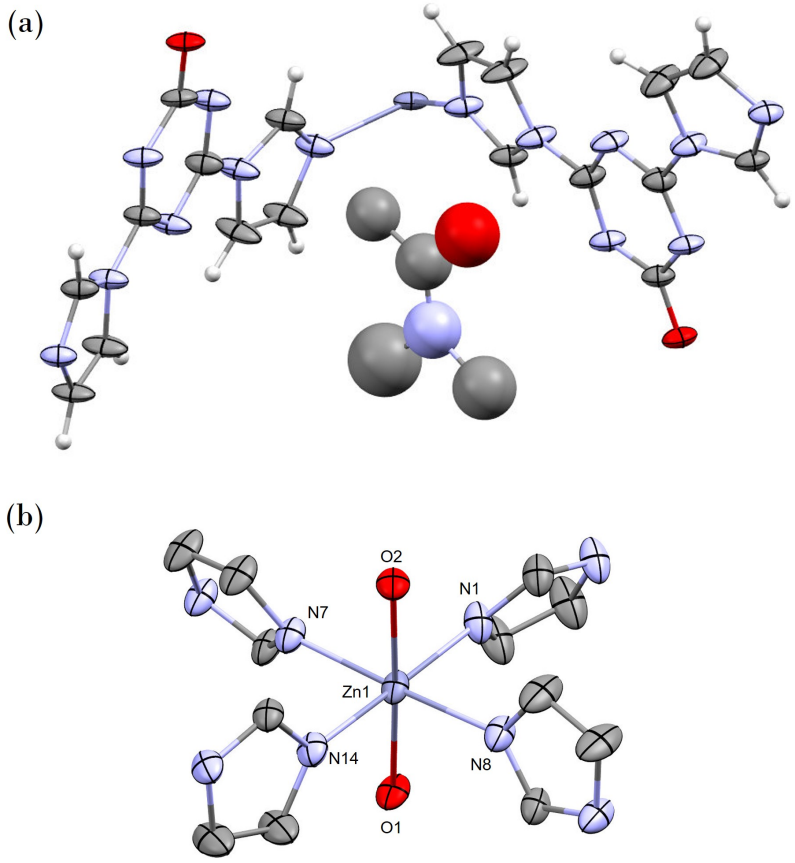

Figure 8.9: (a) Asymmetric unit of **5** and (b) extended structure (hydrogen atoms omitted for clarity).

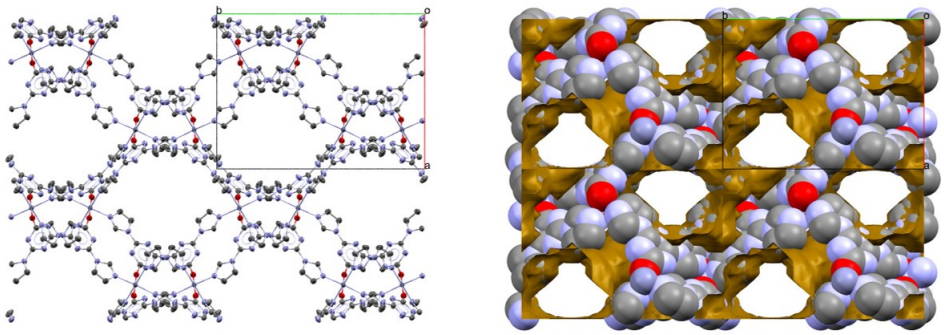

Figure 8.10: Packing diagrams of **5** as viewed down the *a-axis*. (a) Capped stick model (b) spacefilling model showing voids space in orange.

8.3.5.1 **5a**: *[{Zn($C_9H_6N_7O$)$_2$•2(C_9H_8O)}$_n$]*

5a crystallised in the centrosymetric monoclininc space group $P2_1/c$ with formula [{Zn($C_9H_6N_7O$)$_2$•2(C_9H_8O)}$_n$]. The key refinement indicators are reported in Table 8.1, showing the slight unit cell change upon encapsulation of *trans*-cinnamaldehyde into **5**. The asymmetric unit is shown in Figure 8.12, with molecules of *trans*-cinnamaldehyde taking up two unique sites both with 100% occupancy. The guest molecule labelled B displays positional disorder, manifested as minor rotation of the aromatic ring and orientation of the chain (Figure 8.13). Analysis of the extended structures and short-contacts as defined in Mercury[131] gives insight into the dominant interactions anchoring the guest molecules in the pores. There is evidence for both electrostatic interactions and hydrogen bonding. Guest A is positioned by a $\mathrm{CH}\cdots\pi$ interaction with an imidazole ring of the framework, as shown in Figure 8.14. Additionally, contact measurements suggest the presence of a C(H)=O$\cdots$H interaction (2.89 Å) between two symmetry equivalent guests. Guest B appears to be anchored by a parallel offset $\pi\cdots\pi$ interaction (4.04 Å, dihedral angle 8.10°) with a imidazole ring of the framework. A C=O$\cdots$H (3.15 Å) guest-guest was revealed formed between symmetry equivalent molecules. Each aldehyde acts as both an acceptor and donor. This is likely to be responsible for anchoring the end of the *trans*-cinnamaldehyde chain and determining the overall orientation. Both interactions are shown in Figure 8.15.

Analysis using PLATON calculated a void space of 858.0 $\mathrm{Å}^3$ [20.2%] per unit cell, accounting for generation of a level A checkCIF alert for solvent accesible voids. Electron density of 849.4 e^- is present in the voids - the equivalent of 3 additional *trans*-cinnamaldehyde molecules per asymmetric unit. This suggests that either there are areas in the unit cell that are not capable of guest ordering, or that the time given for encapsulation experiments (2 days) was insufficient for guest equilibration in those areas.

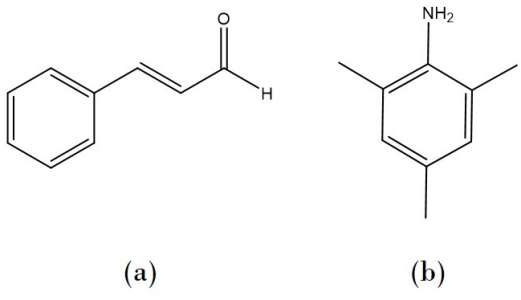

Figure 8.11: Guest compounds (a) *trans*-cinnamaldehyde and (b) 2,4,6-trimethylaniline.

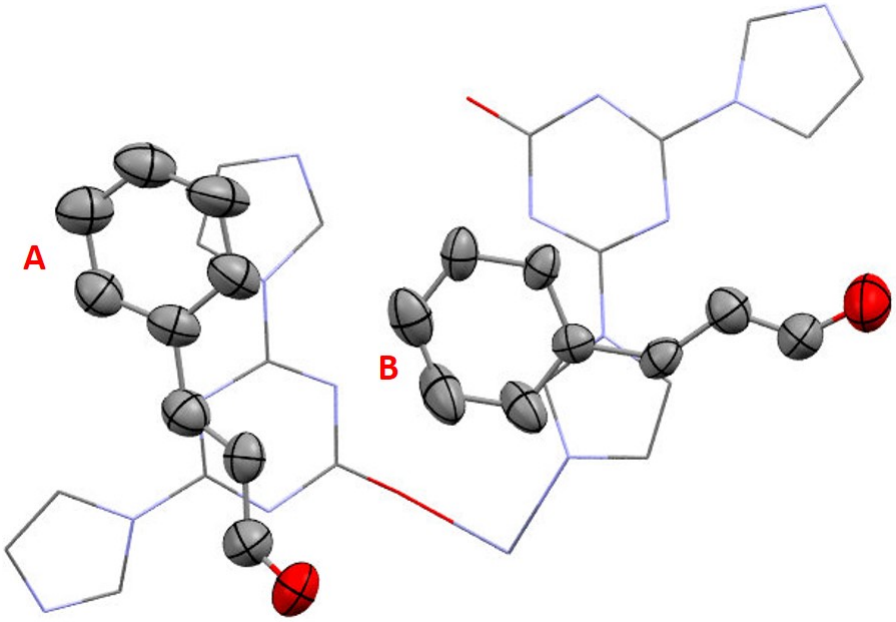

Figure 8.12: Asymmetric unit of **5a**.

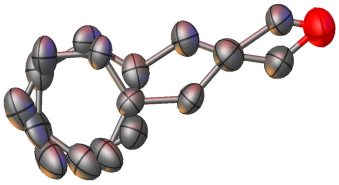

Figure 8.13: Disorder of guest B cinnamaldehyde in **5a**. Atoms are shown as ellipsoids at 50% probability.

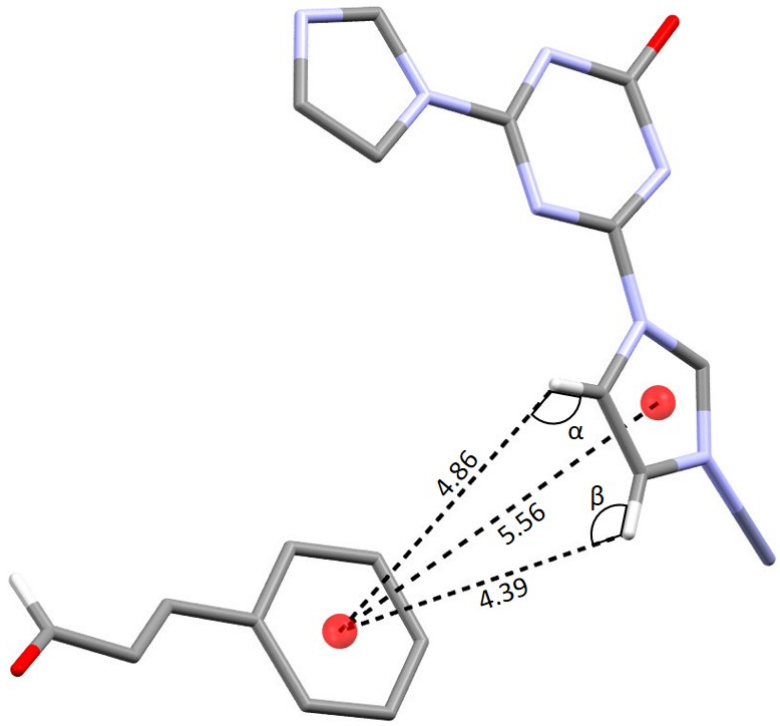

Figure 8.14: Guest(A)-host CH $\cdots$ π interaction in **5a**. α 97.95° and β 113.6°.

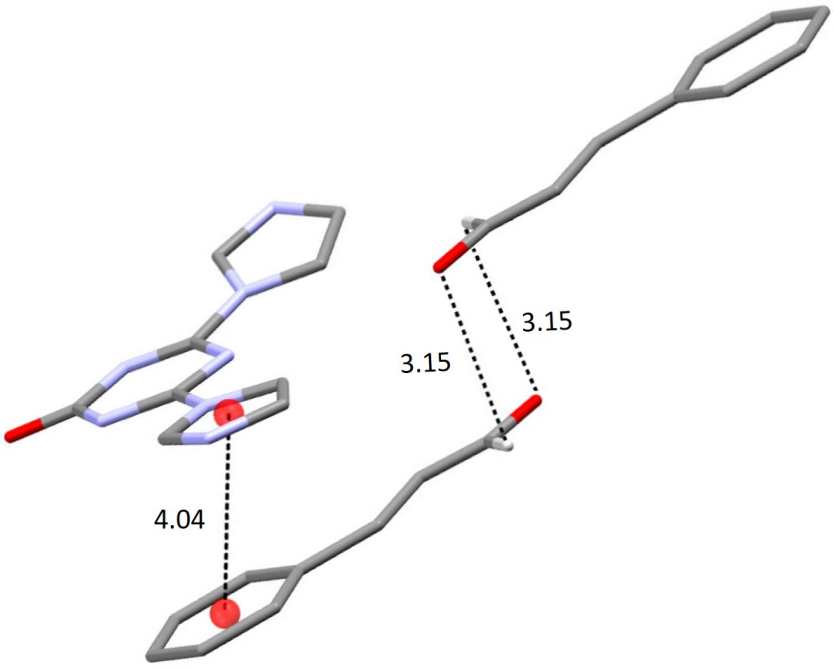

Figure 8.15: The $\pi \cdots \pi$ and hydrogen bond interactions formed in **5a**. Centroids shown as red spheres.

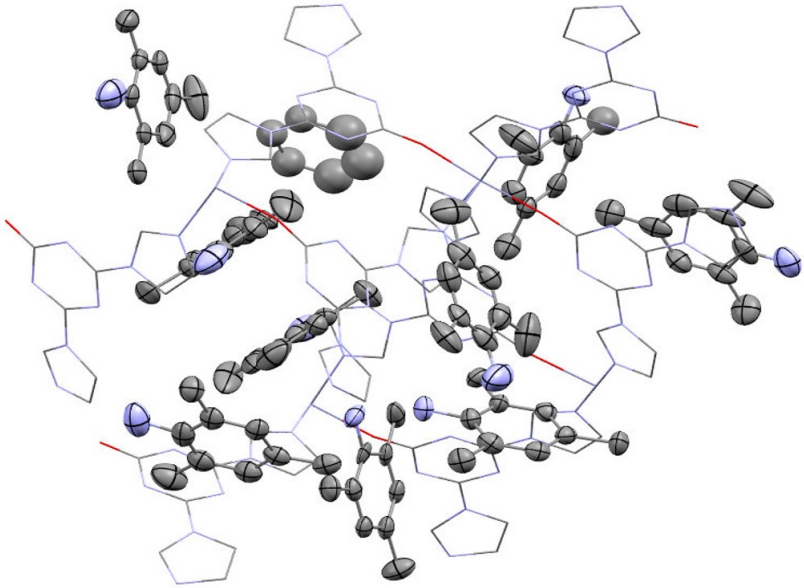

Figure 8.16: Asymmetric unit of **5b**.

8.3.5.2 ***5b***: *[{Zn($C_9H_6N_7O$)$_2$•7.42($C_9H_{11}NH_2$)}$_n$]*

5b crystallised in the monoclininc space group $P2_1$ with formula [{Zn($C_9H_6N_7O$)$_2$•7.42($C_9H_{11}NH_2$)}$_n$] having undergone a single-crystal-single-crystal space group transformation from **5** ($P2_1/c$). This is a interesting examp'e of an achiral compound crystallising in Sohncke space group.[152] The high flack parameter (0.489(10)) reflects the lack of Freidel opposites obtained during data collection. Neither structure inversion nor BASF/TWIN refinement yielded any improvement. Although this resulted in the unsatisfactory arbitrary assignment of the absolute structure, as the guest is non-chiral this structure still allows an important insight into encapsulation complexes with **5**. Inspection of crystal data in Table 8.1 allows a direct comparison of the key unit cell parameters. The framework itself (relieved of any guest molecules) was found to be unchanged and all three are super-imposable in Mercury. This confirms **5b** is isostructural but not isomorphic to **5** and **5a**. The asymmetric unit is shown in Figure 8.16, containing nine unique molecules of 2,4,6-trimethylaniline all of which were refined anisotropically, with occupancies between 91 - 100%. One incomplete, isotropically refined C_6 fragment at 100% occupancy is also present. Indistinguishable electron density around the expected positions of the -Me or -NH_2 groups was apparent but attempts at assign resulted in an unstable refinement.

Analysis of the interactions responsible for the ordering of 2,4,6-trimethylaniline in the pores of **5** again indicate the importance of electrostatic interactions. $\pi \cdots \pi$ interactions were observe in the form of parallel face-centred guest-host$_{triazine}$, and offset

guest-guest interactions. An example of each of these is displayed in Figure 8.17, with centroid· · ·centroid distances of 3.90 Å (dihedral angle 4.16°) and 4.32 Å (0.75°) respectively. Due to the high substitution of the aromatic ring in 2,4,6-trimethylaniline $\mathrm{CH}\cdots\pi$ appear to take on a more unusual form to that observed previously. Figure 8.17 also shows two examples of interactions formed between an imidazole ring of the framework and either -CH_3 and/or $C_{arom}H$ groups of the guest, depending on its specific orientation.

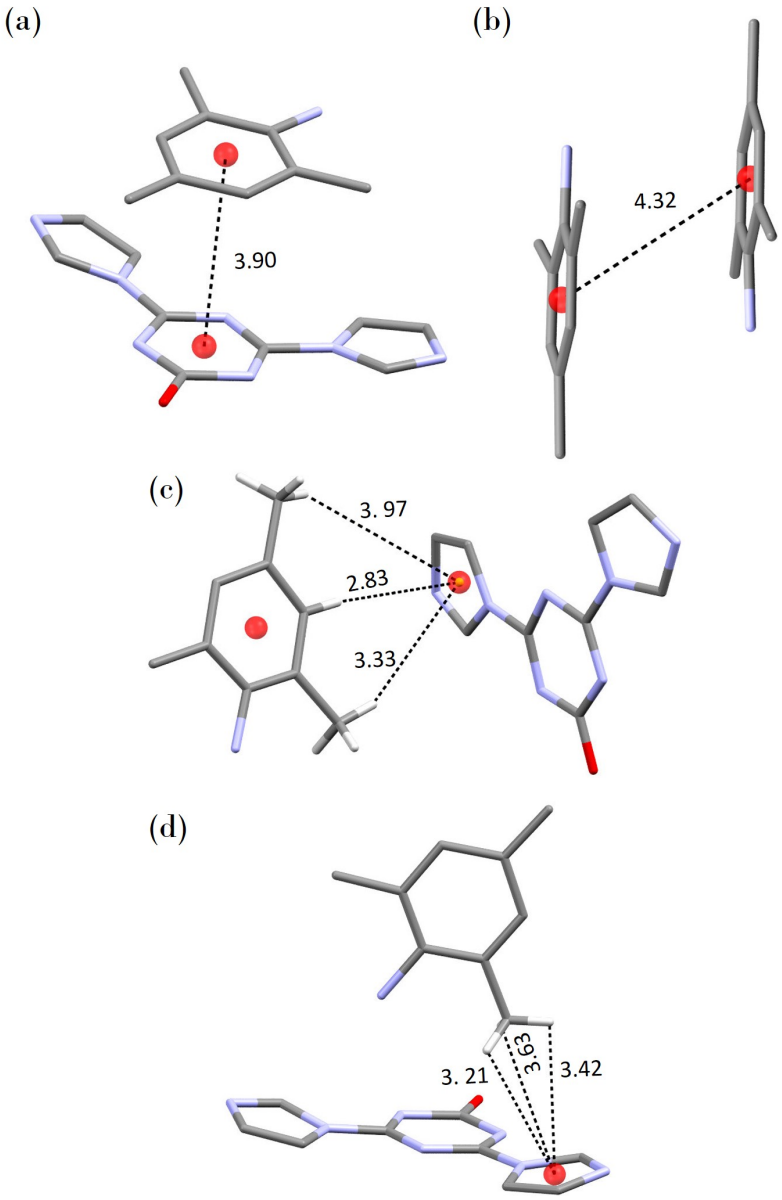

Figure 8.17: Examples of (a) guest-host and (b) guest-guest $\pi\cdots\pi$ interactions, and (c,d) unusual $\mathrm{CH}\cdots\pi$ interactions formed in **5b**. Centroids shown as red spheres.

8.4 CONCLUSION

Four new metal-organic frameworks based on linkers with similar functionality to **TPT** have been synthesised using the interfacial diffusion method. All were obtained as single-crystals and fully characterised by SCXRD. They are: $[\{(Zn_4(OAc)_6)(TPT)\cdot 2(H_2O)\}_n]$ (**2**); $[\{(ZnI_2)_2(TMDP)\cdot C_6H_5NO_2\}_n]$ (**3**); $[\{Co(TMDP)(mand)_2\}_n]$ (**4**); and $[\{Zn(C_9H_6N_7O)_2\cdot 0.56(DMF)\}_n]$ (**5**). The structures of **2**, **3** and **4** were found to be formed of one-dimensional chains with non-porous condensed extended structures. Conversely, **5** was shown to have three-dimensional structure containing solvent accessible voids of 1225.58 $Å^3$ per unit cell (29.6% by volume, approximately half the volume accessible in the pores of **1**). Its potential as a crystalline sponge was probed and encapsulation complexes with *trans*-cinnamaldehyde and 2,4,6-trimethylaniline successfully obtained. Guest molecules were anistropically refined with comparably few restraints to those required for some encapsulation complexes reported here with **1**.

Although the initial aim was to obtain a crystalline sponge with larger pore size, this work displays the potential for **5** to be used as crystalline sponge. Indeed, a smaller pore size may be advantageous in optimising certain guest-host interactions by increased proximity. Its ease of synthesis offers certain advantages to using **5** as a crystalline sponge, compared to **1** and other alternatives discussed in Section 1.8. Firstly the synthesis is rapid, producing a high yield of crystals after only two days. Secondly, the protocol is forgiving to the experimenter; **5** was seen to form with either ZnI_2 or $Zn(OAc)_2$ in DMA or DMF. Thirdly, no solvent exchange is required before guest encapsulation. Additionally, the synthesis of the precursor linker **TIMTZ** on which **5** is based is straightforward to perform in house using inexpensive reagents - a great advantage over **1**, for which **TPT** is routinely purchased at a not insignificant cost.

Certainly more work needs to be preformed to ascertain the scope of **5** in terms of compatible guest size and functionality. However, based on the positive results obtained up to this point, it can be concluded that **5** has a great deal of potential in the field of crystal-free crystallography.

8.5 EXPERIMENTAL

8.5.1 *Synthesis of* ***2***

A vial containing TPT (6.3 mg, 0.020 mmol) and chloroform (4 cm^3) was placed in a ultrasonic bath until dissolved (~5 minutes). The TPT solution was transferred to a borosilicate test tube (15 × 0.5 cm) and a 0.03M methanol solution of $[Zn(OAc)_2.2H_2O]$ (1 cm^3) layered on top. The tube was covered with a double layer of parafilm and left on the bench top for 37 days. After this time a few colourless crystals were harvested using a plastic Eppendorph pipette tip to detached crystals from the test tube surface. Collected crystals were stored in chloroform (~3 cm^3) at 25 °C in a screw cap vial until SCXRD analysis. Cell parameters monoclinic $C2/m$, $a = 24.3951(2)$, $b = 17.03155(16)$, $c = 7.81450(10)$ Å, $\alpha = 90$, $\beta = 90.4886(10)$, $\gamma = 90°$, $V = 3246.70(6)$ $Å^3$ (full details in Appendix A).

8.5.2 *Synthesis of* ***3***

TMDP (30.0 mg, 0.2 mmol) was dissolved in nitrobenzene (4 cm^3) and transferred to a borosilicate test tube (13 × 1 cm). A 0.06 M methanol solution of $Co(NO_3)_2.6H_2O$ (1 cm^3) was layered on top. The tube was covered with a double layer of parafilm and left in an incubator at 25 °C. After 8 days colourless block crystals were harvested and submitted directly for SCXRD analysis. Cell parameters orthorhombic $Pnma$, $a = 21.3050(2)$, $b = 12.59249(11)$, $c = 8.57461(9)$ Å, $\alpha = 90$, $\beta = 90$, $\gamma = 90°$, $V = 2300.42(4)$ $Å^3$ (full details in Appendix A).

8.5.3 *Synthesis of* ***4***

TMDP (46.8 mg, 0.3 mmol) was dissolved in nitrobenzene (5 cm^3) and transferred to a borosilicate test tube (13 × 1 cm). A methanol/nitrobenzene (1:1, 5 cm^3) buffer was carefully layered above. A third layer of $Co(NO_3)_2.6H_2O$ (120 mg, 0.4 mmol) and enantiopure D-mandelic acid (60 mg, 0.4 mmol) in methanol (5 cm^3) was layered on top. The tube was covered with a double layer of parafilm and left in an incubator at 25 °c. After 8 days orange needle crystals were harvested and submitted directly for SCXRD analysis. Cell parameters hexagonal $P6_522$, $a = 11.5256(3)$, $b = 11.5256(3)$, $c = 32.9005(8)$ Å, $\alpha = 90$, $\beta = 90$, $\gamma = 120°$, $V = 3785.0(2)$ $Å^3$ (full details in Appendix A).

8.5.4 *Synthesis of* ***5***

TIMTZ (3.3 mg, 4 mmol) was dissolved in dimethylformamide (1.5 cm^3) and ultrasonically dissolved and transferred to a borosilicate test

tube (7 × 0.8 cm). A buffer of methanol (0.5 cm^3) was layered on top, followed by a solution of ZnI_2 (0.5 mg, 3 mmol) in methanol (0.5 cm^3). The tube was covered with a double layer of parafilm and left in an incubator at 25 °C. After 2 days colourless crystals were harvested using a plastic Eppendorph pipette tip and transferred to a sealed glass vial in the reaction mixture.

8.5.5 *Encapsulation experiments*

Crystals of **5** were immersed directly into 1 cm^3 of the guest compound in a 3 cm^3 vial. Samples were incubated at 22 °C and guest exchange was allowed to proceed for 2 days. Suitable crystals were selected and subjected to SCXRD.

8.5.6 *Crystallography*

Following the procedure described in Section 3.5.3.

8.5.6.1 *Crystal structure refinement*

Structure refinement of encapsulation complexes began with construction of the rigid MOF framework which proved straight forward and once anisotropically refined any guests and/or solvent molecules present were identified. Where required the aromatic rings of guests were constrained using the AFIX 66 command.

For **5a**, anisotropic refinements were performed using DELU on one part of the disordered guest molecule.

For **5b**, anisotropic refinements were performed using SIMU on two of the nine guest molecules, one of which required the addition of DELU to achieve stable refinement. Two pyridyl rings in the framework required SIMU and RIGU, or ISOR restraints to prevent oblate ADPs.

9

SUMMARY OF RESULTS AND FUTURE DIRECTION

9.1 SUMMARY OF RESULTS

The main aims of this project were two-fold. Firstly, to investigate the ability of the metal-organic framework (MOF) $[\{(ZnI_2)_3(\text{tris(4-pyridyl)-1,3,5-triazine})_2.x(\text{solvent})\}_n]$ (**1**) to act as a 'crystalline sponge' for the analysis of non-crystalline compounds *via* single-crystal X-ray diffraction (SCXRD). Secondly, to develop alternative crystalline sponges to expand the scope of the technique by enabling to encapsulation of a broader range of guest compounds.

Studies began with the synthesis of **1** following two most prominent literature procedures. Through this study the challenges of application were explored, and an understanding of the delicacy of the technique developed. The most reliable protocol was identified and high quality single crystals obtained consistently, using the chloroform/methanol method. However, this was accompanied by the interesting but unwelcome discovery of three novel, non-porous Zn-TPT forms along side **1**. Although they decreased the yield of the desired form, their formation did not greatly impact subsequent encapsulation experiments.

This was followed by extensive encapsulation experiments with simple, aromatic guest molecules to obtain novel encapsulation complexes. Repeat experiments with five guest compounds, both solid and liquid, demonstrated the reproducibility of the technique and that guest molecules preferentially take up specific sites within the unit cell of **1**. This study presented the first demonstration of the reproducibility of the technique and showed that routine repetition of encapsulation experiments to be unnecessary.

These findings prompted the author to consider the cause of this specificity, and determine the key interaction that enable **1** to order its guest molecules and enable their visualisation by SCXRD. Two studies based around the encapsulation of systematic series of chemically related guest molecules probed the effect of variation in guest size and functionality on site uptake and ordering. Overall, the extended structures of 14 encapsulation complexes were analysed and short-contact measurements taken, revealing the dominate guest-host interactions. These were $\pi\cdots\pi$ and $CH\cdots\pi$ interactions, of predominately off-set arrangements. Results further suggested the complementary formation of multiple guest-host and guest-guest van der Waals interactions and hydrogen bonds.

Bolstered by the enhanced understanding of the nature of **1** provided by these studies, parallel work sought to over come the limitation of encapsulation into **1** associated with its pore size. This involved the synthesis of novel linkers based on the principle of isoreticular synthesis. Three organic compounds were synthesised to form a series of potential linkers with similar functionality and chemical properties to tris(4-pyridyl)-1,3,5-triazine (used in **1**) whilst displaying systematic variation in size. using Stille and Suzuki coupling reactions. They were; **TPT**, 2,4,6-tri(imidazol-1-yl)-1,3,5-triazine (**TIMTZ**), 4,4'-trimethylenedipyridine (**TMDP**), 2,4,6-tris(4-(pyridin-4-yl)phenyl)-1,3,5-triazine (**TPPT**) and the novel compound 2,4,6-tri(4'-(pyridin-4-yl)-[1,1'-biphenyl]-4-yl)-1,3,5-triazine (**TPPPT**). Work focused on developing interfacial synthesise to produce novel MOFs in single-crystalline form for future use as crystalline sponges. This yielded four novel MOFs: $[\{(Zn_4(OAc)_6)(TPT)\cdot 2(H_2O)\}_n]$ (**2**); $[\{(ZnI_2)_2(TMDP)\cdot C_6H_5NO_2\}_n]$ (**3**); $[\{Co(TMDP)(mand)_2\}_n]$ (**4**); and $[\{Zn(C_9H_6N_7O)_2\cdot 0.56(DMF)\}_n]$ (**5**). The latter of which, **5**, was formed from the product of the indirect zinc catalysed hydrolysis of **TIMTZ**. Of the four novel MOFs, **5** alone displayed any framework porosity, and was therefore tested for guest ordering ability. It was shown to display crystalline sponge properties, with proof-of-concept provided by the successful encapsulation and SCXRD analysis of *trans*-cinnamaldehyde and 2,4,6-trimethylaniline. The encapsulation complexes were analysed and the key guest-ordering interactions were determined as similar to those formed in **1**: $\pi\cdots\pi$ and $CH\cdots\pi$ interactions, along with guest-guest hydrogen bonding. These successful results reflect the merits of a systematic investigation, beginning with understanding the established structure of **1** and utilisation of the acquired knowledge to inform future investigation.

9.2 FUTURE DIRECTION

It has been shown that $[\{Zn(C_9H_6N_7O)_2\cdot 0.56(DMF)\}_n]$ (**5**) has the potential to be a highly valuable crystalline sponge, although the full extent of its capabilities has not yet been assessed. To better understand its scope and limitations, a broader range of encapsulation experiments is required. This would involve the use of guests with a range of functionalities, such as halogens, non-aromatic structures, basic amines and chiral compounds. Experiments to determine the reproducibility of guest positioning upon encapsulation in **5**, as performed with **1**, would be of great interest. This may lead to additional encapsulation complexes and refinements of the protocol, or it may highlight incompatibilities and unsuccessful results - this would all be valuable. The very

first step however, would be simply to ensure the reproducibility of the synthesis of **5** by a chemist other than the author to confirm the protocol's broad applicability. Given the initial difficulty in obtaining quality crystals of **1** from literature procedures and the inherent difficulty of single-crystal growth, this step is of great importance. With the overall aim of crystalline sponge development to offer of a broadly applicable and widely accessible technique, this development of **5** could hope to add a MOF to an arsenal of porous structures suitable for the analysis of non-crystalline compounds.

The linkers **TPPT** and **TPPPT** have not been reported in the literature as forming MOF structures, and offer huge potential for novel large-pored crystalline sponges. Therefore, with more time further attempts to determine optimal conditions for MOF growth (whether powder or crystalline) this goal may be achieved. This would involve investigating a broader range of metal components, solvent combinations and higher-pressure synthesis. Additionally, the crystal structures of **TPPT** and **TPPPT** have themselves not been reported and their full characterisation would complete the study. Crystallisation by sublimation may be attempted.

Part III

APPENDIX

A

CRYSTALLOGRAPHIC DATA

Please find supplementary crystallographic data on the attached CD ROM.

(1) Y. Inokuma, S. Yoshioka, J. Ariyoshi, T. Arai, Y. Hitora, K. Takada, S. Matsunaga, K. Rissanen and M. Fujita, *Nature*, 2013, **495**, 461–466.

(2) P. Stallforth and J. Clardy, *Nature*, 2013, **495**, 456–457.

(3) M. P. Bym, C. J. Curtis, Y. Hsiou, S. I. Khan, P. A. Sawin, S. K. Tendick, A. Terzis and C. E. Strouse, *J. Am. Chem. Soc.*, 1993, **115**, 9480–9491.

(4) S. L. James, *Chem. Soc. Rev.*, 2003, **32**, 276–288.

(5) M. J. Prakash and M. S. Lah, *Chem. Commun. (Camb).*, 2009, 3326–3341.

(6) O. M. Yaghi and H. Li, *J. Am. Chem. Soc.*, 1995, **117**, 10401–10402.

(7) H. Furukawa et al., *Science*, 2010, **329**, 424–428.

(8) J. An, O. K. Farha, J. T. Hupp, E. Pohl, J. I. Yeh and N. L. Rosi, *Nat. Commun.*, 2012, **3**, 604.

(9) P. Z. Moghadam, A. Li, S. B. Wiggin, A. Tao, A. G. Maloney, P. A. Wood, S. C. Ward and D. Fairen-Jimenez, *Chem. Mater.*, 2017, **29**, 2618–2625.

(10) H. Wang, X. Y. Yang, Y. Q. Ma, W. B. Cui, Y. H. Li, W. G. Tian, S. Yao, Y. Gao, S. Dang and W. Zhu, *Inorganica Chim. Acta*, 2014, **416**, 63–68.

(11) M. D. Allendorf, C. a. Bauer, R. K. Bhakta and R. J. T. Houk, *Chem. Soc. Rev.*, 2009, **38**, 1330.

(12) W. M. Bloch, N. R. Champness and C. J. Doonan, *Angew. Chemie Int. Ed.*, 2015, **54**, 2–10.

(13) J. Liu, L. Chen, H. Cui, J. Zhang, L. Zhang and C.-Y. Su, *Chem. Soc. Rev.*, 2014, **43**, 6011–6061.

(14) L. Qiaowei, Z. Wenyu, O. S. Miljanic, C.-h. Sue, Y.-l. Zhao and L. Liu, *Science*, 2009, **325**, 855–860.

(15) D. Sheberla, J. C. Bachman, J. S. Elias, C.-J. Sun, Y. Shao-Horn and M. Dincă, *Nat. Mater.*, 2016, **16**, 220–224.

(16) A. Phan, A. U. Czaja, F. Gandara, C. B. Knobler and O. M. Yaghi, *Inorg. Chem.*, 2011, **50**, 7388–7390.

(17) L.-L. Tan, H. Li, Y.-C. Qiu, D.-X. Chen, X. Wang, R.-Y. Pan, Y. Wang, S. X.-A. Zhang, B. Wang and Y.-W. Yang, *Chem. Sci.*, 2015, **6**, 1640–1644.

(18) H. Li, M. Eddaoudi, M. O'Keeffe and O. M. Yaghi, *Nature*, 1999, **402**, 276–279.

(19) S. S.-Y. Chui, S. M.-F. Lo, J. P. H. Charmant, A. G. Orpen and I. D. Williams, *Science*, 1999, **283**, 1148–1150.

(20) P. Silva, S. M. F. Vilela, J. P. C. Tome and F. A. Almeida Paz, *Chem. Soc. Rev.*, 2015, **44**, 6774–6803.

(21) M. Peplow, *Nature*, 2015, **520**, 148–150.

(22) J. A. Mason et al., *Nature*, 2015, **527**, 357–361.

(23) A. C. McKinlay et al., *Chem. Mater.*, 2013, **25**, 1592–1599.

(24) P. K. Allan et al., *Dalt. Trans.*, 2012, **41**, 4060–4066.

(25) *Retrieved 23/06/2017, https://www.chemistryworld.com/feature/mofs-find-a-use/2500508.article*.

(26) E Leung, U Müller, J. K. W. Sandler, G Skupin, M Yamamoto and A van der Net, *Biodegradable Material Composed Of A Polymer Comprising A Porous Metal-Organic Framework U.S. Patent, 13/257,787, Jan 19*, 2012.

(27) *Retrieved 12/05/2017, https://lukegamon.wordpress.com/tag/makoto-fujita/*.

(28) T. D. Bennett, A. L. Goodwin, M. T. Dove, D. A. Keen, M. G. Tucker, E. R. Barney, A. K. Soper, E. G. Bithell, J. C. Tan and A. K. Cheetham, *Phys. Rev. Lett.*, 2010, **104**, 2–5.

(29) C. Dey, T. Kundu, B. P. Biswal, A. Mallick and R. Banerjee, *Acta Crystallogr. Sect. B Struct. Sci. Cryst. Eng. Mater.*, 2014, **70**, 3–10.

(30) P. Maniam, N. Stock, A. Chemie and D Kiel, 2011, **50**, 5085–5097.

(31) A. Sonnauer, F. Hoffmann, M. Fröba, L. Kienle, V. Duppel, M. Thommes, C. Serre, G. Férey and N. Stock, *Angew. Chemie - Int. Ed.*, 2009, **48**, 3791–3794.

(32) C. E. Wilmer, M. Leaf, C. Y. Lee, O. K. Farha, B. G. Hauser, J. T. Hupp and R. Q. Snurr, *Nat. Chem.*, 2011, **4**, 83–89.

(33) M. Zhang, Y.-P. Chen, M. Bosch, T. Gentle, K. Wang, D. Feng, Z. U. Wang and H.-C. Zhou, *Angew. Chemie Int. Ed.*, 2014, **53**, 815–818.

(34) O. K. Farha and J. T. Hupp, *Acc. Chem. Res.*, 2010, **43**, 1166–1175.

(35) B. Chen, S. Ma, F. Zapata, F. R. Fronczek, E. B. Lobkovsky and H. C. Zhou, *Inorg. Chem.*, 2007, **46**, 1233–1236.

(36) L. Ma, J. M. Falkowski, C. Abney and W. Lin, *Nat. Chem.*, 2010, **2**, 838–846.

(37) O. M. Yaghi, O. K. M, N. W. Ockwig, H. K. Chae, M Eddaoudi and J Kim, *Nature*, 2003, **423**, 705–714.

(38) M. Eddaoudi, J. Kim, N. Rosi, D. Vodak, J. Wachter, M. O'Keeffe and O. M. Yaghi, *Science*, 2002, **295**, 469–472.

(39) D. Zhao, D. J. Timmons, D. Yuan and H. C. Zhou, *Acc. Chem. Res.*, 2011, **44**, 123–133.

(40) F. a. Almeida Paz, J. Klinowski, S. M. F. Vilela, J. P. C. Tomé, J. a. S. Cavaleiro and J. Rocha, *Chem. Soc. Rev.*, 2012, **41**, 1088.

(41) H. Deng, C. J. Doonan, H. Furukawa, R. B. Ferreira, J. Towne, C. B. Knobler, B. Wang and O. M. Yaghi, *Science*, 2010, **327**, 846–850.

(42) S. Yuan, W. Lu, Y. P. Chen, Q. Zhang, T. F. Liu, D. Feng, X. Wang, J. Qin and H. C. Zhou, *J. Am. Chem. Soc.*, 2015, **137**, 3177–3180.

(43) L. K. Cadman, J. K. Bristow, N. E. Stubbs, D. Tiana, M. F. Mahon, A. Walsh and A. D. Burrows, *Dalt. Trans.*, 2016, **45**, 4316–4326.

(44) M. Fujita, D. Oguro, M. Miyazawa, H. Oka, K. Yamaguchi and K. Ogura, *Nature*, 1995, **378**, 469–471.

(45) Y. Inokuma, T. Arai and M. Fujita, *Nat. Chem.*, 2010, **2**, 780–783.

(46) B. F. Abrahams, S. R. Batten, H. Hamit, B. F. Hoskins and R. Robson, *Angew. Chemie Int. Ed. English*, 1996, **35**, 1690–1692.

(47) K. Biradha and M. Fujita, *Angew. Chemie Int. Ed.*, 2002, **41**, 3392–3395.

(48) O. Ohmori, M. Kawano and M. Fujita, *J. Am. Chem. Soc.*, 2004, **126**, 16292–16293.

(49) O. Ohmori, M. Kawano and M. Fujita, *Angew. Chemie - Int. Ed.*, 2005, **44**, 1962–1964.

(50) T. Kawamichi, T. Haneda, M. Kawano and M. Fujita, *Nature*, 2009, **461**, 633–635.

(51) K. Ohara, M. Kawano, Y. Inokuma and M. Fujita, *J. Am. Chem. Soc.*, 2010, **132**, 30–31.

(52) H. Kim, H. Chun, G.-H. Kim, H.-S. Lee and K. Kim, *Chem. Commun.*, 2006, **26**, 2759–2761.

(53) G. J. Halder and C. J. Kepert, *J. Am. Chem. Soc.*, 2005, **127**, 7891–900.

(54) J. Kahr, R. E. Morris and P. A. Wright, *CrystEngComm*, 2013, **15**, 9779.

(55) K. Ikemoto, Y. Inokuma, K. Rissanen and M. Fujita, *J. Am. Chem. Soc.*, 2014, **136**, 6892–6895.

(56) G. Friedel, *C. R. Acad. Sci*, 1913, **157**, 1533 –1536.

(57) C. Bokhoven, J. C. Schoone and J. M. Bijvoet, *Acta Crystallogr.*, 1951, **4**, 275–280.

(58) J. M. Bijvoet, *Proc. Acad. Sci. Amst.*, 1949, **B52**, 313 –314.

(59) A. J. v. B. Bijvoet, J. M., A. F. Peerdeman, *Nature*, 1951, **168**, 271 –272.

(60) H. D. Flack and G. Bernardinelli, *Acta Crystallogr. Sect. A Found. Crystallogr.*, 1999, **55**, 908–915.

(61) H. D. Flack, *Acta Crystallogr. Sect. A Found. Crystallogr.*, 1983, **39**, 876–881.

(62) H. Burrows, R Weir and J. Stohner, 1995, **67**, 1307–1375.

(63) M. P. Byrn, C. J. Curtis, I. Goldberg, Y. Hsiou, S. I. Khan, P. A. Sawin, S. K. Tendick and C. E. Strouse, *J. Am. Chem. Soc.*, 1991, **113**, 6549–6557.

(64) M. P. Byrn and C. E. Strouse, *J. Am. Chem. Soc.*, 1991, **113**, 2501–2508.

(65) M. P. Byrn, C. J. Curtis, S. I. Khan, P. A. Sawin, R. Tsurumi and C. E. Strouse, *J. Am. Chem. Soc.*, 1990, **112**, 1865–1874.

(66) S. Kaabel et al., *Chem. Sci.*, 2017, **8**, 2184–2190.

(67) D. J. Cram, *Nature*, 1992, **356**, 29–36.

(68) F. Jia, Z. He, L.-P. Yang, Z.-S. Pan, M. Yi, R.-W. Jiang and W. Jiang, *Chem. Sci.*, 2015, **6**, 6731–6738.

(69) S. Yoshioka, Y. Inokuma, M. Hoshino, T. Sato and M. Fujita, *Chem. Sci.*, 2015, **6**, 1–4.

(70) S. Takizawa, K. Kishi, Y. Yoshida, S. Mader, F. A. Arteaga, S. Lee, M. Hoshino, M. Rueping, M. Fujita and H. Sasai, *Angew. Chemie Int. Ed.*, 2015, **127**, 15731–15735.

(71) G. Brunet, D. A. Safin, K. Robeyns, G. A. Facey, I. Korobkov, Y. Filinchuk and M. Murugesu, *Chem. Commun.*, 2017, **53**, 5645–5648.

(72) T. Haneda, M. Kawano, T. Kawamichi and M. Fujita, *J. Am. Chem. Soc.*, 2008, **130**, 1578–1579.

(73) M. Yoshizawa, J. K. Klosterman and M. Fujita, *Angew. Chemie - Int. Ed.*, 2009, **48**, 3418–3438.

(74) K. Ikemoto, Y. Inokuma and M. Fujita, *J. Am. Chem. Soc.*, 2011, **133**, 16806–16808.

(75) J. V. Knichal, H. J. Shepherd, C. C. Wilson, P. R. Raithby, W. J. Gee and A. D. Burrows, *Angew. Chemie - Int. Ed.*, 2016, **55**, 5943–5946.

(76) V. Duplan, M. Hoshino, W. Li, T. Honda and M. Fujita, *Angew. Chemie - Int. Ed.*, 2016, **55**, 4919–4923.

(77) Y. Inokuma, T. Ukegawa, M. Hoshino and M. Fujita, *Chem. Sci.*, 2016, **7**, 3910–3913.

(78) S. Urban, R. Brkljača, M. Hoshino, S. Lee and M. Fujita, *Angew. Chemie Int. Ed.*, 2016, **55**, 2678–2682.

(79) S. Yoshioka, Y. Inokuma, V. Duplan, R. Dubey and M. Fujita, *J. Am. Chem. Soc.*, 2016, **138**, 10140–10142.

(80) M. Hoshino, A. Khutia, H. Xing, Y. Inokuma and M. Fujita, *IUCrJ*, 2016, **3**, 139–151.

(81) Y. Inokuma, S. Yoshioka, J. Ariyoshi, T. Arai, Y. Hitora, K. Takada, S. Matsunaga, K. Rissanen and M. Fujita, *Nature*, 2013, **501**, 262–262.

(82) T. R. Ramadhar, S.-L. Zheng, Y.-S. Chen and J. Clardy, *Chem. Commun.*, 2015, **51**, 11252–11255.

(83) E. Sanna, E. C. Escudero-Adán, A. Bauzá, P. Ballester, A. Frontera, C. Rotger and A. Costa, *Chem. Sci.*, 2015, **6**, 5466–5472.

(84) S.-Y. Zhang, L. Wojtas and M. J. Zaworotko, *J. Am. Chem. Soc.*, 2015, **137**, 12045–12049.

(85) G.-H. Ning, K. Matsumura, Y. Inokuma and M. Fujita, *Chem. Commun.*, 2016, **52**, 7013–7015.

(86) S. Lee, E. A. Kapustin and O. M. Yaghi, *Science*, 2016, **353**, 808–811.

(87) F. Gándara, H. Furukawa, S. Lee and O. M. Yaghi, *J. Am. Chem. Soc.*, 2014, **136**, 5271–5274.

(88) J.-S. Qin, S. Yuan, A. Alsalme and H.-C. Zhou, *ACS Appl. Mater. Interfaces*, 2017, In Press DOI:10.1021/acsami.6b16264.

(89) I. Union, O. F. Pure and A. Chemistry, 1994, **66**, 1077–1184.

(90) A. Bondi, *J. Phys. Chem.*, 1964, **68**, 441–451.

(91) S. Zuluaga, P. Canepa, K. Tan, Y. J. Chabal and T. Thonhauser, *J. Phys. Condens. Matter*, 2014, **26**, 133002.

(92) C. M. Roth, B. L. Neal and a. M. Lenhoff, *Biophys. J.*, 1996, **70**, 977–87.

(93) K. Autumn, M. Sitti, Y. a. Liang, A. M. Peattie, W. R. Hansen, S. Sponberg, T. W. Kenny, R. Fearing, J. N. Israelachvili and R. J. Full, *Proc. Natl. Acad. Sci.*, 2002, **99**, 12252–12256.

(94) E. Arunan et al., *Pure Appl. Chem.*, 2011, **83**, 1637–1641.

(95) J. Emsley, *Chem. Soc. Rev.*, 1980, **9**, 91.

(96) G. P. Schiemenz, *Zeitschrift fur Naturforsch. - Sect. B J. Chem. Sci.*, 2007, **62**, 235–243.

(97) G. R. Desiraju and T. Steiner, *The Weak Hydrogen Bond*, Oxford University Press, Oxford, 1st, 2001.

(98) L. Pauling, *Nature of the Chemical Bond,* Cornell University Press, Ithaca NY, 3rd, 1960, p. 464.

(99) J. D. Dunitz, *ChemBioChem*, 2004, **5**, 614–621.

(100) J. D. Dunitz and R. Taylor, *Chem. - A Eur. J.*, 1997, **3**, 89–98.

(101) T. S. Thakur, M. T. Kirchner, D. Bläser, R. Boese and G. R. Desiraju, *CrystEngComm*, 2010, **12**, 2079.

(102) J. a. K. Howard, V. J. Hoy, D. O'Hagan and G. T. Smith, *Tetrahedron*, 1996, **52**, 12613–12622.

(103) V. R. Thalladi, H.-C. Weiss, D. Bläser, R. Boese, A. Nangia and G. R. Desiraju, *J. Am. Chem. Soc.*, 1998, **120**, 8702–8710.

(104) J. L. Alonso, S. Antolínez, S. Blanco, A. Lesarri, J. C. López and W. Caminati, *J. Am. Chem. Soc.*, 2004, **126**, 3244–3249.

(105) C. A. Hunter, K. R. Lawson, J. Perkins and C. J. Urch, *J. Chem. Soc. Perkin Trans. 2*, 2001, **5**, 651–669.

(106) C. R. Martinez and B. L. Iverson, *Chem. Sci.*, 2012, **3**, 2191.

(107) C. a. Hunter and J. K. M. Sanders, *J. Am. Chem. Soc.*, 1990, **112**, 5525–5534.

(108) S. Tsuzuki, K. Honda, T. Uchimaru, M. Mikami and K. Tanabe, *J. Am. Chem. Soc.*, 2002, **124**, 104–112.

(109) M. O. Sinnokrot and C. D. Sherrill, *J. Am. Chem. Soc.*, 2004, **126**, 7690–7.

(110) M. L. Waters, *Curr. Opin. Chem. Biol.*, 2002, **6**, 736–741.

(111) C. Livage, C. Egger and G. Férey, *Chem. Mater.*, 2001, **13**, 410–414.

(112) D. J. Tranchemontagne, J. R. Hunt and O. M. Yaghi, *Tetrahedron*, 2008, **64**, 8553–8557.

(113) R. Ameloot, F. Vermoortele, W. Vanhove, M. B. J. Roeffaers, B. F. Sels and D. E. De Vos, *Nat. Chem.*, 2011, **3**, 382–387.

(114) K. Uemura, S. Kitagawa, M. Kondo, K. Fukui, R. Kitaura, H. C. Chang and T. Mizutani, *Chem. - A Eur. J.*, 2002, **8**, 3586–3600.

(115) S. Vujovic, E. C. Constable, C. E. Housecroft, C. D. Morris, M. Neuburger and A. Prescimone, *Polyhedron*, 2015, **92**, 77–83.

(116) P. M. Forster, P. M. Thomas and A. K. Cheetham, *Chem. Mater.*, 2002, **14**, 17–20.

(117) A. Banerjee, P. Mahata and S. Natarajan, *Eur. J. Inorg. Chem.*, 2008, **2008**, 3501–3514.

(118) Y. Inokuma, S. Yoshioka, J. Ariyoshi, T. Arai and M. Fujita, *Nat. Protoc.*, 2014, **9**, 246–252.

(119) T. R. Ramadhar, S.-l. Zheng, Y.-s. Chen and J. Clardy, *Acta Crystallogr. Sect. A*, 2015, **71**, 46–58.

(120) G. W. Waldhart, N. P. Mankad and B. D. Santarsiero, *Org. Lett.*, 2016, **18**, 6112–6115.

(121) G. R. Desiraju, *J. Am. Chem. Soc.*, 2013, **135**, 9952–9967.

(122) D.-K. Bučar, *Cryst. Growth Des.*, 2017, **17**, 2913–2918.

(123) G.-G. Luo, J.-X. Xia, K. Fang, Q.-H. Zhao, J.-H. Wu and J.-C. Dai, *Dalton Trans.*, 2013, **42**, 16268–71.

(124) D.-K. Bučar, R. W. Lancaster and J. Bernstein, *Angew. Chemie Int. Ed.*, 2015, **54**, 6972–6993.

(125) J. D. Dunitz and J. Bernstein, *Acc. Chem. Res.*, 1995, **28**, 193–200.

(126) CrysAlisPro, *Agilent Technologies UK Ltd, Yarnton, England*.

(127) R. Caliandro, B. Carrozzini, G. L. Cascarano, C. Giacovazzo, A. Mazzone and D. Siliqi, *J. Appl. Crystallogr.*, 2009, **42**, 302–307.

(128) G. M. Sheldrick, *Acta Crystallogr. Sect. A Found. Crystallogr.*, 2008, **64**, 112–122.

(129) O. V. Dolomanov, L. J. Bourhis, R. J. Gildea, J. a. K. Howard and H. Puschmann, *J. Appl. Crystallogr.*, 2009, **42**, 339–341.

(130) I. A. Guzei, *J. Appl. Crystallogr.*, 2014, **47**, 806–809.

(131) C. F. Macrae, P. R. Edgington, P. McCabe, E. Pidcock, G. P. Shields, R. Taylor, M. Towler and J. Van De Streek, *J. Appl. Crystallogr.*, 2006, **39**, 453–457.

(132) A. Mohammad and a Forghaniha, *Heterocycles*, 2004, **63**, 1897–1901.

(133) M. Fujita, H. Oka and K. Ogura, *Tetrahedron Lett.*, 1995, **36**, 5247–5250.

(134) N. Miyaura, K. Yamada and A. Suzuki, *Tet. Lett.*, 1979, **36**, 3437–3440.

(135) A. Suzuki, *J. Organomet. Chem.*, 1999, **576**, 147–168.

(136) A. J. J. Lennox and G. C. Lloyd-Jones, *Chem. Soc. Rev.*, 2014, **43**, 412–443.

(137) D. G. Brown and J. Bostrom, *J. Med. Chem.*, 2016, **59**, 4443–4458.

(138) D. Blakemore, in *Synth. Methods Drug Discov.* Ed. D. Blakemore, P. C. Doyle and Y. M. Fobian, The Royal Society of Chemistry, 2016, vol. 1, pp. 1–69.

(139) D. Milstein and J. K. Stille, *J. Am. Chem. Soc.*, 1979, **101**, 4992–4998.

(140) P. Espinet and A. M. Echavarren, *Angew. Chemie - Int. Ed.*, 2004, **43**, 4704–4734.

(141) C. Cordovilla, C. Bartolomé, J. M. Martínez-Ilarduya and P. Espinet, *ACS Catal.*, 2015, **5**, 3040–3053.

(142) C. Reichardt, *Solvent Effects in Organic Chemistry*, Wiley-VCH Publishers, 3rd, 2003.

(143) R. Seetharaj, P. V. Vandana, P. Arya and S. Mathew, *Arab. J. Chem.*, 2016, In Press DOI:10.1016/j.arabjc.2016.01.003.

(144) G Férey, C Mellot-Draznieks, C Serre, F Millange, J Dutour, S Surblé and I Margiolaki, *Science*, 2005, **309**, 2040–2042.

(145) W.-Y. Gao, S. Palakurty, L. Wojtas, Y.-S. Chen and S. Ma, *Inorg. Chem. Front.*, 2015, **2**, 369–372.

(146) D. Feng et al., *Nat. Commun.*, 2014, **5**, 5723.

(147) L. Peng, M. Asgari, P. Mieville, P. Schouwink, S. Bulut, D. T. Sun, Z. Zhou, P. Pattison, W. van Beek and W. L. Queen, *ACS Appl. Mater. Interfaces*, 2017, **9**, 23957–23966.

(148) D. N. Dybtsev et al., *Chem. - A Eur. J.*, 2010, **16**, 10348–10356.

(149) M. Moriya et al., *Inorg. Chem.*, 2012, **51**, 4689–4693.

(150) W.-Y. Guo, M.-L. Li, Y.-J. Shi, H.-H. Song and H.-T. Yu, *J. Coord. Chem.*, 2015, **68**, 4224–4241.

(151) Y.-f. Zhu and H. Xia, *J. Chem. Res.*, 2012, **36**, 169–171.

(152) E. Pidcock, *Chem. Commun.*, 2005, **27**, 3457–3459.